The authors would like to thank the 3 referee's comments and the editor's efforts in helping us to improve the manuscript. We have made replies to the comments and corresponding revisions. This general reply include the major and common revisions that are made to the manuscript. The replies to each referee's comments are attached after this document. Besides, a marked up version of the revised manuscript is also provided to highlight the specific revisions (yellow for the replies to the comments from referee #1, cyan for those from referee #2, and red for those from referee #3).

There are several major changes to the manuscript (among which many are also common questions raised by the referees):

(1) In the revised manuscript, we have adopted the sea ice strength parameterization scheme in Hibler (1929), denoted H79, and re-run all the experiments. All the contents, including figures and texts, are updated accordingly. Although the scheme in Rothrock (1975), denoted R75, is used by default in CICE and CESM, we attain a more reasonable basin-scale sea ice thickness distribution with H79 under the NYF forcing dataset. Some detailed analysis of the sensitivity is in the reply to the referee comments. We consider the choice of strength parameterization an important and relevant issue, but beyond the scope of this study. We intend to explore it further in future studies.

(2) We have changed the spatial and temporal coverage for the scaling analysis. First, we have changed the region of study to be within the basin but excluding area close to land. This avoids the inclusion of semi-permanent deformation regions, which is an issue raised by two referees. Second, we have added the results of wintertime spatial scaling with daily deformation fields. This content forms an added section (Sec. 3.3) in the manuscript. Due to the variety of the factors that contribute to the kinematics (including its statistics), the scaling coefficients cannot be simply attributed to AO. Rather, it remains an open question of how various factors (such as sea ice state, fine-scale atmospheric forcings) influence the spatial scaling, and furthermore, whether current models have the potential to reproduce related processes. In this regard, we present the wintertime scaling coefficients in Sec. 3.3 and add the planned work for attributing of various factors in discussion.

(3) Model details, including the choice of model parameters, are now in an added appendix (Appendix B), as required by all 3 referees. We keep the same model parameters as used across the resolutions (0.45-deg, 0.15-deg and 0.05-deg), since we have attained very consistent climatology without extra model tuning. For example, the wintertime sea ice volume only differs by 5% among the three resolutions. We do consider model tuning a necessary step, especially when comparing against observations. However, due to the use of NYF forcing, we lack the exact observational dataset to compare against. We plan to carry out parameter-based tuning when moving to IAF and historical experiments in the future.

(4) Spatial scaling methodology are covered in detail in a newly added appendix (Appendix C), which is required by the 3$^{rd}$ referee.

(5) We restrain from the statements about temporal scaling. A Lagrangian tracking

based approach is needed for a formal examination of temporal scaling (Hutter, 2018; Weiss & Dansereau, 2017), the mean of Eulerian ice speeds is improper for such analysis. Therefore, we only show the results with 3-day mean ice fields without using temporal scaling. Temporal scaling, as well as spatial-temporal scaling can be carried out with our model output with a Lagrangian tracking based diagnosis in the future.

The replies to the 3 referees' comments are attached after this document (**page 3 to 15** for the reply to referee #1, **page 16 to 22** for those to referee #2, and **page 23 to 41** for those to referee #3). Again, we sincerely thank the referee's for the professional and helpful review to help us improve the contents of the manuscript.

**References:**


Hibler, W.D. (1979). A dynamic thermodynamic sea ice model. J. Phys. Oceanogr., 9:817846.

Hutter, N., Losch, M., and Menemenlis, D. (2018). Scaling properties of Arctic sea ice deformation in a high-resolution viscous-plastic sea ice model and in satellite observations, Journal of Geophysical Research: Oceans, 123, 672–687, doi:10.1002/2017JC013119.

Rothrock, D.A. (1975). The energetics of the plastic deformation of pack ice by ridging. J. Geophys. Res., 80:4514–4519

Weiss, J. and Dansereau, V. (2017). Linking scales in sea ice mechanics. Phil. Trans. R. Soc. A, 375: 20150352. http://dx.doi.org/10.1098/rsta.2015.0352

The authors would like to thank Dr. Nils Hutter (the referee) for the invaluable comments. The following are the replies for each comment, together with specific revisions that are made. The original comments are in *green italic* font, and the revisions are highlighted in the revised manuscript in yellow.

**Reply to comments of Referee #1:**

*The paper describes the creation of a multi-resolution suite of grids for CESM with a focus on their use for sea-ice modelling in the Arctic. The authors study the effect of grid resolution and number of EVP subcycling steps on the statististical properties of sea ice deformation as well as sea ice extent and volume. In particular, the localization of sea ice deformation in shear and failure lines such as leads and pressure ridges is studied. The authors present their model configuration as a starting point for more dedicated studies on sea ice dynamics and climate simulations and share the corresponding code and data. The simulations are analysed without optimising model parameters to the specific grid resolution and the evaluation of the simulations need to be improved. Therefore, I recommend the manuscript for publication in Geoscientific Model Development after consideration of my general and specific comments.*

*General comments:*

*1) The authors present untuned model runs with biased ice thickness fields (with too thick ice in the Beaufort Gyre) and also the ice volume in the simulations differs with the resolution used. However, the authors describe good agreement of sea ice coverage and volume of all simulations although a comparison with a sea ice thickness product, e.g. PIOMAS, is missing. So first, I suggest a thorough evaluation of the ice thickness and to study the differences in sea ice state between the different resolution simulations. I see two potential ways how to handle these different resolutions simulations that produce different sea ice state:*

**Reply to the general comment (1)**: the authors thank the referee's comment on the modeled sea ice thickness, and would like to make the following reply. Based on extra numerical experiments, we have discovered sensitivity of modeled ice thickness to the strength parameterization scheme. By default, CESM utilizes an ice strength parameterization in Rothrock (1979), detailed in Lipscomb et al. (2007). Instead of the traditional scheme in Hibler (1975) in which ice strength is related to mean ice thickness, the ice strength is closely related to the energy conversion and dissipation during the ridging process. Fig. 1 (below) compares the equilibrium Arctic sea ice thickness with the two ice strength schemes for TS045 (CESM D-type). With the scheme of Hibler (1975), the sea ice is considerable thinner in the Beaufort Gyre (BG), and arguable more reasonable with respect to observed sea ice climatology. We further confirm that thinner ice in BG is independent of the specific grid we use, showing similar differences for the default built-in grid of GX1V6 in CESM (Fig. 2). We have also found similar results with TS015 (CESM D-type experiment) as well as CESM G-type experiment (ocean-ice coupled run) with TS045 (results not shown).
Since Rothrock (1979) and Lipscomb et al. (2007) are used by CESM, including its scientifically validated experiments, we consider this choice of ice strength parameterization reasonable for the experiments and analysis within the realm of this study.
Furthermore, in a recent paper (Stewart et al., 2020), ocean-ice coupled experiments with both CORE2 NYF and normal-year based forcings from JRA55-do are compared. Fig. 18 of

the reference confirms our findings above, showing thick ice in BG for CESM (version 2), as well as drastically different ice thickness fields modeled when different years of JRA55-do are used for normal-year forcings. This indicates that NYF based experiments that produce reasonable sea ice distribution can serve the study of certain aspects of model performance, but not necessary representation of the mean status of sea ice in reality.
In summary, we consider the model output attained with CORE2 NYF in our experiments reasonable for the comparative study across the resolutions. Furthermore, we look forward to exploring the attribution of strength scheme dependent sea ice thickness in the future.

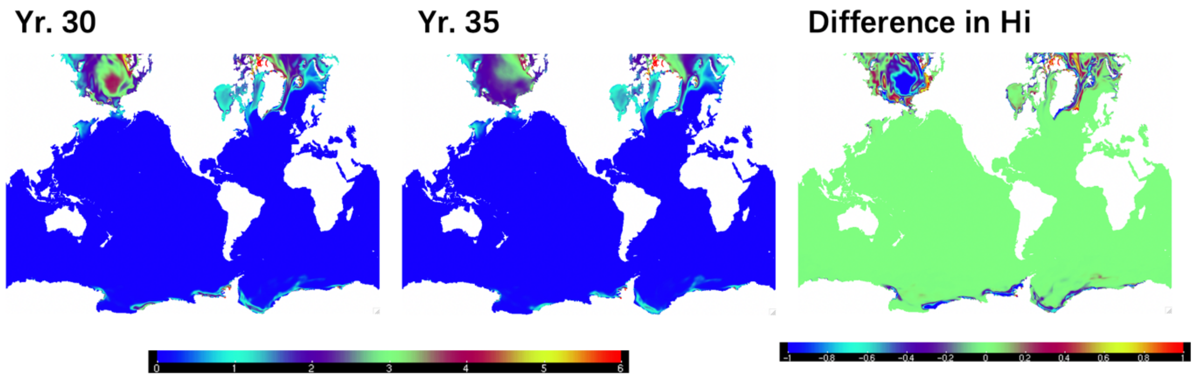


Fig. 1. March sea ice thickness difference for TS045 grid at equilibrium states under CESM D-type experiments. Left: Rothrock (1975) scheme; Middle: Hibler (1979) scheme; Right: difference (middle *minus* left). All values are in meters.

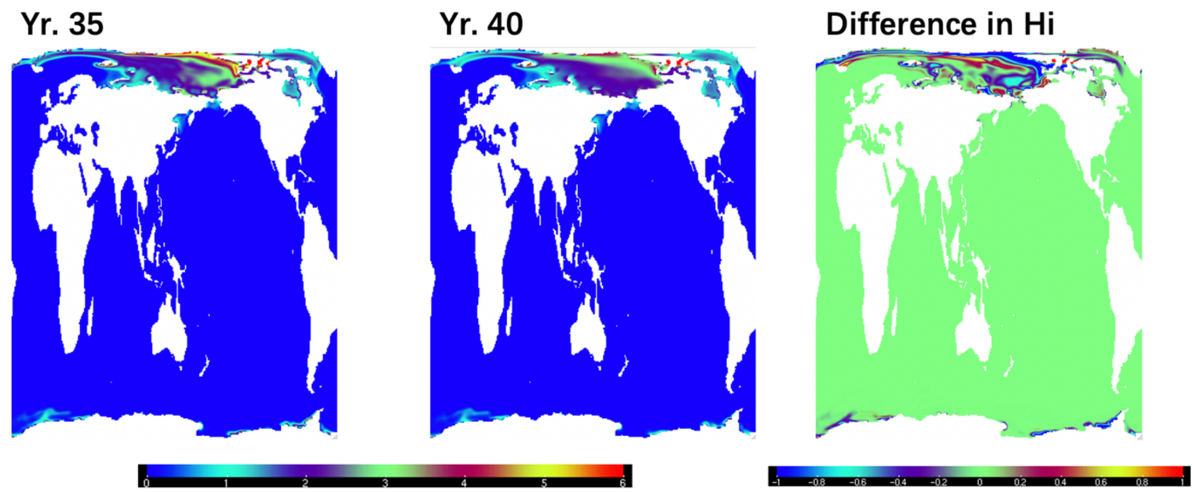


Fig. 2. March sea ice thickness difference for GX1V6 grid at equilibrium states under CESM D-type experiments. Left: Rothrock (1975) scheme; Middle: Hibler (1979) scheme; Right: difference (middle *minus* left). All values are in meters.

*(a) If you are interested to study the effect of different resolution on sea ice dynamics (which is the topic of Section 3.3), all simulations should produce comparable sea ice distributions (concentration fields thickness as well volume and extent). Otherwise it is not possible to disentangle the effect of the change in resolution and the change in sea ice state on the dynamics. Systematic tuning methods (Massonnet et al., 2014; Ungermann et al., 2017; Sumata et al., 2019) could be used for all three simulations to optimize the parameter choices for each simulations by minimizing the model-observations misfit (for*

*instance concentration, thickness, and drift). To resolve the issue of too thick ice in the Beaufort Gyre, drag coefficients and the ice strength parameterization could be tuned. The tuned simulations are then a good starting point for further multi-resolution studies and also the various parameters determined in the optimization will provide insight in how model physics change with resolution.*

**Reply to the general comment (1.a)**: the authors fully agree with the referee that it is necessary to tune the model in order to improve modeled sea ice distribution and comparability. In our study, our original intention is to align the parameterization across the resolution to ensure good comparability, at least the thermodynamics should be kept the same across the resolution range. As indicated by the referee, we have found sea ice thickness in BG greatly dependent on the ice strength parameterization scheme, as shown above. Although the scheme we have adopted is used by default in CESM, we consider it to be replaced with the more commonly used scheme in Hibler (1979) in future studies.

*(b) If such systematic tuning is not possible due to limited computational resources, the authors should be more cautions with statements regarding the good agreement of ice thickness fields and agreement of all three simulations. The differences between the three simulations should be described and interpreted in details. Possible reasons for the different sea ice distributions should be provided along with guidance what limitations with regard to the kinematic studies originate from the different sea ice distributions.*

**Reply to the general comment (1.b)**: according to the referee's suggestions, we further compare the Arctic sea ice climatology among the 3 grids. However, based on experiments that evaluate the effects of sea ice strength parameterization (shown above), we argue that ice strength parameterization causes much more uncertainty than the differences among the 3 grid resolutions. Since we have limited computational resource for the model runs, we follow the criteria below for the new experiments and related analyses. We align the thermodynamic parameterization schemes as well as parameter values across the 3 resolutions. We examine in detail the ice strength parameterization (including its parameters) in the modeled climatology. Furthermore, we include a new appendix showing all the parameters that are utilized in our study.

*2) The analysis of deformation rates in the manuscript is limited to two 3-day intervals. Since the scaling properties of sea-ice deformation are highly variable (Stern & Lindsay, 2009) and strongly impacted by atmospheric winds (Herman & Glowacki, 2010), limiting the analysis to such a short time interval does not allow robust conclusions on the model capability to simulate multi-fractal deformation rates. It can not be excluded that the two dates chosen for the analysis mainly highlight the imprint of the atmospheric forcing. Another problem with the too short interval are the CDF of deformation rates that do not show power-law tails due to strong fluctuations (although stated differently by the authors). I suggest to extend this analysis to at least one entire winter. This will reduce the impact of specific wind conditions, smoothen the CDFs, and allow a more robust interpretation of the presented results with regard to the models ability to simulated strongly localized deformation rates along leads and pressure ridges. In addition I recommend to remove all statements on temporal scaling based on these two 3-day intervals from this manuscript, as now temporal scaling analysis is performed by the authors.*

**Reply to the general comment (2)**: regarding to the referee's comment on the analysis of deformation fields, we have made the following two revisions. First, we extend the study to the full winter, including the study of C-CDF and scaling analysis. The discussion on these two representative days are further carried out on daily deformation fields during the winter months. Second, as pointed out by the referee, the temporal scaling has not been carried out in strict manner, and therefore we remove the statements involving temporal scaling. Specifically, we only present the 3-day results without relating them to (or drawing any conclusion on) temporal scaling properties.

*3) The good agreement of deformation fields between the different resolutions surprised and impressed me. In your simulations only the degree of detail in deformation feature increases, but the general patterns agree across the different resolutions. Knowing that ice fracture is a chaotic process that is very sensitive to small variations in ice strength these results puzzles me, as I was expecting that the deformation fields diverge very fast due to the different deformation history. At high resolution, a deformation event which is associated with divergence reduces concentration and thickness, and thereby the ice strength, such that deformation is more likely to appear in the same spot again. This effect should not be so effective in coarse resolution simulations as the reduction in concentration and thickness is much smaller due to the size of the grid box. This different memory should cause different reactions to the same atmospheric forcing. Do you see a reduction in concentration and thickness along the simulated LKFs in all your simulations? Do you see reoccuring deformation lines in all simulations? Your results indicate rather that in general this described feedback is not so strong and that fracture is mainly driven or better prescribed by the forcing, which would be an interesting result. This aspect of your results is definitely worth more discussion in the paper and maybe some additional analysis.*

**Reply to the general comment (3)**: regarding to the referee's comments, we in the first place were also a little bit surprised about the consistency of deformation features across the 3 vastly different resolutions. We conjecture that this is due to the specific experiment design of using NYF forcing, as well as the specific strength parameterization scheme we have adopted. We are yet to explore deeper and carry out attribution study of why the kinematic features agree and find the factors can break such consistency. Specifically, we have 2 aspects to look into. First, we want to explore the effect of inter-annually changing forcings on the system. A constantly alternating forcing may deviate the pathway of different resolutions in terms of spatial distribution of thick/thin ice, and may cause differences in the deformation events (or strengths). Also with the ice strength parameterization scheme of Hibler (1979), we also want to carry out similar analysis comparing the deformation fields. Regarding the two specific questions, first, we do witness concentration changes with LFKs if divergence is present. Second, we witness some cases of re-occurrence of the LKFs, but we haven't carried out systematic analysis yet.

----

*Specific comments:*

*P1, Line 3, "multi-fractality": of what? Please add scaling of sea-ice deformation*

**Reply**: revised as indicated by the referee.

*P1 Line 19, "kilometer-scale" satellite observations: SAR images have a resolution in the range of tens of meters. The drift and deformation products derived from consecutive SAR images have a kilometer-scale resolution. Please be more specific.*

**Reply**: according to the referee's comment, we have revised the sentence as follows: "… kilometer-scale sea ice drift and deformation estimates with Synthetic Aperture Radars …"

*P2 Line 1, "Linear kinematic features": You have not described what these linear kinematic features are. Please describe once what they are (failure and shear lines where deformation is localized).*

**Reply**: revised by replacing "Linear kinematic features …" as "Linear kinematic features, including local deformation regions of sea ice failures and shearing, …"

*P2 Line 7: In the VP framework, the transition between viscous and plastic deformation depends on the stress states and not the concentration. The concentration influences the stress states by scaling the ice strength, but there is no direct link as suggested by your description. Please clarify.*

**Reply**: the sentence is revised to be more precise, as follows: "it describes the sea ice as a two dimensional continuum with nonlinear viscosity and plastic deformations under high stress conditions of compression and shear".

*P2 Line 14: CMI -> CMIP (here and elsewhere in the manuscript)*

**Reply**: replaced here and every use throughout the text.

*P2 Line 15: This is true for VP/EVP models. For other rheologies that include memory of past deformation, as the Maxwell elasto-brittle rheology, also coarser grid resolution might produce similar deformation statistics.*

**Reply**: we revise the sentence to be more precise, as follows "With VP rheology, the capability of sea ice models to resolve fine-scale deformations is inherently bounded by the resolution of the models' grid."

*P2 Line 18: The continuum assumption is part of all continuum sea-ice models regardless what rheology they use. Please consider not explicitly mentioning the rheology here.*

**Reply**: the sentence is revised by removing the specific rheology of VP, as follows "Although the continuum assumption of the sea ice cover does not necessarily hold at these resolutions, …"

*P2 Line 22, "main driver": It is not clear to me what you mean with main driver. Please clarify this sentence.*

**Reply**: the sentence is revised as "… adopted by various research groups in the world for climate studies."

*P4, Table1: Please be more specific with the grid descriptions in the "Notes: column, such that the table is understandable without reading the text. There is enough space for that.*

**Reply**: the last column (Notes) of the table is extended for a more understandable description.

*P4 Line 21-22: at the grid location and 60 vertical layers,. . .*

**Reply**: revised according to the suggestion.

*P4 Line 25: Please rewrite sentence.*

**Reply**: we reformulate the sentence as "Second, we configure the model according to the grid resolution, including the choice of parameterization schemes and related parameters that are used."

*P6 Figure 3: Please think about using the same limits for the contour plots for both grids. This would make it easier to see the difference between them. The contour lines are also hardly visible, you might also want to use a brighter red instead.*

**Reply**: the figure is revised to improve clarity and readability, according to the referee's suggestion.

*P8 Line 6-8: The thickness anomaly in Beaufort Gyre could also be caused by too weak ice and not properly tuned ice strength parameterization. The thick ice north of CAA and Greenland is then advected by the ice drift and accumulates within the Gyre.*

**Reply**: the authors have carried out experiments which show very large sensitivity of equilibrium sea ice thickness (including BG) with respect to the ice strength parameterization. By replacing the default scheme adopted by CESM with Hibler (1979), the anomalously thick ice in BG is now gone. Considering the fact that the default scheme adopted by CESM is widely used in many scientifically validated experiments, including OMIP and CMIPs, we plan to carry out detailed attribution study in the future on this issue.

*P8 Line 13, "With the warm start-up, the experiments with TS005 approaches equilibrium towards year 42.": Only for the extent, the volume is still decreasing. Please clarify.*

**Reply**: we further make analysis and attribution of the differences among the 3 grid resolutions. Before that, the experiments are also continued to allow TS005 to reach an equilibrium after year 45.

*P8 Line 17, "The overall sea ice coverage and volume of TS005 is also in good agreement with satellite observations and PIOMAS dataset.": I would not describe the strong overestimation of sea ice extent in winter as a good agreement. In addition, I miss the comparison with the PIOMAS dataset in the figure. Please state where to find this comparison.*

**Reply**: we revise the sentence as “In general, the overall sea ice coverage and volume as modeled with TS005 are consistent with satellite observations and PIOMAS dataset”. In Fig. 5.b we also add the climatological seasonal cycle from PIOMAS dataset. The years of 1979-2000 are adopted, same as the SIE climatology from NSIDC data.

*P8 Line 17-19: I do not understand why using the same parameterizations for all three grids is a reason for reasonable results. It is known that model parameters need to be adapted to different grid resolutions to show similar physics (e.g. Williams & Tremblay, 2018). Please clarify or rewrite.*

**Reply**: regarding the comment, we would like to make the following clarifications. First, we expect the thermodynamic parameterization schemes, along with the parameter values, to be consistent across the resolutions. The dynamics across the resolutions definitely will cause differences in the distribution of ice (both local ridging and spatial re-distribution), but we do not want to compensate these errors (or uncertainties) with thermodynamics. Second, we fully agree that in order to quantitatively improve the model’s performance, the modeler (or model user) should tune the model to available observations. However, since under NYF there is no exact sea ice climatology for us to match, we therefore focus on the consistency among the 3 resolutions as long as they attain reasonable results. For future studies we look forward to carrying out IAF based experiments, for which a full suite of model tuning to match observed sea ice historical changes is planned.

*P9 Line 8, "removed of seasonal cycle": -> and the seasonal cycle is removed*

**Reply**: revised.

*P10 Figure5, "satellite-observed": Please state which satellite product is used for this comparison*

**Reply**: the mean annual cycle of NSIDC SIE product of year 1979-2000 from SSMI/SMMR sensors is retrieved and used as climatological seasonal cycle. The figure caption is revised to include this information.

*P10-11 AO index analysis It is not clear why this analysis is needed here. As the corresponding explanation is rather complex, please consider to remove them from manuscript for clarity.*

**Reply**: regarding the comment on AO analysis, the authors want to clarify that the inclusion of AO indices is to ensure that the NYF dataset is not untypical in terms of wintertime atmospheric forcings. If prominent negative or positive AO is present in the NYF dataset, we would expect much different sea ice circulation and thickness distribution.

*P11 Line 8: sybcycle count -> subcycles*

**Reply**: revised as indicated.

*P11 Line 17-18: "The kinematic features with TS005 are richer and much narrower, such as the network of shearing in Beaufort Sea." Do you want to say that in TS005 more and finer features are simulated?*

**Reply**: yes, and we revise the sentence as "With TS005, the model simulates more and finer sea ice kinematic features".

*P11 Line 35: The region for the analysis you have chosen is problematic as it mixes pack-ice regions with coastal regions. In coastal regions stable deformation features, like flaw lead, are found that show nearly constantly very high deformation rates, which impacts the presented CDFs. I suggest to use the entire Arctic Ocean as study region and filter all grid points that are closer than 150-200km to the coast as done in other scaling studies.*

**Reply**: we agree with the referee's comment on the effect of coastal region on the PDF and scaling analysis. We therefore update the results by limiting the analysis within the basin, to the common regions according to TS045 (the coarsest resolution among the three).

*P12 Line 3: Please be cautious for two reasons: (1) just because the PDF/CDF of sea ice deformation shows a power-law tail does not mean it is multi-fractal. To show mulit-fractality a scaling analysis of the moments of sea-ice deformation need to be performed that shows a non-linear convex structure function (you do this analysis but it is described later). (2) The distributions shown in Figure 9 show hardly power-law distributions. I suggest to use the methodology of Clauset et al. (2009) to test for power-law distributions.*

**Reply**: the authors fully agree with the referee. We have made a mistake that we have included the texts describing the spatial scaling results to the analysis of C-CDF. We have removed the description of multi-fractality from this part of the paragraph.
Regarding the power-law distribution, since for the end of the C-CDF tail (which corresponds to relatively larger deformation events) we are hit with very small sample count, therefore, the determination of slopes is carried out for the range of 0.05 and 0.25 for the C-CDFs (noted in the figure caption).

*P12 Line 6: What do you mean with "spatial scaling"? Are you coarse-graining the high resolution simulation to coarser grid resolution? Please clarify.*

**Reply**: yes, and we revise the sentence as " … we carry out: (1) the spatial coarsening of the model output of TS005 onto TS015 and TS045, and (2) that of TS015 onto TS045."

*P12 Line 6-21: (1) The CDF in Figure 9 hardly show power-law tails and deviate from strait tails. It is not clear how you determine the power-law slopes. I recommend to use larger time intervals for the analysis to reduce the imprint of certain atmospheric forcing conditions and second to use the methodology presented in Clauset et al. (2009) to test for power-law distributions.*

**Reply**: the authors have extended the analysis to winter months and limited the analysis to strictly within the basin (away from coast) to attenuate atmospheric noises and avoid potential problems on coastal regions. Details and results are presented separately in the revised Sec. 3.2.

*(2) It is unclear to me how you relate the slopes the CDF-tails of coarse-grained deformation rates to the nominal resolution of the grid. Please describe this concept more in detail.*

**Reply**: the authors have rewritten the paragraph to include a more formal introduction of the methodology we have adopted. In brief, we use the simulation results from TS005 as a reference, by spatial coarsening of the results with TS005 to a coarser grid such as TS045, we compute the difference between the tail slopes at the grid scale of TS015. As shown, the slopes are flatter for TS005, indicating that with TS015 the model cannot simulate reasonable sea ice deformation rates with respect to the reference of TS005. We consider this difference due to that the grid-cell scale deformation is actually not realistic for TS015, and therefore a coarser spatial scale can be determined with coarsening, when the slopes from TS015 finally matches that of TS005. This scale we consider is the effective resolution of TS015 for simulating sea ice deformations.

*P12 Line 22-26: Given the limitations of your analysis (short-time interval, no clear power) I do not recommend a direct comparison with observations or at least mention these limitations.*

**Reply**: according to the referee's comment, we revise the paragraph to avoid direct comparison with Marsan et al. (2004) or any observational dataset. Afterall, due to the use of NYF, there is no direct comparability of these data.

*P12 Line 32, "about 1.3 on Feb. 6th for all three grids": I see values from 1.2 to 1.3.*

**Reply**: according to the referee's comment, we revised the sentence as "and between 1.2 and 1.3 on Feb. 6th for all three grids."

*P13 L1-2, "Furthermore, no positive value of β is detected at q = 0.5, which is consistent with Marsan et al. (2004) (Fig. 4 of the reference).": Please clarify. In Marsan et al. (2004) beta is positive for q=0.5. Also in your Figure 9 beta seems to be positive for q=0.5. What would be the physical interpretation of negative scaling exponents if you find them in your model?*

**Reply**: we correct the mistake in citing the value of beta from Marsan et al (2004), by changing "positive" to "negative". For reported data with observations [such as Marsan et al. (2004)], the value of Beta is still positive for q=0.5. For the model to report negative values for Beta, statistical issues might be the cause. Since the usual practice of using linear fittings in the analysis in Fig. 10 (left side of each panel), we usually ignore the different statistical confidence on different scales. For larger spatial scales, the sample count is significantly smaller than small scales, given that the analysis is carried out on the same dataset. Uncertainty in estimating the mean deformation rate could play an important role for the estimation of Beta, causing statistically insignificant negative values for Beta.

*P13 Line 6-8: Please be more specific. Do you mean that with increasing resolution, deformation rates are more localized with yields to more pronounced scaling?*

**Reply**: regarding the referee's comment, we consider this description applies to the contrast between the two days (Dec. $20^{th}$ and Feb. $6^{th}$). But this description is not very strict, since we lack the analysis of relating it to general cases and convincing attribution studies. For revision, since we have the model results from the whole winter, we relate the difference in scaling properties to various factors including circulation and forcing data.

*P13 Line 8-9: Temporal scaling is indicated by the decrease in β for the daily field and 3-day field for Dec. 20th, and not evident for Feb. 6th. This could be also caused by just smoothening of deformation fields due to advection. To test for for temporal scaling a Lagrangian analysis is needed that follows the ice deformation with the drift. Please remove this sentence or add analysis.*

**Reply**: the authors agree with the referee that the temporal scaling analysis formally involves Lagrangian based analysis. Besides, we want to clarify that a pure Lagrangian diagnosis with our model (which is based on Eulerian grids) is not practical, since we cannot attain the Eulerian drift speed at every time step. Therefore, we use daily mean sea ice drift speed for all the spatial analysis. We project that using smaller time interval for the computation of mean sea ice drift speed, the analysis results would converge to a pure Lagrangian based analysis.

*P13 Line 14, "indicating less dominant large-scale 15 features on Feb. 6th.": or a more heterogenous distribution of deformation rates along the LKFs.*

**Reply**: the authors agree with the referee's insight on this issue. We consider this scaling property inherent to the specific scenario of circulation/forcing. The LKFs on Feb. $6^{th}$, as a result of the thickness distribution and circulation, are indeed more localized and heterogeneous when compared with Dec. $20^{th}$.

*P13 Line 15-16, "Furthermore, there is more effective temporal scaling on Dec. 20th than Feb. 6th, as shown for C-CDFs in Figure 9 and structure functions in Figure 10.": Please remove this sentence since no temporal scaling analysis is done.*

**Reply**: we agree with the referee that due to the lack of Lagrangian perspective, the analysis we carried out here is not strictly a temporal scaling analysis. We have revised the sentence to remove the statement of "temporal scaling".

*P14 Line 4, "Figure 7": Do you mean Figure 12?*

**Reply**: corrected.

*P14 Line 6, "noisier": It is really hard to spot the noise in Fig. 12 except you zoom very strongly in certain regions. Could you find better ways to show this? For instance, plot or average the difference between the deformation rates in a grid cell and its local surrounding (couple of grid cells). This would shift the focus on the noise. Or just zoom on a certain subdomain where the noise is seen.*

**Reply**: according to the referee's comment, we add a supplementary figure showing the details in region around and north of CAA for the experiments with TS005. This will highlight the noise due to non-convergent EVP solutions.

*P17 Figure 9: This figure needs more explanation in the caption: What do the colors refer to (NDTE?)? Are 0.05 ◦ , 0.15 ◦ , and 0.45 ◦ the grid resolution and why do you not use the names T005, etc. here?*

**Reply**: the figure as well as the caption are revised to be more precise. The lines are colored by the grid name, while different shapes represent different spatial scales (0.05-deg, 0.15-deg, and 0.45-deg).

*P17 Line 5, "equilibrium in sea ice thickness and volume": But volume is still increasing, please clarify how this fits to the claimed equilibrium.*

**Reply**: we further carry out continued experiments to ensure that a quasi-equilibrium status is attained for TS005.

*P22 Line 17: MITGcm -> MITgcm*

**Reply**: corrected.

*P22 Line 20, "with initial study with temporal scaling analysis with 3-day mean drift fields": Please remove, since you have not done a temporal scaling analysis.*

**Reply**: corrected as "with initial study of 3-day mean sea ice drift fields".

*P23 Line 22-23: Remove one "in our study".*

**Reply**: corrected by removing one of the "in our study"

*P22 Line 28 - P23 Line 3: This paragraph is rather a summary of on going research in the sea ice modelling community and your future plans and not a conclusion of your study. Please remove it here or move to the state of research in the introduction.*

**Reply**: the whole paragraph is moved into Sec. 1 (on page 4), as suggested by the referee.

*P23 Line 5: Which efforts? Please add citations.*

**Reply**: citations are added for EVP convergence, including Lemieux et al. (2012), Kimmritz et al. (2015), and Koldunov et al. (2019).

*P23 Line 30 is -> are*

**Reply**: revised.

*P24 Line 3-4, "Given that the modeled sea ice climatology is reasonable and consistent among the three resolutions": In the high resolution run, the sea ice climatology is distinctively different from the two coarser runs, which indicated that parameters of the sea-ice model need to be tuned for each specific resolution to reach the same climatology. I agree that using a slab-ocean in this study is fine, but further tuning of sea ice model parameters would be required to obtain runs with comparable sea ice climatology. Please elaborate on this.*

**Reply**: the authors agree with the referee's comment on the model output presented in the original manuscript. Two aspects are improved with add-on experiments. First, we further carry out continued experiments to ensure that a quasi-equilibrium status is attained for TS005. Second, in this study we have used NYF to force the sea ice model, and this hinders the comparison with observational datasets and the ensuing tuning process, since we do not expect the model exactly match any climatology we choose. Therefore, in this study we focus on the consistency and inter-comparison of the modeled sea ice states across the resolutions, given that the climatological sea ice status is reasonable. We intend to carry out IAF based experiments for future studies, in which a formal model tuning process is planned by using observed sea ice changes as reference datasets.

**References:**

Flato, G.M. and W. D. Hibler (1995). Ridging and strength in modeling the thickness distribution of Arctic sea ice. J. Geophys. Res.–Oceans, 100:18611–18626.

Hibler, W.D. (1979). A dynamic thermodynamic sea ice model. J. Phys. Oceanogr., 9:817–846.

Kwok, R. (2010). Satellite remote sensing of sea-ice thickness and kinematics: a review, Journal of Glaciology, 56(200):1129-1140

Lipscomb, W.H., E. C. Hunke, W. Maslowski, and J. Jakacki (2007). Improving ridging schemes for high-resolution sea ice models. J. Geophys. Res.–Oceans, 112:C03S91, doi:10.1029/2005JC003355

Marsan, D., Stern, H., Lindsay, R., and Weiss, J. (2004). Scale Dependence and Localization of the Deformation of Arctic Sea Ice, Phys. Rev. Lett., 93, 178 501, doi:10.1103/PhysRevLett.93.178501.

Rampal, P., Dansereau, V., Olason, E., Bouillon, S., Williams, T., Korosov, A., and Samaké, A. (2019). On the multi-fractal scaling properties of sea ice deformation, The Cryosphere, 13, 2457–2474, doi:10.5194/tc-13-2457-2019.

Rothrock, D.A. (1975). The energetics of the plastic deformation of pack ice by ridging. J. Geophys. Res., 80:4514–4519

The authors would like to thank Dr. Frederic Dupont (the referee) for the invaluable comments. The following are the replies for each comment, together with specific revisions that are made. The original comments are in *green italic* font, and the revisions highlighted in the revised manuscript in cyan.

**Reply to comments:**

*General comments:*

*The authors present the results of one component of a new earth system, namely the sea-ice. They first introduced a new grid generation for a tripolar grid. Then, they show initial results of the sea-ice component under normal-year-forcing (a kind of climatological forcing with synoptic scales sampled from different years), including multi-scale analysis of the sea-ice deformation. Finally, they show the sensitivity of the dynamics of the model to a long-debated parameter in the dynamics, namely the number of subcycling in order that allows for artificially slow elastic waves in order to solve for the viscous plastic equations. This is to my mind the most interesting bit.*

*The manuscript is well-written. The experiments are well described. The results are well presented and analyzed using existing diagnostic tools.*

*1-One comment about the grid generation, it looks very similar to the ORCA grid we use in NEMO, but I see only a short mention in Appendix (p25) to Madec and Imbard (1996). It would be important to mention how your method differs and improves on existing ones, otherwise it sounds like you are reinventing the wheel. One additional suggestion would be give more context on why you are doing this.*

**Reply to the general comment (1)**: the authors fully acknowledge the pioneering work on ocean model grid generation in Madec & Imbard (1996), as well as the similarity with our study. Specifically, in Madec & Imbard (1996), the details of the grid generation method with embedded ellipses are only briefly mentioned by the end of the paper. The resulting grids are adopted further in NEMO with various grid resolutions in different applications.
However, there are three major reasons that we design and implement the grid generation method for our own use. First, we use CESM (v1.2.1) and its component models for all the experiments. Both POP and CICE use Arakawa-B staggering with a U-fold for the tripolar grid. On the other hand, as far as I know, NEMO uses Arakawa-C staggering with a T-fold tripolar grid. Although a seemingly minor issue, it does greatly affect all the numbering with many associated code changes to existing grid generation method.
Second, we want to have more flexible control of all the grid generation method and tool for the grid. The requirements include the control of grid cell size anisotropy in the polar regions, the grid size transition to the two grid poles on Eurasia and North American continents. For the TS grids in study we have adopted polynomial form (Fig. A1.b and Appendix A), but other options are possible, including exponential function and sinusoidal function. Different forms result in differences in grid scales in the Arctic region. Therefore we are yet to explore the various options of the grids, including resolution differences in CAA. Utilizing a fully-fledged grid generation toolkit enables aforementioned tasks.
Finally, the proposed tripolar grid generation method, including its implementation, serves as the basis for a comprehensive toolset for future development. In specific, we look forward to combining several grid generation methods into a complete toolset, including tripolar grids

(as in this study) and coastline/bathymetry-following techniques with complex conformal mappings (Xu et al., 2015).
In summary, we attain more flexibility with the proposed grid generation method for our ongoing model development. The similarity between Madec & Imbard (1996) and this study is that both adopt embedding ellipses, but the specific methods differs including in the construction of these ellipses as well as the numerical method to construct the grid lines.

*2-One general concern would be that the experiments are done with climatological atmospheric forcing and slab ocean, which means that, while it helps standardizing the experimental framework, it is not necessarily realistic as it lacks the increasing spectrum at high wave numbers present in the atmospheric and oceanic fields as one increases the resolution of the model.It is not a major problem but it would be worth discussing.*

**Reply to the general comment (2)**: the authors would like to reemphasize that the purpose of using Normal-Year Forcing based experiments, as also stated by the referee, is to align the experiments across the different grids. The NYF dataset includes synoptic signals from the atmospheric reanalysis, but lacks inter-annual variability as well as long-term trend. Therefore, NYF is also used in Ocean Model Inter-comparison Project (OMIP) to study climatological and equilibrium status of the ocean-sea ice coupled system. In response, in Section 3.1 and 4, we add further discussion of the methodology of using NYF in our study, and potential extension to Inter-Annual Forcing (IAF) dataset in the future.

*3-One important metric which seems to be missing is the ice drift error (only Fig.6 shows it for two different dates). Given the experimental framework chosen here, would it possible to add one? It is important to support that overall sea-ice volume, ice export out of the Arctic ocean or the convergence in the Beaufort gyre are reasonably modelled.*

**Reply to the general comment (3)**: regarding this comment, the authors have made the 2 revisions and an add-on experiment for the attribution of extra-thick ice in Beaufort Gyre. First, we have carried out comparison of Arctic basin sea ice drift for winter months. In specific, we have compared DJF sea ice drift from the model output against the climatological sea ice drift of NSIDC (corresponding months for 1980-2000). Second, we re-evaluate the modeling results against comparable sea ice volume by PIOMAS. The annual cycle of PIOMAS sea ice volume for the year from 1980 to 2000 is used to compute the climatology.
The add-on experiments mainly dealt with the sensitivity of modeled Arctic sea ice volume (especially in Beaufort Sea) to ice strength parameterization. In our experiments, as well as those in standard CESM settings, the ice strength parameterization follows Rothrock (1975) and Flato & Hilber (1995), instead of Hibler (1979) which is arguably more widely used. In specific, in the strength parameterization adopted by CESM (Lipscomb et al., 2007 JGR), the sea ice strength is assumed to be proportional to the change in ice potential energy with respect to compressive deformation, which in turn relates to the ridging (with exponential redistribution) and the specific ITD settings. For contrast, in Hibler (1979), the ice strength is directly computed with prognostic status including sea ice thickness (in linear relationship), concentration, as well as prescribed parameters of which Pstar is treated as a tunable constant. As a result of the choice of strength parameterization, the equilibrium sea ice thickness across the basin is considerably different, with thick sea ice in Beaufort Sea absent when using Hibler (1979). The figure below (Fig. 1) shows the comparison with TS045 grid.

Besides, we have also confirmed that this phenomenon is qualitatively similar with CESM's native grid (e.g., GX1V6, shown in Fig. 2), as well as TS015 (not shown). Given that Lipscomb et al., (2007, JGR) is used by default in scientifically checked cases of CESM relevant to our study, we consider this choice a reasonable choice for our experiments and analysis here. However, we consider this an important issue that should be further explored in future studies.

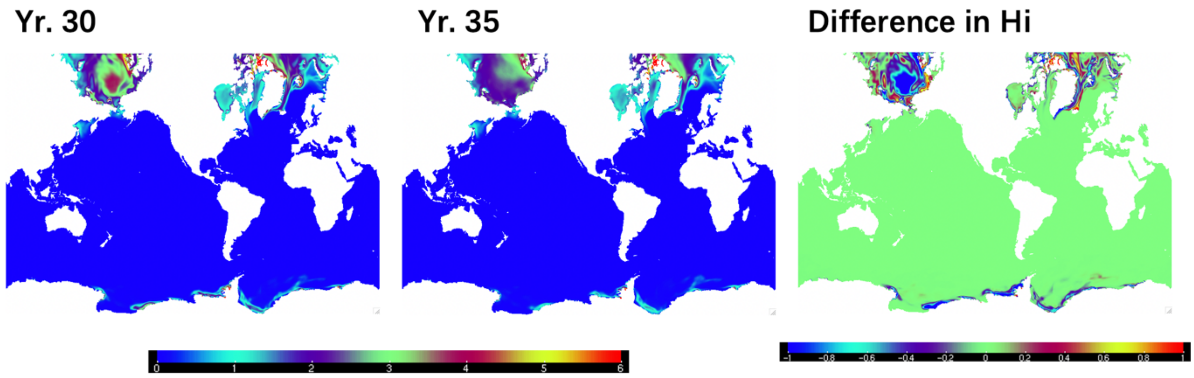


Fig. 1. March sea ice thickness difference for TS045 grid at equilibrium states under CESM D-type experiments. Left: Rothrock (1975) scheme; Middle: Hibler (1979) scheme; Right: difference (middle *minus* left). All values are in meters.

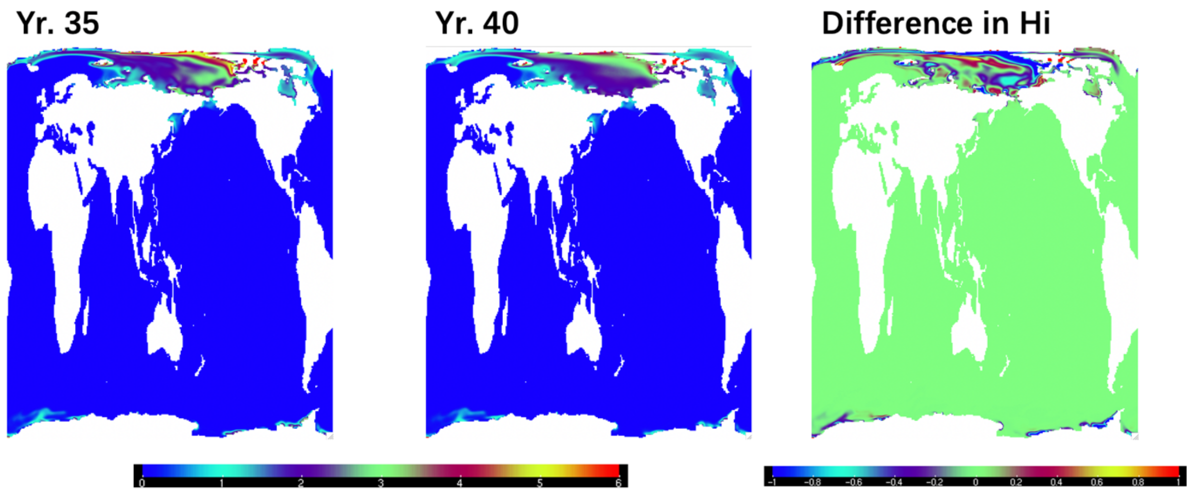


Fig. 2. March sea ice thickness difference for GX1V6 grid at equilibrium states under CESM D-type experiments. Left: Rothrock (1975) scheme; Middle: Hibler (1979) scheme; Right: difference (middle *minus* left). All values are in meters.

*4-Another is that as Lemieux et al. (2012, JCP) showed, one cannot claim a true convergence of the EVP solver (it does not convergence in the numerical sense). Please also add a discussion on this and define what you mean by "convergence".*

**Reply to the general comment (4)**: the authors apologize for using "convergence" in a less strict sense. The convergence we mentioned for EVP is not in the strict numerical sense. Rather, there is asymptotic behavior of the sea ice deformation and kinematic features with respect to EVP subcycling count. Fig. 7, 8 and 11 show the asymptotic convergence. For example, the PDFs of the deformation rates (Fig. 11) attain a good match when the NDTE is large enough especially for TS045 and TS015. Also with larger NDTE values, the kinematics features become more refined in structure and match well when NDTE goes beyond a certain value (e.g., comparing NDTE=480 and NDTE=960 for TS045). Here we revise the manuscript of Sec. 3.3 by adding extra text to formally explain what we mean by "convergence".

*5-Since the paper goes relatively in depth in analyzing sea-ice deformation –which is usually an prelude for intense discussion on rheology models– I recommend that you broaden a bit more your discussion at the end (p.22-23). For instance, about the effect of the form of the yield curve in viscous-plastic models, Bouchat and Tremblay (2017, JGR) for instance claims that decreasing the ice strengh and eccentricity improves their simulation (thickness, drift and deformation), while Ringeisen et al. (2018, cryosphere) claim that the angle in intersecting fractures from viscous plastic models is nowhere realistic...*

**Reply to the general comment (5)**: following the referee's comment, the authors have added extra discussion in Section 4 on rheology models and related dynamics-related parameterization schemes, especially regarding related works. In particular, we consider the ice strength parameterization a key discussion point here. As many works on tuning the model have adopted the scheme of Hibler (1979) [including Bouchat & Tremblay (2017) which is also mentioned by the referee], the most straightforward tuning parameters are Pstar and eccentricity of the yield ellipse. But for the scheme we have adopted, we have not observed much tuning work especially regarding basin-scale simulations. One particular parameter that can be subjected to tuning is the empirical parameter of C_f that is used to characterize frictional energy dissipation, which can be scale-dependent (details in CICE documents).

*Minor comments (given in the order of appearance in the text and figures):*

*1-any other changes to the ice physics except for ndte? There is only a reference to CESM D-type experiments and a short list of default schemes (p3 line 25 to p7 line 14), but it would be good that those are listed somewhere with chosen parameters.*

**Reply**: we confirm that the thermodynamic parameterizations are kept the same across all 3 grids and different NDTE values. In our original design of the experiments, the parameters are kept the same in order to improve the comparability of the simulation results. To revise, we have now added a separate appendix (Appendix B) that includes all parameterization schemes and related parameters that are used in the experiments, including both thermodynamics and dynamics.

*2-line 14: operational forecast BASED on Dupont et al. (2015), i.e. we were not reporting on the operational implementation in this paper but on the general long hindcast prior to it.*

**Reply**: the text is corrected to be more precise, as "the hindcast experiments for operational sea ice forecasts in Dupont et al. (2015)".

*3-line 22: main driver OF*

**Reply**: corrected.

*4-line 32: NCEP CORE: requires a reference and likely mislabed (CORE 2 might be more accurate)*

**Reply**: corrected to be CORE 2.

*5-page 5, line 4-5 (and last column of table 2), giving the number of subcycling per hour is misleading as in CICE the restoring time for the elastic waves is function anyway of the larger transport+thermodynamic timestep. I see no argument in reporting this (#/hour) except artificially increasing the cycling number when resolution is below 1 degree. Table 2 in fact shows that you did not go above 1000 cycles per timestep. Please remove.*

**Reply**: according to the referee's suggestion, the authors have removed the last column which showed the total subcycling count per model hour. Besides, we confirm that the maximum subcycle count per timestep is 960, which is indeed under 1000 cycles.

*6-page 5, line 12, "ocean status" might be "ocean processes"?*

**Reply**: revised as indicated, by changing "ocean status" into "ocean processes".

*7-Fig.5a: missing what years are used in the NSIDC climatology.for the comparison*

**Reply**: the climatological sea ice extent is computed as the annual cycle of monthly mean sea ice extent for the year from 1979 to 2000. The text is also revised to include this information.

*8-the text refers to PIOMAS but Fig.5b does not show the comparison. Can you add it please?*

**Reply**: the authors have added the climatological sea ice volume annual cycle from PIOMAS on Fig. 5.b. The same years (1979-2000) from PIOMAS are used to compute the annual cycle.

*9-p11 line 1, Nice analysis of NYF Artic Oscillation. I was always concerned of a particular bias with repeatingly using NYF. So at least the winter wind pattern is mildly neutral. What about summer though? Can we say it is also neutral?*

**Reply**: we have extended the analysis of AO to the summer months of NYF dataset, which is now incorporated into Fig. S1. In general, the summertime AO index pf CORE2 NYF is also neutral.

*10-p13, line 17 "geostrophic" is mispelled*

**Reply**: corrected.

*11-Fig.7: TS005 appears too smooth in the central Arctic (this is also noted in the text). Could it be an issue with the "convergence"?*

**Reply**: we do not consider the relative lower deformation rates in Fig. 7 an abnormal behavior of TS005. As sea ice thickness is generally thinner on the outer rim of the sea ice cover (i.e., marginal seas), the deformation rates tend to be higher as well (Kwok, J-Glaciol., 2010). In the central Arctic, for the two representative days, the seemingly smooth deformation field actually have certain shearing but low convergence/divergence (lower left panel of both Fig. 7 and 8). The convergence we mentioned is related to the concentration of deformation to local regions when NDTE is large enough.

*12-Fig.9 has an unclear color key (it seems to be function of the run and spatial filter) and Fig.10: is missing one altogether. Please elaborate so that the figure is selfreadable.*

**Reply**: both Fig. 9 and Fig. 10 are revised to include more information of the scaling curves for different resolutions. Texts that correspond to these figures are also revised.

*13-Fig.11: values are getting noisy past 1e-1 for TS045, sounds like a lack of resolution compared to TS015 and TS005.*

**Reply**: at the deformation rate of 10%/day for TS045 (shear, div, and total deformation) appear to be noisy, since with lower resolution of TS045, **we do not have sufficient samples** to compute the proper shape (i.e., tail) of the PDF. Therefore, we consider this a sampling issue, rather than the direct issue of the lack of resolution.

*14-Fig.13: interesting that ndte has such an impact on thickness even for the lowest resolution (TS045), whereas pattern of deformation are equivalent (top row of Fig.12). [please check that the top row is indeed showing different ndte results!]. I suspect this is because most of the changes in thickness are insise the Canadian Arctic Archipelago (CAA) where the deformation is not plotted. I suspect that the ice in the CAA is referred as "landfast", but it would be nice to have a more rigorous definition (is it in terms of some velocity threshold?).*

**Reply**: the difference in deformation rate between NDTE values for TS045 are mainly in the range of small values (less than 0.5%/day), as shown in the top row in Fig. 12. Note the color difference in CAA. As indicated by the referee, we revise the manuscript adopting the sea ice drift speed criterion of characterizing sea ice as landfast when the 2-week mean drift speed is lower than 5e-4m/s, as introduced in Lemieux et al (2015). The region of landfast ice (with the newly adopted criterion, as a supplementary figure) agrees well with the region of analysis.

**References:**


Bouchat, A., and Tremblay, B. (2017), Using sea-ice deformation fields to constrain the mechanical strength parameters of geophysical sea ice, J. Geophys. Res. Oceans, 122, 5802– 5825, doi:10.1002/2017JC013020.

Dupont, F., Higginson, S., Bourdallé-Badie, R., Lu, Y., Roy, F., Smith, G. C., Lemieux, J.-F., Garric, G., and Davidson, F. (2015). A high-resolution ocean and sea-ice modelling system for the Arctic and North Atlantic oceans, Geoscientific Model Development, 8, 1577–1594, doi:10.5194/gmd-8-1577-2015

Flato, G.M. and W. D. Hibler (1995). Ridging and strength in modeling the thickness distribution of Arctic sea ice. J. Geophys. Res.–Oceans, 100:18611–18626.

Hibler, W.D. (1979). A dynamic thermodynamic sea ice model. J. Phys. Oceanogr., 9:817–846.

Kwok, R. (2010). Satellite remote sensing of sea-ice thickness and kinematics: a review, Journal of Glaciology, 56(200):1129-1140

Lemieux, J.-F., Tremblay, L. B., Dupont, F., Plante, M., Smith, G. C., & Dumont, D. (2015). A basal stress parameterization for modeling landfast ice. Journal of Geophysical Research: Oceans, 120, 3157–3173. https://doi.org/10.1002/2014JC010678

Lipscomb, W.H., E. C. Hunke, W. Maslowski, and J. Jakacki (2007). Improving ridging schemes for high-resolution sea ice models. J. Geophys. Res.–Oceans, 112:C03S91, doi:10.1029/2005JC003355

Madec, G. and Imbard, M. (1996). A global ocean mesh to overcome the North Pole singularity, Climate Dynamics, 12, 381–388, doi:10.1007/BF00211684

Ringeisen, D., Losch, M., Tremblay, L. B., and Hutter, N. (2019). Simulating intersection angles between conjugate faults in sea ice with different viscous-plastic rheologies, The Cryosphere, 13, 1167–1186, doi:10.5194/tc-13-1167-2019

Rothrock, D.A. (1975). The energetics of the plastic deformation of pack ice by ridging. J. Geophys. Res., 80:4514–4519

The authors would like to thank Dr. Véronique Dansereau (the referee) for the invaluable comments. The following are the replies for each comment, together with specific revisions that are made. The original comments are in *green italic* font, and the revisions are highlighted in the revised manuscript in red.

**Reply to comments:**

*This study compares EVP sea ice simulations at different spatial resolutions and with different level of convergence (i.e., number of subiterations of the solver) of the model solution. The comparison is made on the basis of the simulated deformation rates, which are analyzed in terms of their spatial distribution (fields), probability density function, cumulative probability density function and scaling properties, in space. Unlike recent studies which have used these metrics (e.g., Rampal et al., 2019, Hutter et al., 2018 and others), the authors use a climatology as their atmospheric forcing and analyze the simulated deformation rates after spin-up and stabilization of their modeled seasonal cycle. Daily and 3-days mean deformation rate fields are used as the basis of their analyses. Two days are compared, which correspond to different AO scenarios and hence circulation patterns in the Arctic.*

*Analyses of the statistical properties of the simulated deformation rates (i.e., the shape of the PDF) are performed for different level of convergence of the model solution and demonstrate that simulation at higher resolution require a larger number of subiteration of the EVP solver to obtain heavy-tailed PDFs that are indicative of spatial scaling properties in sea ice deformation.*

*While the climatological approach is different than previous studies and perhaps eases the comparison of the modeled dynamics under different atmospheric forcing scenarios, it also precludes a direct, quantitative comparison between the model and observations, which I believe is a weakness of this study, especially considering that the physical processes that could be responsible for the difference in the results between the two atmospheric scenarios analyzed are only vaguely discussed. It also makes it hard to put the study into a temporal context (e.g., sea ice thickness and extent fields cannot be related to a specific time period and especially do not seem representative of recent sea ice conditions).*

**Reply to the major comment**: the authors thank the referee's comment on the comparability aspects of our study. We agree with the referee on the comparison of model output with observations. We would like to make the following clarifications. First, the purpose of the experiment methodology, including using atmospheric NYF dataset as well as coupling to slab ocean model, is to increase comparability across the resolution range. Second, since the NYF dataset is used to force the ice model, there is no direct comparable observation available. In turn, the comparison we have carried out are mainly between different (grid) resolutions, including deformation, scaling properties, and EVP convergence. Third, regarding the limited results and analysis as pointed out by the referee, for revisions, we extend the analysis beyond the two representative days to the whole winter, and carry out attribution study of the scaling properties and differences among the different resolutions. Lastly, this work is a first step of our effort in using the grid hierarchy with the ocean-ice coupled settings and inter-annually forced experiments. Both aspects (coupling to dynamic ocean and IAF experiments) would require a much more higher computational overhead (especially for the TS005 grid) which we look forward to exploration in the future.

*I note that a lot of care has gone into building the grid and chosing the model (atmosphere and ocean) components. These choices are clearly explained and justified. However, while a lot of information is given on the model grid, surprisingly little information is given on the dynamics part of the sea ice component (thickness resdistribution scheme parameters, rheology/mechanical parameters), which is obviously of high importance in determining the simulated dynamics. References should be included to redirect the reader towards the EVP parameter values used. I also suggest including a table with these values (P*, ellipse ratio, etc.) so that to avoid having to dig for these values into other papers and ease eventual comparisons to other similar scaling analyses.*

**Reply to the major comment**: regarding the referee's comment, we now add a separate appendix (Appendix B) to include all the parameterization schemes and the specific values of parameters we have adopted in the experiments. All the schemes, especially thermodynamic processes are kept the same as much as possible across the 3 resolutions, for the sake of improved comparability.

*Importantly, no information is given on the method used for the scaling analyses. A subsection to 3.2 that explains the steps taken towards these analyses should definitely be included in a revised version of the paper. Information on the impact of the choice of the region, period of time, the exclusion or not of grid cells close to coasts, the exclusion or not of scaling data points to evaluate the structure functions, etc., should also be given, as all of these factors can have a significant impact on the results. Also, how do your results differ if other days than Dec 10 and Feb 6 are chosen?*

**Reply to the major comment**: regarding to comment on the lack of the details of the methodology for scaling analysis, we now include another appendix (Appendix C) to cover these details. Specifically, the method involves line integrals that cover different spatial scales in the model's grid system, which follows Marsan et al. (2004) and Rampal et al. (2019). Besides, we update the region of scaling analysis and remove those close to land, and the results are also updated accordingly. Last but not the least, besides Dec. 20$^{th}$ and Feb. 6$^{th}$, we extend the analysis of daily deformations to winter months, and in Sec. 3 the new contents are added.

*Overall, section 3.2, which presents the scaling and PDF analysis, is very hard to follow. It includes some contradictions, uses of wrong words, some important misunderstandings, etc. I make several specific comments to this effect below. The figures associated with this section are in my point of view incomplete, which makes the appreciation of the results difficult. I also give suggestions below on how to improve them.*

**Reply to the major comment**: the authors thank the referee for the careful examination of the manuscript and detailed comments on Sec. 3.2. We have made specific replies to each comment, and the following revisions in general. First, we update the scaling analysis of Cumulative Probability (C-CDF in previous manuscript) to be more accurate, including a more formal introduction of the effective resolution. Second, the scaling analysis for multi-fractality and structure functions are now revised. Third, we include the analysis of other wintertime days for the sake of completeness and further analysis of contributing factors.

*Section 3.3 contains some intersting results on the effect of the convergence of the EVP model on the simulated dynamics.*

*Overall, the paper needs some proof-reading to improve the conciseness and accuracy of the formulations used. I also found many grammar mistakes but stopped raising them up at some point. I moreover found that sometimes, jargon-like formulations were used that unfortunately hide the real meaning of the sentences. An important point is the use of the term "multi-scale modeling" for what is really a comparison of model simulations across resolution. This crucially needs to be clarified.*

**Reply to the major comment**: the authors would make thorough check and proof reading on the grammatical usage after all revisions have been made. Specifically, the term of "multi-scale modeling" are replaced with "multi-resolution simulation (or modeling)" throughout the paper. Indeed, as raised by the referee, the approach is multi-resolution with parallel experiments at different grid resolutions, but not multi-scale within a single experiment. We also take care to differentiate the multi-scale deformation of the sea ice cover, and the multi-scale (or multi-resolution) experiments we have carried out.

*In brief, I consider that major revisions are required. In my point of view, the points I raise in the specific comments below need to be adressed in a first time. Another review of the paper should be conducted in a second time, in order to better appreciate the results, their meaning and their importance, in the context of this study and provide further suggestions on how to improve the manuscript it its gobality.*

**Reply to the major comment**: the authors thank the referee for these invaluable comments, and the replies (with explanations and revision to be made) are as follows for each specific comment from the referee.

*Page 1, title: I find the use of the term ''multi-scale modeling" unfortunately misleading and inapropriate. The paper is effectively about comparision of model simulations performed at various spatial resolutions, while multi-scale modeling refers to codes that can effectively resolve processes occuring different space/time scales by coupling physically and numerically models of these specific processes. A more appropriate title would be "Comparison of sea ice kinematics at different spatial resolutions modeled with a hierarchy CESM..." or "Cross-resolution comparison of CESM sea ice simulations". Please also correct any mention to multi-scale modeling in the text for consistency.*

**Reply**: the authors acknowledge the comment on the use of term "multi-scale modeling". Therefore, we modify the title of the article to: "Comparison of Sea Ice Kinematics at Different Resolutions Modeled with a Grid Hierarchy in Community Earth System Model (version 1.2.1)"

*Abstract, line 2 : "Sea ice kinematics is the most prominent feature of high-resolution simulations." There is no need to use high-resolution for kinematics features to be prominent in sea ice simulations. Please sea my comment just below about alternative rheological models, which do resolve the signature of kinematic features at medium and low resolution (> 20 km, Rampal et al., 2019).*

**Reply**: we agree with the referee that with Lagrangian framework and MEB rheology, neXtSIM could model realistic sea ice deformation at lower nominal resolution (Rampal et al. 2019). We would argue, however, that the nominal resolution of the Lagrangian models are not the limitation in resolving multi-scale deformations of sea ice, which is a great advantage of the methodology as compared with Eulerian grid based ones. Therefore, the statement we made apply to these traditional models with non-moving grids. The text is revised accordingly, as follows: "In traditional Eulerian grid based models, sea ice kinematics is the most prominent feature of high-resolution simulations". The introduction to neXtSIM and related works, including references, are now moved to Sec. 1 (from the last section), to give a better background introduction.

*Abstract, line 3 : "such as Viscous Plastic" current models are able to reproduce multifractality and linear kinematic features". This is one of my major comments: please be carefull as to make the distinction between multi-fractality in space and in time, throughout the entire text.*

**Reply**: the authors have revised the sentence to be more precise. Since this sentence is to introduce the community's status quo, it is revised as follows: "… with rheology models such as Viscous Plastic (VP) and Maxwell Elasto-Brittle (MEB), sea ice models are able to reproduce multi-fractal sea ice deformation and linear kinematic features that are witnessed in high-resolution observational dataset".

*Abstract, line 4 : "we carry out multi-scale sea ice modeling". No, you carry out a comparison of simulations at different resolutions.*

**Reply**: revised as "we carry out modeling of sea ice with multiple grid resolutions"

*Abstract, lines 6-7 : "including multi-fractal deformation and scaling properties that are temporally changing". In the light of my other comments below, I would precise "multifractal deformation in space" and not put too much weight on the temporal part. Your abstract should highlight your strong results and the temporal aspect of the scaling analysis is not one.*

**Reply**: we revise the sentence to include spatial scaling only, as follows "… including multi-fractal spatial scaling of sea ice deformation that depends on atmospheric circulation pattern and forcings". The abstract is also revised to be more precise.

*Abstract, line 8 : "effective spatial resolution". This effective spatial resolution has not been defined and cannot be understood here. I believe you mean that the model can resolve kinematic features that are 6 or 7 times the width of a model's grid cell? If so, this should be explained clearly and in simple words (i.e., rewrite lines 8-9) in the abstract and redefine later (see my other comment below).*

**Reply**: we rewrite the sentence to be more clear as follows: "By using high-resolution runs as references, we evaluate the model's effective resolution with respect to the statistics of sea ice kinematics. In specific, we find the spatial scale at which the PDF of the scaled sea ice deformation rate of low-resolution runs match that of high-resolution runs. This critical scale is treated as the effective resolution of the coarse resolution grid, which is estimated to be about 6 to 7 times of the grid's native resolution."

*Page 2, line 1 : "scale-invariance properties" Cite Marsan et al., 2004 there and Kwok et al., 2008 after "linear-kinematic features". Also, many other and more recent references can be added to Marsan et al., 2004 regarding scale-invariance, especially scale-invariance in time.*

**Reply**: as suggested by the referee, the order of references is modified, and we have added the references for scale invariance including Rampal et al. (2008) and Weiss and Dansereau (2017).

*Page 2, line 6 : "most popular". A more objective term would be "most widely used".*

**Reply**: revised as suggested by the referee.

*Page 2, line 7-8 : "a plastic medium for packed ice under shear and pressure". This formulation is vague and unfortunately not accurate: the VP model describes sea ice as undergoing plastic deformation for over-critical shearing and compressive stresses only. Please modify the sentence accordingly.*

**Reply**: the sentence is revised as follows "…, and sea ice undergoes plastic deformations over critical shearing and compressive stresses."

*Page 2, lines 15-19 : "In order to reproduce the observed properties of the sea ice kinematics, grids of 0.1 degree resolution or finer are usually required". This is true perhaps only in the VP or EVP rheology cases. The MEB rheology has the capability to localize deformation in space at the nominal grid cell scale, whatever the resolution of the grid (Dansereau et al., 2016, Rampal et al., 2019). Mention of this fact unfortunately come only in the conclusion, whereas an adequate literature review in your introduction should distinguish between the VP/EVP and other existing continuum rheologies (EB, MEB, Elastic-decohesive).*

**Reply**: the authors agree with the referee that the statements we have made apply to models with Eulerian grids. Lagrangian model (neXtSIM) with MEB rheology does not suffer from the resolution limitation of non-moving Eulerian grids. We have also moved the paragraph introducing Lagrangian and novel rheology models in Sec. 4 to Sec. 1.

*Page 2, line 20 : "multi-resolution sea ice modeling". I think that "we carry a comparison of sea ice model simulations at different spatial resolutions", or "cross-resolution comparison" would be clearer and more accurate.*

**Reply**: we revise the sentence as "… we carry out comparison of sea ice model simulations at different spatial resolutions with the coupled model …"

*Page 3, line 12 : "For the SP (...) For the NP". And the same for the lines below.*

**Reply**: revised.

*Page 4, line 4 : "a suite", a series?*

**Reply**: revised.

*Page 4, line 16 : This sentence is not clear: is there a repetition of "for TS015" there?*

**Reply**: removed the first "for TS015"

*Page 4, line 19 : "within the Arctic Ocean".*

**Reply**: revised

*Page 5, lines 2-3 : This sentence is unclear and a bit repetitive.*

**Reply**: the sentence is revised as "We choose shorter time steps for both thermodynamics and dynamics with respect to the resolutions of the grids (Tab. 2)"

*Page 5, line 4 : "a series", replace by "different subcycle numbers". Maybe rephrase as "We choose shorter thermodynamics and dynamics time steps for our higher resolution grids"?*

**Reply**: revised "…, different subcycle numbers are chosen for each grid". See also the revision above.

*Page 7, line 4 : "Potential compromises of using SOM". This needs to be rephrased, for instance as "Potential compromises pertaining to the use of SOM".*

**Reply**: revised as suggested by the referee.

*Page 7, line 6 : "in the Ocean Model Intercomparison Project".*

**Reply**: revised by adding "the", as suggested by the referee.

*Page 7, lines 8 to 12 : I understand here that you interpolate the same wind field onto your different (3) resolution grids. Does the interpolation ensures that the input (wind) energy is conserved accross resolutions? If not, this will impact your scaling results. I believe that a clear mention to this effect, in this paragraph, would be a valuable addition.*

**Reply**: for the interpolation between the atmosphere and ocean (or sea ice), we follow the standard protocol of CESM. In specific, interpolation of air-ocean (or ice) fluxes are always kept conservative. For the dynamic coupling (i.e., treatments of winds), high-order method (Patch-Recovery) is adopted. The text is revised accordingly.

*Page 7, lines 7-8 : Can you specify to which years corresponds the climatological annual cycle based on NCEP atm. reanalysis that you use? It would help understanding the ice coverage and thickness value that you obtain in your simulations at equilibrium (see my comment about these results just below).*

**Reply**: regarding the CORE2 NYF dataset, the authors make the following statements [details in Large & Yeager (2004)]. First, the fluxes are computed with 43-year NCEP reanalysis. Second, the synoptic signals are mainly from year 1995 of the reanalysis, with transition by the end of December carried out through interpolation with data in December of 1994. We consider this a limitation for future study, and will move to inter-annual forcings in further experiments.
Furthermore, as shown in Stewart et al. (2020) in which JRA55-do reanalysis is used to generate new NYF datasets, the specific year that is chosen greatly affects the model's equilibrium status for simulating Arctic sea ice (Fig. 18 of the reference).
In our opinion, the sensitivity of sea ice climatology to the NYF forcing should be studied further, with the reanalysis's behavior in the Arctic at least a focus point (instead of the current status quo).

*Page 7, line 18 : Can you perhaps spell NDTE?*

**Reply**: revised as "number of timesteps for elastic wave damping, or NDTE"

*Page 7, line 25 to page 8, line 4 : You mention here a minor overestimation in the sea ice extent (cover) in some parts of the Arctic and underestimations in others. What is the basis for this comparision? From figure 5, I understand it is satellite sea ice edge data (from NSIDC), but this should be clearly mentionned in the text as well. Also the year or period of this satellite data should be mentionned with the corresponding years on which the climatology used to force your model is based.*

**Reply**: we revise the text to include the description over the specific region with overestimation of sea ice (mainly during winter in marginal seas). We also add in the texts the years (1979-2000) for the definition of sea ice extent climatology from NSIDC data.

*Page 8, lines 4-5 : "consistent with existing sea ice thickness reconstructions by PIOMAS". Also, in the same line as my previous comment, please mention the year for these PIOMAS thickness reconstruction, or insert a figure. It seems to me that there is indeed a lot of ice* *stocked into the Beaufort Sea and that such thick ice conditions (up to 5 meters and more than 4 meters over a wide region, in September!) have not been seen at least in the last decade.*

**Reply**: we add on Fig. 5.b the PIOMAS sea ice volume seasonal cycle (computed with 1979-2000 monthly means) and revise the figure caption and texts to include necessary description. This period (1979-2000) aligns with that for the observational sea ice extent data from NSIDC. They are used as climatological sea ice extent/volume, since we do not have exact match between the model's climatology with existing observations/renanlysis.

*Page 8, line 10 : Can you explain in a few words what is a warm start-up?*

**Reply**: by "warm start-up" we mean "starting up the high-resolution simulation with a spun-up status from low-resolution ones". Therefore we revise the sentence as "With the spun-up climatological status of TS015, the experiment with TS005 approaches equilibrium towards year 42."

*Page 8, line 15 : "a minor decrease" of what? Please specify "both sea ice extent and volume" or merge this part of the sentence within the next one.*

**Reply**: according to the referee's suggestion, we have merged the two sentences as one: "Similar to TS045 and TS015, the experiment with TS005 produces reasonable sea ice climatologies, but with a minor decrease in both sea ice coverage (mainly in summer) and sea ice volume (all season) with respect to TS045 and TS015."

*Page 8, line 30 : "two years' daily mean sea ice fields (...)". Rephrase, eg. "two years (41-42) of daily mean sea ice fields for all three TS grids".*

**Reply**: rephrased as "two years (41-42) of daily mean sea ice fields for all three TS grids".

*Page 8, lines 28–30 : This is one of my major comment/concern. In this paragraph, you mention computing the deformation invariants from the daily mean sea ice drift speeds. This is the time scale set throughout your scaling analysis of daily deformation rates. You do not however mention how deformation rate components (du/dx, dv/dy, du/dy, dv/dx) are calculated, in particular at space scales larger than that of the cells of your Eulerian grids (with Arawaka-B staggering). Because you use Eulerian grids, I am guessing that your are following a coarse-graining method such as the one used in Marsan et al., 2004, but what are the details of the method? Do you, for instance, define square boxes and use a contour integral calculation to estimate each of the deformation rate components? Or just sum the components over each box? Most importantly, in estimating deformation rates at a given space scale, do you effectively sum (i.e., average) the deformation rate components and then calculate the corresponding invariants at that scale or do you sum (i.e, average) the deformation invariants themselves over that space scale? Also, why do you choose the region outlined in Figure 7 for your scaling and PDF analyses especially? How do you deal with the presence of coasts? Do you to eliminate data within a margin of the coasts? How do you deal* *with coarse graining boxes that might contain land regions? All of these details will most probably affect your scaling results and should be mentionned.*

**Reply**: the authors would like to clarify that the computation of scaled deformation rates are strictly following the coarse-graining algorithm of line integration for the specific scale (for our case a square region of the grid), as carried out in Marsan et al. (2014) and Rampal et al. (2019) (Sec. 3 of the reference). In specific, a region of a certain area (in our case, a number of adjacent cells that form a square), we compute its scale (L) as well as the deformation rates by computing line integration around its outer walls. The values of u_x, u_y, v_x and v_y are computed and then used to compute the deformation rates. We have added an appendix to specify the computations we have carried out in more detail.
The region we chose (as shown in Fig. 7) covers the majority of the Arctic basin, and due to its square shape, it facilitates the computation of aforementioned scaled deformation rates.
The authors agree with the referee that the treatments on the outer rim of the sea ice cover (including coastal regions) affects the analysis results. For our study, in the case of adjacency to coast, since we use Arakawa-B grids in CICE, we omit any T-points that have any single vertex on land.
In the revised version of the paper, we carry out the analysis without any points close to land. We confirm that there is slight change, but no qualitative difference in the new results.

*Section 3.2, pages 8-9 : I my point of view, readability would be improved if the second and third paragraphs were included after the first sentence of paragraph one of section 3.2. Then, after paragraph 6, you a paragraph or sub-section describing your method for the estimation of deformation rates at different space scales, and of the scaling exponents, is necessary.*

**Reply**: according to the suggestion of the referee, revisions are made to re-arrange the contents of these paragraphs. First, the characteristic of the forcing data and the choosing of the representative days are covered. Second, a general description of the modeled deformation of the two days. Third, the analysis of the PDF and scaling properties, including the methodology, consistency checks, scaling analysis results.

*Page 11, line 22 : "There is good agreement". I think it would be more accurate to say that the results are consistent accross spatial resolution, since the comparison here is not done on the basis of observational data.*

**Reply**: we revise the sentence as "The simulation results are consistent across the three grid resolutions …"

*Page 11, line 23 : "large shearing belts accross the basin". There are indeed large shearing belts and diffuse regions of shearing rates seen at all model resolutions. Are these diffuse shearing belts physical? How do they compare, for instance, to shearing rates fields inferred from RadarSAT data? To what process, physical or numerical, do you think they are related?*

**Reply**: the authors agree that the comparison and validation with observational dataset (such as SAR-based deformation) is important. But because we use a NYF dataset from CORE2 for the experiments, there is no direct correspondence of the modeled sea ice field to any observations. In this paper we mainly focus on comparing the simulation of various

resolutions with certain consistency among them, but we do acknowledge this a limitation of our current work. We are looking forward to work with IAF dataset that improve comparability with observations such as RGPS.
In our opinion, very large deformation structure (such as shearing belt) is an aggregate response of the sea ice cover to large-scale forcings. Especially, there is very large variability of the (sea ice) transpolar drift on the daily scale (i.e., within synoptic scale), regarding both direction and strength. There is a wide spatial scale involved surrounding the either side of the transpolar drift. Another possible mechanism is that low-pressure systems entering the Arctic, causing large-scale deformation events.

*Page 11, line 25 : "There is a clear".*

**Reply**: corrected.

*Page 11, line 26 : Please change "more well-defined" by "better defined".*

**Reply**: revised.

*Page 11, lines 31-33 : The last sentence of this paragraph is not clear. Please define clearly what you mean by "effective" resolution of the model. I guess it corresponds to the width of the simulated LKFs?*

**Reply**: the authors would like to clarify that the model's native resolution serves as the basis of the simulation of certain phenomena (such as waves in geofluid dynamics or sea ice kinematic features), but these phenomena are not realistic on the spatial scales of the native resolution. Rather, the "effective resolution" of the model, which is usually coarser than the native resolution, is the spatial scale on which the model could realistically produce these realistic phenomena. Here we do not focus on the widths of the LKFs, but rather the shape of the modeled LKFs do not agree well with observations, in which the both ends of the (relatively) larger LKFs should feature even smaller LKFs. On the contrary, the ends of the many modeled LKFs end in a larger region with a spread-out, smaller deformation rates, with no clear structure.

*Page 11, line 34 : "the distribution of total deformation rates follow power-law distributions". What distribution? Please be precise here, e.g., "the statistical (or probability density) function of total deformation rates follow a power law".*

**Reply**: revised as "… the probability density function of total deformation rates follows a power law distribution"

*Page 12, line 1 : I find the accronym C-CFD to be confusing here. You are calculating the cumulative probability density function of both daily and 3-days mean deformation rates. This term and the accronym cumulative PDF is used in most published scaling analyses within the sea ice community. I suggest for clarity that you use similar terms.*

**Reply**: the authors would like to clarify that we use complementary cumulative distribution function (or C-CDF) for the cumulative PDF (which is more widely used by the sea ice community, as mentioned by the referee). In response to the comment, we replace the use of C-CDF with Cumulative PDF or Cumulative Probability as revisions.

*Page 12, line 3 : "For both daily and 3-days cumulative distributions, we attain multifractality accross the three resolutions". I am confused here: how do you conclude that deformation rates are multifractal from the cumulative distributions in Figure 9? This information is rather given by a scaling analysis based on different moments of the distribution of deformation rates and the estimation of the convexity of the quadratic function describing the dependance of the scaling exponents on the moment. Please clarify or remove.*

**Reply**: the authors remove this statement of multi-fractality, since this is actually the result drawn from the scaling analysis later in this sub-section.

*Page 12, lines 7-21 : This paragraph is very confusing and I do not understand your method here. First you say that you carry out the spatial scaling of one grid onto another? How do you do that? Do you mean that you interpolate deformation rates from one grid to another? Line 7 : you mention that the slopes become steeper for the higher resolution grids for one given day but not the other. I suspect you mean the slope of the "CFDs/C-CDFs" in log-log space? How do you compute these slopes from figure 9? Can you please show these slopes on the figure so that one can evaluate at least qualitatively the goodness of fit? Lines 9-10 : "the slopes of C-CFDs from scaled rates". Do you mean interpolated doformation rates? Also, putting all of the curves on each panel of figure 9 makes it very difficult to read the figures. I would suggest separating the "non-scaled" or non-interpolated and interpolated results on different figures, or use different levels of opacity for the non-interpolated and interpolated results. Lines 13-14 : what is a realistic shape for the distribution? On what data do you base your evalution of a "realistic shape"? Also, a realistic shape for a "power-law distribution" is by definition a power law! Hence I suggest you write simply "a realistic shape of the distribution of deformation rates". Also see my previous comment about defining the "effective" resolution of the model. Line 16 : "we attain the same slope" Lines 18-19 : "the CFD of sea ice deformation rates", not kinematics. Also, please explain how you evalute this effective resolution, which is 6-7 times higher than that of the TS015 grid and what are the different days that you are analyzing.*

**Reply**: the authors apologize for the lack of clarity of this paragraph. The central role of the analysis is to compute and compare the scaled C-CDFs (or cumulative probability) from different grids. For example, we can scale the model output from TS005 to the grid resolution of TS015, and directly compare the C-CDF with that of TS015. Another example is that we scale the model output from TS005 to the resolution of TS045, and scale the model output of TS015 to the resolution of TS045. Then, we can compare the tail slopes of the Cumulative Probability. Suppose that we want to evaluate the effective resolution of TS015, by using the results from TS005 as a reference, we can find the spatial scale at which the slopes of scaled C-CDF from TS015 matches that of TS015. This spatial scale is then viewed as the effective resolution of the model output of TS015.
This analysis inherently relies on high-res. (TS005) model outputs as references. Also, we compute the slope as the slope of the linear least-square fitting between 0.05 and 0.25 for the

cumulative probability (y-axis). We have re-written the whole paragraph to increase clarity. Besides, Fig. 9 is also revised to include necessary information of statistical fittings.

*Page 12, lines 22-26 : Why do you think the (absolute) slopes you are estimating are smaller than that of Marsan et al. 2004 at a similar time scale? It would be relevant to offer possible explanations here.*

**Reply**: the authors would like to clarify that the absolute values of slopes we have in the analysis (-1.6 to -2.7) are indeed smaller than that of Marsan et al. (2004), which is -2.5 at the spatial scale of 13~20km. This is only to cite these values, since there is inherently no comparability among them (different date, different time duration, models not forced with realistic atmospheric forcings). We conjecture that this value of slope is time-variant and changes with forcing and ice conditions, but this could be investigated in the future.

*Page 12, line 26 : "to evaluate the structure function".*

**Reply**: revised (on line 28).

*Page 12, line 31 : "At q = 3, the structure function is in the range...". Do you mean beta instead of the structure function?*

**Reply**: corrected to be beta(q), according to the referee's suggestion.

*Page 12, last paragraph : I do not think it is relevant to cite the differences in the values of beta(q) or in the shape of the structure functions between the two analyzed days if you do not try to explain these differences physically.*

**Reply**: in the revised version the authors extend the scaling analysis of structure function to the potential contributing factors including the atmospheric forcings.

*Page 12, line 35 : "the average deformation rate". It would be more specific to refer to the mean deformation rate or to the moment of order 1.*

**Reply**: revised to "the mean deformation rate".

*Figure 10 : On the scaling figures (left panels) please indicate the moment order corresponding to each set of curves and insert a legend for the different colors/model resolutions. Also, you label the y-axis with epsilon for the total deformation rate, whereas in equations (1) to (3) you use dot(varepsilon) (indeed not available in MATLAB) for this variable and the other deformation invariants. Please use consistant symbols accross the text and figures. On the x-axis of the same figure, you use the label "space scaling", which would rather be appropriate as a title for these figures. I believe you mean "space scale". Your structure function is estimated using the moment of order 0.5, but it is not shown in the scaling analyses (left panels), why? Your structure function results could also be appreciated*

*more objectively if you included error bars for beta for each of the moments (see e.g., Rampal et al, 2019 for the definition of the error bars on beta(q)).*

**Reply**: the authors apologize for the missing of legend for different (grid) resolutions. Actually the starting points of different resolutions differ, since only TS005 (purple) reaches down to the spatial scale of 2km, and TS015 (red) reaches down to 7km. For the sake of clarity, we add a legend to these panels and corresponding texts in the figure caption. Symbols for deformation rates are also revised to be consistent across the article, as suggested by the referee.
"Space scaling" are replaced with "Spatial scale" in the figures. We have also included the moment-order of 0.5 in the scaling analyses. Besides, error bars are added for the panels for structure functions, by using formulations in Rampal et al. (2019).

*Most importantly, for the December case in particular it is apparent from the scaling figures (left panels) that the slope (beta) of the moments of order 2 and 3 is calculated by leaving out at least the two last points of the scaling analysis, corresponding to the largest space scales. Why is that and how considering/rejecting these points affects your results? If some data points are left out or attributed less weigth in the analyses, this should be definitely be clearly mentionned and argued for in the text.*

**Reply**: the authors thank the referee for the careful examination of the figures. Indeed at very large spatial scales, we are potentially hit with the problem of lacking samples. Actually across all the spatial scales, the effective sample counts change (or decrease) dramatically. The confidence level on the mean value at these largest scales are much wider, as a result. We further examine the results in the revised version of the manuscript with the exclusion of the scales larger than 200km, which corresponds to the last points mentioned by the referee.

*Page 13, line 4 : Please specify that your result support multifractality of the simulated sea ice deformation in space (i.e, not in time), hence not "multifractality of sea ice kinematics".*

**Reply**: revised to be more precise by only mentioning spatial scaling.

*Page 13, line 5 : How does the inclusion of the deformation rates at the two larger space scales for the moments 2 and 3 change the value of the estimated curvature? (see my previous comment on figure 9).*

**Reply**: We further examine the results in the revised version of the manuscript with the exclusion of the scales larger than 200km, which corresponds to the last points mentioned by the referee (also replied above).

*Page 13, line 6-8 : This sentence is a generic comment and does not offer a satisfactory explaination for the difference in results between the two time period analyzed. Either offer some physical hypotheses or refrain from comparing the two results.*

**Reply**: regarding to this comment, we extend the analysis to daily deformation fields during the winter and carry out attribution study by relating the scaling to circulation pattern and forcing data.

*Page 13, line 8-9 : If there is a slight drop between the values of beta or the curvature of the structure functions between the daily and 3-days deformation rates and this difference is not evident for the Feb. 6 case, my opinion is that this is no sufficient evidence that the model can reproduce temporal scaling. Such assumption should rather be based on a proper temporal scaling analysis that spans several orders of time scales, not a comparision between 1 and 3-days fields. This comment in my point of view should be removed because not supported from your results (and mention to it should be removed from the abstract as well, which should only state your strong results).*

**Reply**: the authors agree with the referee that the method (based on Eulerian means) and the ensuing analysis do not strictly correspond to temporal scaling analysis. We have revised it to include the results above, but removed related statements on temporal scaling.

*Page 13, line 12 : "existing studies with observational datasets and modeling results". Please put some references here.*

**Reply**: references are added, as suggested by the referee, including Marsan et al. (2004) and Rampal et al. (2019).

*Page 13, line 14-15 : Why is there a comparison here? This does not make sense. Do you mean "more convex on Feb. 6 than Dec. 20"? Also, why would this support less dominant large-scale features on Feb. 6? Please clarify.*

**Reply**: the authors have revised the manuscript to remove this statement. Attribution to the various circulation pattern and forcing data are made in relevant part of the paper instead.

*Page 13, line 15 : What is a ''more effective temporal scaling"? How does the results on figure 9 and 10 support temporal scaling?*

**Reply**: (according to previous comment and reply related to temporal scaling) during revision we remove statements involving temporal scaling.

*Page 13, lines 16-24 : I do not understand the link between these sentences and the previous sentences of this paragraph. What point are you trying to make? Please explain. Also, I think it would be more accurate not to refer to Lindsay et al., 2003 as current RGPS observations. RGPS is currently not running. Maybe just drop the reference.*

**Reply**: as noted by the referee, there is missing link in the logic linking the analysis of typical days to atmospheric forcings. We make the following revisions that potentially improve the inherent logic in the argument. We extend the analysis to winter time daily deformation fields, and carry out attribution study of the deformation statistics (scaling, PDF, etc.) to various factors including circulation and forcings.

*Page 13, line 26 : "we evaluate the sensitivity? of the modeled kinematics".*

**Reply**: revised as "… we evaluate the sensitivity of the modeled sea ice kinematics to the EVP subcycling …"

*Page 13, line 27 : "the probability density function (PDF)".*

**Reply**: corrected.

*Page 13, line 28 : and figure 11 : I suggest adding the estimated slope of the tail of each PDF on the graphs of figure 11 to illustrate how you estimate it from your results. It would also help putting a Gaussian distribution on each graph to visually identify the fat tails of the PDFs.*

**Reply**: as suggested by the referee, we add the estimation of slopes from the fittings, the range (on the y-axis) that is used to estimate the slopes, as well as the theoretical slope on Fig. 11.

*Page 13, line 28 : "for the total deformation rate".*

**Reply**: corrected.

*Page 13, Section 3.3, 1st paragraph : To support your claim that insufficient convergence of the model solution (i.e., nb of subcycles) is responsible for the absence of convergence between the PDFs of the simulated distribution rates at high resolution, I think you could also mention that the tail of the log-log PDF at the higher resolution and lowest number of sub-iteration does not seem linear as in the other cases.*

**Reply**: according to the referee's comment, we add another 2 sentences in the first paragraph of Sec. 3.3 (specifically, on line 1 of page 14), as follows "Besides, the PDFs of high-resolution runs (TS015 and TS005) show better tail structure, and furthermore, the slopes are also better characterized (i.e., closer linear fittings at -3) with larger values of NDTE. For TS045, the tail of the PDF suffers from the lack of samples for large deformation events."

*Page 14, line 6 : I think you mean figure 12, not 7.*

**Reply**: corrected.

*Page 14, line 8 : I think you mean figure 11, not 12.*

**Reply**: corrected

*Page 14, line 8 : What is the "physical" deformation rate? Please explain more clearly.*

**Reply**: the authors would like to clarify that by "physical deformation rate" we are referring to the inherent deformation when the EVP convergence is attained. Actually for regions outside LKFs, the deformation rate drops (without the noise), and the structure of LKFs becomes more defined. Therefore this sentence is less accurate, and we revise it as follows "With larger values of NDTE, the noise level decreases and the deformation rate around the linear kinematic features becomes smaller. As a result, a convergent PDF and linear feature maps are attained."

*Page 14, lines 10-12 : Instead of convergence of the kinematics, it is the convergence of the model solution, or simulated kinematics. Also, instead of "deterioration of simulation speed", I would write "increase in simulation time or cost" for more clarity.*

**Reply**: revised as indicated by the referee.

*Page 15, line 1 : "in the Canadian Arctic Archipelago". Line 3, "the CAA" again. Same mistake in other places on page 18.*

**Reply**: adding missing word of "the" for this case and all other cases.

*Page 15, line 2 : "an ice arch"*

**Reply**: corrected.

*Page 15, lines 8-10 : It would be helpful for the reader if you could further explain how you can separate these contributions in your model, by showing the term of the the dynamics/thermodynamics equation associated with each of them.*

**Reply**: according to the suggestion from the referee, this paragraph is extended to include a formal description of the different contributing terms to sea ice thickness, as well as the details of how to compute in the model (we adopted CICE).

*Page 18, line 2 : "due to the fact that the thermodynamic growth".*

**Reply**: revised according to the referee's suggestion

*Figure 13 : Please increase the fonts of the figure titles and colorbars.*

**Reply**: this figure is modified to improve readability.

*Page 22, line 1 : Please rephrase that sentence, which is not clear at all, both in the meaning and construction.*

**Reply**: this sentence is revised as: "In this paper we carried out sea ice simulations with a multi-resolution framework with Community Earth System Model."

*Page 22, line 2 : Change "grid stepping" for "grid resolution".*

**Reply**: revised according to the referee's suggestion.

*Page 22, lines 6-8 : "Multi-fractal sea ice deformation is accurately modeled by all three resolutions": please see my comment above on the inclusion or not of the all the points in your scaling analysis for the case of Dec 20. "with good agreement with observational works in terms of scaling properties" : have you try to compare the slopes of the scaling analyses (beta) for the three moments and the curvature of the structure functions with observational analyses at equivalent spatial resolution, e.g., based on RGPS data? If not, this comment should be revised.*

**Reply**: the authors revise this sentence according to the referee's suggestion, as follows "As shown in the spatial scaling analysis on the representative days, multi-fractal sea ice deformation is accurately modeled by all three resolutions."

*Page 22, line 12 : "multi-scale modeling studies". Please consider my previous comment on the meaning of "multi-scale modeling".*

**Reply**: we correct this case, along with all other cases, of "multi-scale modeling" to the more precise statement of "multi-resolution simulations"

*Page 22, line 19-21 : This sentence is incomprehensible, what is the "initial study with temporal scaling analysis with 3-day mean drift fields"? I did not see these results. If you are referring to the comparison of the daily mean and 3-days mean results, see my previous comment about how a much larger range of timescales would be necessary to conduct a meaningful temporal analysis.*

**Reply**: the authors agree with the referee's comment on temporal analysis. We remove the statements of referring the analysis of 3-day mean drift as temporal scaling.

*Page 22, line 21 : Repetition of "in our study".*

**Reply**: removed the second instance of "in our study"

*Page 22, lines 23-27 : Scaling analyses of modeled deformation fields and their comparison with equivalent analyses of observed deformation fields date from around 2010. Such* *analyses and model-observation comparisons have been made by only a few sea ice research groups and besides, techniques for comparing accurately Lagrangian/Eulerian model outputs to observational deformation data, especially in the context of time scaling analyses, are complex and have been recently developped and applied. Hence I would not qualify scaling analysis as a "traditional" tool for evaluating sea ice kinematics. For further validating sea ice deformation properties simulated with your multi-resolution framework, I also suggest a comparison of simulations to observations of sea ice deformation.*

**Reply**: the authors agree that the scaling analysis involving modeled sea ice kinematics, including validation with observed high-resolution kinematics is a recent development in the community. Therefore we remove the term "traditional" from our statements. We also look forward to carrying out historical simulations with the multi-resolution grid system and coupling with a fully dynamic ocean component. We plan to start this work by using inter-annual forcing (IAF) dataset and comparing with historical observational dataset.

*Page 22, lines 31 to 33 : It is clearly stated in the paper by Rampal et al., 2019 that the MEB rheology of Dansereau et al., 2016 is used, not the EB rheology of Girard et al., 2011. Please read the paper and correct your sentence. Also, replace "which are shown" by "which is shown" and for a demonstration of the MEB model capability to localize deformation at the nominal grid cell scale, whatever the grid resolution, which explains the fact that neXtSIM does not encounter "effective" resolution issues and does not require using a sub-LFK spatial resolution to simulate adequately these features, therfore reproducing the scaling properties accross model resolutions, see Dansereau et al., 2016.*

**Reply**: the authors apologize for the imprecise statement of the rheological model in neXtSIM. Revisions have been made for both corrections to Maxwell Elasto-Brittle (MEB) rheology in neXtSIM and the addition of reference (Dansereau et al., 2016). Other errors including grammatical ones are also corrected.

*Page 22, line 6 : It is hard from the figures shown here only to witness the asymptotic convergence of the simulated modeled kinematics. Please remove that sentence or include a figure that shows this clearly.*

**Reply**: as suggested by the referee, we revise this sentence to be more precise: "Based on a traditional implementation of EVP in our model, we have witnessed asymptotic converging behavior of sea ice kinematics fields with increased EVP subcycle count."

*Page 23, line 6 : "we have witnessed that".*

**Reply**: corrected.

*Page 23, line 15 : What is your choice of ice strength parameterization scheme? See my previous comment about the importance of including at least a reference to the dynamic equations of the model and a table listing the EVP rheology parameter values.*

**Reply**: the ice strength parameterization scheme is based on Rothrock (1975) with details of implementation in Lipscomb et al., (2007). This scheme is used by CESM in its scientifically validated experiments. We have now included a new appendix to include a complete list of the specific parameterization schemes and parameters that are used in the experiments.

*Page 23, line 29 : "Multi-scale simulations". I belive you mean that the comparison of simulations across spacial resolutions is becoming common in the climate modeling community.*

**Reply**: revised as "Simulation with multiple spatial resolutions".

**References:**


Dansereau, V., Weiss, J., Saramito, P., and Lattes, P. (2016). A Maxwell elasto-brittle rheology for sea ice modelling, The Cryosphere, 10, 1339–1359, doi:10.5194/tc-10-1339-2016

Large, W., and Yeager, S. (2004). Diurnal to decadal global forcing for ocean and sea-ice models: the data sets and flux climatologies. NCAR Technical Note: NCAR/TN460+STR. CGD Division of the National Center for Atmospheric Research.

Lipscomb, W.H., E. C. Hunke, W. Maslowski, and J. Jakacki (2007). Improving ridging schemes for high-resolution sea ice models. J. Geophys. Res.–Oceans, 112:C03S91, doi:10.1029/2005JC003355

Marsan, D., Stern, H., Lindsay, R., and Weiss, J. (2004). Scale Dependence and Localization of the Deformation of Arctic Sea Ice, Phys. Rev. Lett., 93, 178 501, doi:10.1103/PhysRevLett.93.178501.

Rampal, P., Dansereau, V., Olason, E., Bouillon, S., Williams, T., Korosov, A., and Samaké, A. (2019). On the multi-fractal scaling properties of sea ice deformation, The Cryosphere, 13, 2457–2474, doi:10.5194/tc-13-2457-2019.

Rampal, P., J. Weiss, D. Marsan, R. Lindsay, and H. Stern (2008), Scaling properties of sea ice deformation from buoy dispersion analysis, J. Geophys. Res., 113, C03002, doi:10.1029/2007JC004143.

Rothrock, D.A. (1975). The energetics of the plastic deformation of pack ice by ridging. J. Geophys. Res., 80:4514–4519

Stewart, K.D., W.M. Kim, S. Urakawa, A.McC. Hogg, S. Yeager, H. Tsujino, H. Nakano, A.E. Kiss, and G. Danabasoglu (2020). JRA55-do-based repeat year forcing datasets for driving ocean–sea-ice models, Ocean Modelling, 147, 111557

Weiss, J. and Dansereau, V. (2017). Linking scales in sea ice mechanics. Phil.Trans. R.Soc.A 375: 20150352. http://dx.doi.org/10.1098/rsta.2015.0352

# Comparison of Sea Ice Kinematics at Different Resolutions Modeled with a Grid Hierarchy in Community Earth System Model (version 1.2.1)

Shiming Xu[1,2], Jialiang Ma[1], Lu Zhou[1], Yan Zhang[1], Jiping Liu[3], and Bin Wang[1,3]

[1]Ministry of Education Key Laboratory for Earth System Modeling, Department of Earth System Science (DESS), Tsinghua University, Beijing, China

[2]University Corporation for Polar Research (UCPR), Beijing, China

[3]State Key Laboratory of Numerical Modeling for Atmospheric Sciences and Geophysical Fluid Dynamics (LASG), Institute of Atmospheric Physics, Chinese Academy of Sciences, Beijing, China

*Correspondence to:* Shiming Xu (xusm@tsinghua.edu.cn)

**Abstract.** High-resolution sea ice modeling is becoming widely available for both operational forecasts and climate studies. In traditional Eulerian grid based models, sea ice kinematics is the most prominent feature of high-resolution simulations, and with rheology models such as Viscous Plastic (VP) and Maxwell Elasto-Brittle (MEB), sea ice models are able to reproduce multi-fractal sea ice deformation and linear kinematic features that are witnessed in high-resolution observational datasets. In this study, we carry out modeling of sea ice with multiple grid resolutions by using Community Earth System Model (CESM) and a grid hierarchy (22 km, 7.3 km, and 2.4 km grid stepping in the Arctic). By using atmospherically forced experiments, we simulate consistent sea ice climatology across the 3 resolutions. Furthermore, the model reproduces reasonable sea ice kinematics, including multifractal spatial scaling of sea ice deformation that partially depends on atmospheric circulation pattern and forcings. By using high-resolution runs as references, we evaluate the model's effective resolution with respect to the statistics of sea ice kinematics. In specific, we find the spatial scale at which the PDF of the scaled sea ice deformation rate of low-resolution runs match that of high-resolution runs. This critical scale is treated as the effective resolution of the coarse resolution grid, which is estimated to be about 6 to 7 times of the grid's native resolution. Besides, we show that in our model, the convergence of the Elastic-Viscous-Plastic (EVP) rheology scheme plays an important role in reproducing reasonable kinematics statistics, and more strikingly, simulates systematically thinner sea ice than the standard, non-convergent experiments in landfast ice regions of Canadian Arctic Archipelago. Given the wide adoption of EVP and subcycling settings in current models, it highlights the importance of EVP convergence especially for climate studies and projections. The new grids and the model integration in CESM are openly provided for public use.

## 1 Introduction

Sea ice is the interface between the polar atmosphere and ocean, and therefore an important modulating factor of the polar air-sea interactions. The momentum input into the sea ice from the atmosphere and the ocean causes sea ice drift, as well as failures and deformations at a wide range of temporal and spatial scales. As revealed by high-resolution, kilometer-scale sea ice drift and deformation estimates with Synthetic Aperture Radars, the deformation of the sea ice is shown to be multi-fractal, with scale-invariance properties (Marsan et al., 2004; Rampal et al., 2008; Weiss and Dansereau, 2017) and quasi-linear kinematic features by visual inspections (Kwok et al., 2008), including local deformation regions of sea ice failures and shearing. Furthermore, the these kinematic features are accompanied by the formation of sea ice leads and pressure ridges, and tightly coupled to sea ice and polar thermodynamic processes. While sea ice leads are hot-spots of heat and moisture fluxes during winter, sea ice ridging is responsible for producing the thickest sea ice in both polar regions.

Sea ice rheology models provide mathematical description and numerical treatments for sea ice dynamic processes, and thus essential components of sea ice models. Viscous-Plastic [VP, (Hibler, 1979)] is the most widely used rheology model, and it describes the sea ice as a two dimensional continuum with nonlinear viscosity which undergoes plastic deformations over critical shearing and compressive stresses. In order to overcome the numerical stiffness of the VP model, modelers usually adopt explicit solvers for the derived models of VP such as Elastic-Viscous-Plastic [EVP, (Hunke and Dukowicz, 1997)] instead of the original VP, or implicit solvers (Hibler, 1979; Lemieux et al., 2010). With the introduction of an artificial term of elastic waves into the VP model, the numerical solving process is transformed into an explicit formulation. An iterative process, called subcycling, is carried out in EVP in order to numerically attenuate the elastic wave and attain the solution to VP model. Due to its good numerical stability and straightforward implementation, EVP is adopted by many climate models participating in Coupled Model Intercomparison Projects (CMIP6), as well the hindcast experiments for operational sea ice forecasts (Dupont et al., 2015).

With VP rheology, the capability of sea ice models to resolve fine-scale deformations is inherently bounded by the resolution of the models' grids. In order to reproduce the observed properties of the sea ice kinematics, grids of 0.1° resolution or finer in sea ice regions are usually required. State-of-the-art high-resolution studies reach 2 km or finer grid stepping in the Arctic (Hutter et al., 2018; Scholz et al., 2019). Although the continuum assumption of the sea ice cover in VP (or EVP) does not necessarily hold at these resolutions, VP models are shown to be capable in reproducing realistic sea ice kinematics (Hutter et al., 2018). Unstructured grid based models and Lagrangian models have unique capabilities in modeling sea ice. Regionally focused studies can be easily carried out with variable grid sizes, such as the Arctic simulation with FESOM (Wang et al., 2018; Koldunov et al., 2019). Purely Lagrangian models such as neXtSIM (Rampal et al., 2019) are potentially free of the resolution issues for resolving small deformation features. Specifically, neXtSIM utilizes Maxwell elasto-brittle rheology (Dansereau et al., 2016; Girard et al., 2011), which is shown to simulate reasonable sea ice kinematics and scaling properties even at moderate resolution settings (Rampal et al., 2019). Although the continuum assumption of the sea ice cover does not necessarily hold at these resolutions (Hutter and Losch, 2020), there exists efforts to improve certain aspects such as reproducing observed anisotropy in deformation fields as well repeating deformation features (Tsamados et al., 2013).

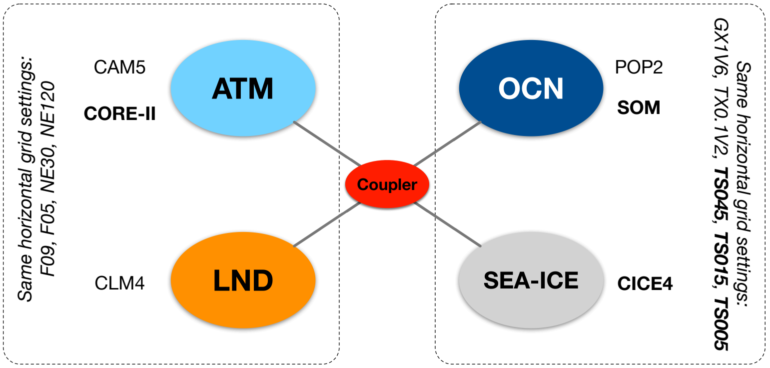


**Figure 1.** Ocean and sea ice grids and air-sea coupling in Community Earth System Model (CESM).

In this study, we carry out comparison of sea ice model simulations at different spatial resolutions with the coupled model of Community Earth System Model (CESM, version 1.2.1). CESM (http://www.cesm.ucar.edu) is developed at National Center for Atmospheric Research (NCAR) and adopted by various research groups in the world for climate studies. The component models of CESM include: Community Atmospheric Model (CAM), Parallel Ocean Program (POP, version 2), Community Ice CodE model (CICE, version 4) and Common Land Model (CLM). The coupling between these components is carried out with the flux coupler CPL. Components can be configured to the specific experiment needs, such as atmospherically forced ocean and (or) sea ice simulations. Figure 1 shows the the coupling schematics in CESM and the common configuration of high-resolution coupled runs. The horizontal model grids (and associated spatial resolutions) of CICE and POP are the same, and the two standard configurations in CESM are: nominal 1° (GX1V6, a dipolar grid) and 0.1° (TX0.1v2, a tripolar grid). Specifically, CICE, the sea ice component of CESM, includes comprehensive thermodynamic and dynamic processes of sea ice, including discretized ice thickness distribution, prognostic enthalpy, complex shortwave albedo and penetration schemes with snow and pond processes, EVP rheology, ridging parameterization, etc. CICE in CESM can be run in three major settings: (1) forced by with atmospheric reanalysis (NCEP CORE 2) with coupling to a slab ocean model (SOM), (2) ice-ocean coupled simulation under atmospheric forcings, and (3) fully atmosphere-ocean-ice coupled runs.

In our study, we design a grid hierarchy for the ocean and the sea ice model and incorporate them in CESM, including its component models of CICE and POP, as well as the coupling to the atmospheric forcings. The grid hierarchy includes three tripolar grids with the nominal resolution of 0.45°, 0.15° and 0.05°, covering the wide range of climate modeling and sub-mesoscale oriented studies. In Section 2 we introduce the grid generation method, and the integration of the grid hierarchy in CESM. Furthermore, atmospheric forcing based experiments are carried out with the new grids, and Section 3 includes the details of the experiments and the analysis of modeled sea ice climatology and kinematics. Especially, we carry out scaling analysis and cross-resolution comparisons of the sea ice kinematics, and study the convergence behavior of EVP. In Section 4 we summarize the article and provide discussion of related topics and future research directions including multi-scale modeling.

## 2 Grid Generation and Model Integration

### 2.1 TS grids – a tripolar grid hierarchy

We design a new tripolar grid generation method for global ocean-sea ice modeling. The generated grid is orthogonal and compatible with many existing ocean and sea ice models, including POP, CICE, and MOM. As shown in Figure 2, it consists of two patches, the southern patch (SP) and the northern patch (NP), divided by a certain latitudinal circle ($\phi$) in the northern hemisphere. For the SP, the grid lines are purely zonal or meridional. For the NP, there are two north poles for the grid, which are placed on the Eurasia and North America land masses. However, unlike many tripolar grids such as TX0.1V2 in CESM, this new grid features smooth grid scale transition on the boundary of SP and NP. In order to achieve this, a non-trivial grid generation process is carried out on the stereographic projection of NP. Specifically, a series of embedded ellipses are constructed based on resolution requirements, with: (1) the outermost ellipse as the projection of the latitudinal circle at $\phi$ (i.e., a circle), and (2) the innermost ellipse as the line linking the two grid poles. The foci of the outermost ellipse are both at the North Pole, and with the progression to inner ellipses, they gradually move towards the two grid poles, respectively. The ellipses form the "zonal" grid lines in NP. After the ellipses are constructed, the "meridional" grid lines in NP are constructed, starting from the southern boundary of NP, down to the innermost ellipse. During this process, it is ensured that: (1) the grid lines are constructed consecutively between adjacent ellipses, with starting points on the outer ellipse; and (2) they are linked with the meridional grid lines in SP to ensure overall continuity of the global grid. The details of the construction of ellipses and the smooth transition of meridional grid scales are further described in Appendix A. Furthermore, the meridional grid scales in both SP and NP are constructed to alleviate the grid aspect ratio, reducing meridional grid sizes in higher latitudes.

By using the grid generation method, we generate a series of tripolar grids: TS045, TS015 and TS005. These grids all have the the boundary between SP and NP ($\phi$ ) at $10°N$, and grid poles at: $(63°N, 104°W)$ and $(59.5°N, 76°E)$. Table 1 shows the detailed configuration of these grids. TS045 is the coarsest grid with the nominal resolution of 0.45°, and it targets at climate modeling and the typical resolution range for ocean component models in Coupled Model Intercomparison Projects (CMIP6). TS015 and TS005 are about 3 times (or nominal 0.15°) and 9 times (or nominal 0.05°) the resolution of TS045, respectively.

Figure 3 shows the horizontal grid scale ($s = \sqrt{(dx^2 + dy^2)/2}$) in polar regions for TS015 and TS005. The average grid scale in TS005 is 2.45 km in the Arctic oceanic regions (north of $65°N$), and the scales of TS015 and TS045 are 7.34 km and 22.01 km, respectively. From the ocean modeling perspective, we use the Rossby deformation radii ($R$) as the proxy for mesoscale (Chelton et al., 1998), and investigate the capabilities of each grid. In specific, the criterion in Hallberg (2013) is adopted: the mesoscale resolving is attained when $s$ is smaller than the half of the local value of $R$. Based on the annual mean WOA13 climatology of salinity and temperature (Locarnini et al., 2013; Zweng et al., 2013), we construct the global distribution of $R$. In Table 1 we note that TS015 is "almost eddying", because this grid attains mesoscale-resolving for 65% of the global ocean's area. As outlined in Figure 3, in polar regions, the ratio of $s$ to $R$ is all higher than 0.5 for TS015, indicating no mesoscale resolving capability for this grid for these regions. But for TS005, the mesoscale processes in polar regions with relatively deep bathymetry (e.g., within the Arctic Ocean) can be resolved.

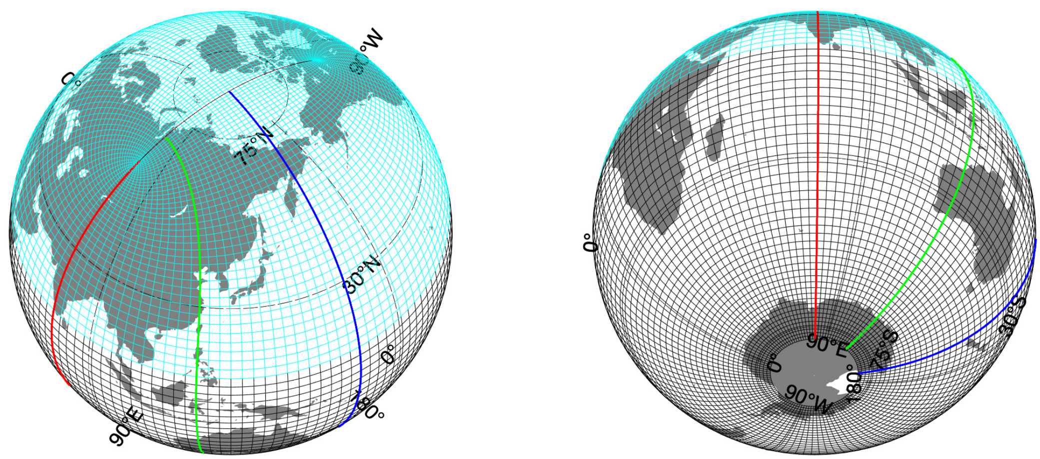


**Figure 2.** Global tripolar TS grid with northern patch (in cyan) and southern patch (in black). 0.05° grid (TS005) is shown (1 in every 60 grid points). On the boundary of the two patches, smooth grid size change is ensured in the meridional direction. Typical meridional grid lines are also shown in thick lines (red, green and blue).

**Table 1.** TS grid hierarchy

| Name | Nominal Resolution (°) | Dimension (i & j) | Zoom Level | Notes |
|---|---|---|---|---|
| TS045 | 0.45 | 800 × 560 | 1 | Long-term, climate simulation |
| TS015 | 0.15 | 2400 × 1680 | 3 | Eddy-resolving in 65% oceanic area ("almost eddying") |
| TS005 | 0.05 | 7200 × 5040 | 9 | Fine-scale, submesoscale ocean modeling |

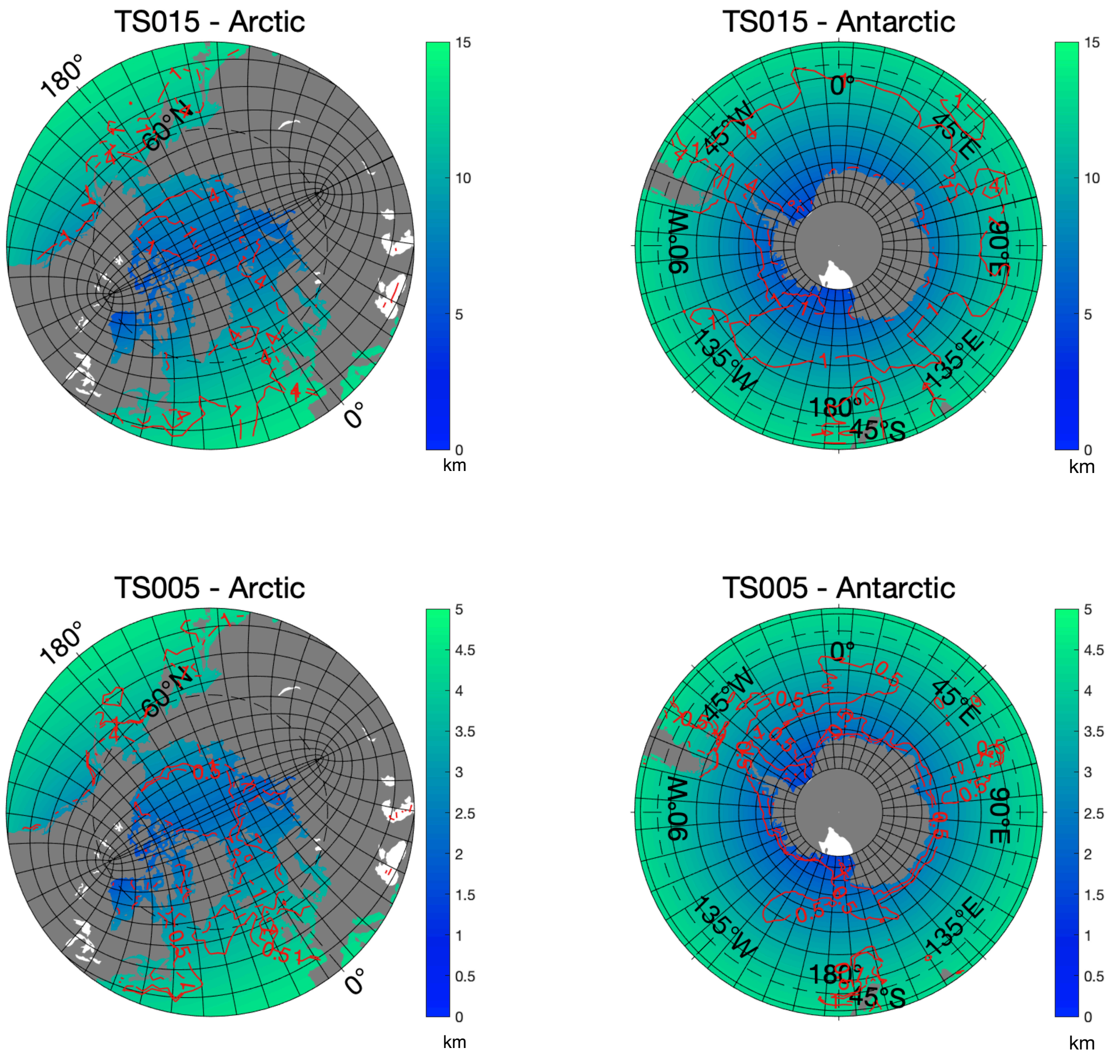


**Figure 3.** Horizontal grid scale of TS015 and TS005 in the polar regions. For grid lines, 1 in 60 (or 180) points are shown for TS015 (or TS005) grid. $\sqrt{(dx^2+dy^2)/2}$ is shown by filled contour (in kilometers), and regions of mesoscale-resolving capability ($s/R < 0.5$) outlined by red contour lines.

### 2.2 TS grid integration in CESM

The integration of the TS grids in CESM involves the following 3 steps. First, the generation of land-sea distribution and bathymetry, as well as the technical implementation of the grids in both POP and CICE. Model bathymetry is generated at the grid locations and 60 vertical layers, based on ETOPO1 dataset (ETO). The vertical coordinate consists of 10-meter equal-depth layers in the top 200 meters, with gradual increase of layer depth to 250 meters in the deep oceans (up to 5500 meters).

Second, we configure the model according to the grid resolution, including the choice of parameterization schemes and related parameters. Specifically, we adopt the full thermodynamic and dynamic model processes in CICE, mainly following the standard configurations of parameterization schemes in Hunke and Lipscomb (2008). The main processes relating to sea ice dynamics include: EVP rheology model (Hunke and Dukowicz, 1997), the ridging/rafting scheme and ice strength model (Lipscomb et al., 2007; Hibler, 1979), and transport-remapping based advection (Dukowicz and Baumgardner, 2000). Model configuration and parameters are aligned across the three grids, with details shown in Appendix B. The major difference among the grids is that we choose shorter thermodynamics and dynamics time steps for grids with higher resolution (Tab. 2). Furthermore, since sea ice kinematics is the focus of this study, different EVP subcycle numbers are chosen for each grid. While 120 subcycles per hour is adopted for some 1° resolution CMIP simulations (Jahn et al., 2012; Xu et al., 2013), we experiment with larger values of cycle counts (up to 960 subcycles per dynamic time step), as shown in Table 2.

In our study, CICE is coupled to the slab ocean model (SOM) in CESM, which provides a climatological seasonal cycle of ocean mixed layer depth and heat potential. The same configuration for SOM is used for experiments with TS045, TS015 and TS005. The reason why we use SOM instead of a fully dynamic-thermodynamic ocean model (such as POP) is three fold. First, in this study we focus on the simulation of sea ice kinematics and the inter-comparison across different resolution settings. Therefore, by using a single-column model for the ocean, we eliminate the factors that may compromise the comparability, including the inconsistency in modeled ocean processes across the resolution range, ocean and coupled turbulence, etc. Second, since atmospheric forcing is the major driver of sea ice drift and kinematics, we consider SOM eligible for the purpose of this study. Third, using SOM with CICE in CESM greatly alleviate the computational overhead for long-term simulations, especially for TS005 (0.05° grid). As is shown in the next section, with CICE coupled to SOM, we simulate comparable Arctic sea ice climatology and kinematic features (cracking events, etc.) among TS045, TS015 and TS005, and the computational cost and time-to-solution remains manageable. Potential compromises pertaining to the use of SOM are discussed further in Section 4.

Fourth, we force the sea ice component with TS grids with atmospheric forcings from CORE 2 dataset, which is also used in the Ocean Model Intercomparison Project (Griffies et al., 2016). Specifically, CORE 2 dataset contains a Normal-Year Forcing (NYF) with the climatological annual cycle based on NCEP atmospheric reanalysis, and it has a spatial resolution of about 2° (T62) with four-times daily wind stress fields. NYF dataset is mainly based on year 1995 of NCEP atmospheric reanalysis, with interpolation-based smoothing at the end of December with data from year 1994, and flux corrections to ensure overall energy balance. Following the common practice in CESM, for the coupling of atmospheric state variables (such as air temperature, humidity, etc.), a bilinear interpolator is used between T62 and each TS grid. For wind stress, the patch-recovery algorithm is

**Table 2.** Time stepping and EVP configurations.

| Grid | $\Delta_t$ for thermodynamics | $\Delta_t$ for dynamics | EVP subcycles per dynamics step |
|---|---|---|---|
| TS045 | 60 min | 30 min | 120 / **240** / 480 / 960 |
| TS015 | 20 min | | 120 / **240** / 480 / 960 |
| TS005 | 15 min | 7.5 min | 120 / **240** / 960 |

adopted to ensure good structure of wind fields on the ocean-sea ice grid. Patch-recovery is a high-order interpolation method based on local reconstruction of the forcing fields, and it ensures consistent wind stress forcing across the 3 grid resolutions in this study. For fluxes, a first-order conservative interpolator is utilized. All these interpolators (in total 6) are generated through CESM mapping toolkit and ESMF regridding toolkit (https://www.earthsystemcog.org/projects/esmf/).

All the model integration for TS grids in CESM, including grid files in the format of POP, and interpolation files, are openly available (details in *Code and data availability*).

## 3 Experiments and Analysis

### 3.1 Spin-up experiments and Arctic sea ice climatology

The spin-up simulations with the new grids are based on CESM D-type experiments, and configured specifically for each grid. CESM D-type experiments are based on CORE 2 NYF dataset and coupling to SOM, and it is usually used for the spin-up for the sea ice and ocean-sea ice coupled system. For CICE, the time stepping are based on 240 EVP subcycles (i.e., the number of timesteps for elastic wave damping, or NDTE) per dynamics time step for all three grids, following the settings in Table 2. The experiments are outlined in Figure 4.a. Specifically, the experiment with TS045 starts on Jan. 1st with no sea ice, and the model is gradually reaching an equilibrium state for both sea ice coverage and volume. After 25-year's experiment with TS045, the spun-up status is migrated onto TS015. Similarly, after another 5-year's experiment with TS015, the spun-up status is further migrated onto TS005. Specifically, we carry out the analysis of Arctic sea ice climatology based on experiments with the default value for NDTE (240) for TS045, TS015 and TS005. The experiments with other values for NDTE show little differences in overall sea ice coverage and volume, but does greatly impact the modeling of kinematics (details in Sec. 3.2).

As shown in Figure 4.b, for TS045, the Arctic sea ice extent (SIE) and volume (SIV) approach equilibrium after about 5 and 30 years, respectively. Besides, with migrated status from experiments with lower-resolution grids, the runs with TS015 and TS005 attain quasi-equilibrium status towards the end of the 37th model year. The annual cycles of the sea ice coverage, computed as the mean monthly SIE and SIV of the last 5-year's model output, agree well among the three grids (Fig. 4.b and Fig. 5.a). The differences in SIE and SIV are within 5%. The spatial distributions of sea ice are also consistent (Fig. 5.c through h). The model results are also in good agreement with observational climatology of seasonal cycle for sea ice extent (NSIDC sea ice index, year 1979 to 2002), with minor overestimation of the sea ice coverage during winter (Fig. 5.a). As shown in Figure 5.f through g, the overestimation in March is present in outer regions to the Arctic Ocean, including Okhotsk Sea, Labrador Sea, southern part of Greenland Sea (near Iceland), and the southern part of Barents Sea. During summer when the sea ice coverage is mainly present within the Arctic Basin, and all three grids reproduce reasonable sea ice coverage regarding observations (Fig. 5.c through e).

The modeled SIV peaks in April (Fig. 5.b), and the modeled seasonal cycle is consistent with existing sea ice thickness reconstructions of PIOMAS (Schweiger et al., 2011). The overall thickness pattern show thick ice (over $3m$) in the regions north of the Canadian Arctic Archipelago (CAA) and Greenland, as well as within CAA. Among the three grids, higher resolution grids simulates slightly higher sea ice volume by the end of winter (by only 4%), which is witnessed in central Arctic (Fig. 5.f through h). During summer and early months of the winter, all three grids simulate lower SIV as compared against PIOMAS (Fig. 5.b), with one particular region with underestimation of ice thickness in the Atlantic sector of the Arctic (Fig. 5.c through e). In general, we consider the model simulates reasonable Arctic sea ice climatology, especially during winter. Furthermore, with good consistency across the three resolutions, we carry out the analysis of sea ice kinematics with high-frequency outputs of these experiments.

One major obstacle of running high-resolution models is the huge amount of computational overhead and the long durations for climate simulations. In this study, we utilize an Intel processor-based cluster with 24 cores/node for all the experiments. For TS045 and TS015, more than 5 simulated year per day (SYPD) can be attained with less than 1000 cores for all the experiments. For TS005, the simulation speed is about 1 SYPD with 1920 cores and NDTE=240, which is reasonable given the high resolution of the grid. The utilization of larger computational facilities for TS015 and TS005 remains an important direction of future work.

### 3.2 Sea ice kinematics and scaling on representative days

In order to study the sea ice kinematics, we output two years (36-37) of daily mean sea ice fields for all three TS grids (Fig. 4.a). Spatial scaling analysis of these deformation rates are performed by using the methods in Marsan et al. (2004). The deformation rates in their invariant forms are defined in Equation 1 through Equation 3, including: shearing rate ($\dot{\varepsilon}_{shear}$), divergence rate ($\dot{\varepsilon}_{div}$) and total deformation rate ($\dot{\varepsilon}_{total}$). They are computed from the daily mean prognostic sea ice drift speeds ($u$'s and $v$'s) defined on Eulerian grid locations (with Arakawa-B staggering in CICE). Specifically, the line integral of a specified model region is computed to for the spatial derivatives and the associated spatial scale (Fig. C1). The deformation rates are then computed and binned according to the specific spatial scale, in order to derive statistics including the probability density of deformation rates at different scales. Appendix C includes a detailed routine for the Arakawa-B staggered grid of CICE.

$$\dot{\varepsilon}_{div} = \frac{\partial u}{\partial x} + \frac{\partial v}{\partial y} \tag{1}$$

$$\dot{\varepsilon}_{shear} = \sqrt{(\frac{\partial u}{\partial x} - \frac{\partial v}{\partial y})^2 + (\frac{\partial u}{\partial y} + \frac{\partial v}{\partial x})^2} \tag{2}$$

$$\dot{\varepsilon}_{total} = \sqrt{\dot{\varepsilon}_{div}^2 + \dot{\varepsilon}_{shear}^2} \tag{3}$$

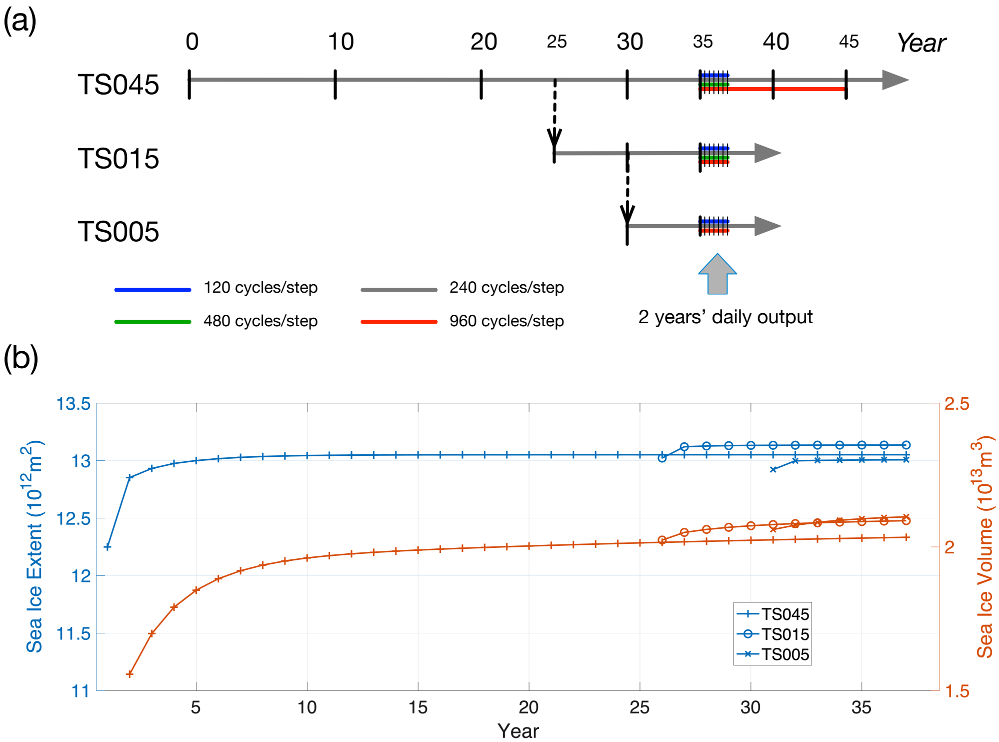


**Figure 4.** Spin-up experiments of sea ice simulations with TS grids (a) and spin-up of Arctic sea ice extent and volume (SIE and SIV, in panel b) up to year 37. These experiments are based on D-cases in CESM: the sea ice component CICE is forced with Normal Year Forcing of CORE and coupled to the Slab Ocean Model. For TS045, the model is initialized with an ice-free condition, and the numerical integration is carried out until equilibrium. For TS015, a snapshot of the spun-up conditions of TS045 at the end of year 25 is used to initialize the integration, and the experiment is carried out for 12 years, up to year 37. For TS005, a snapshot of the spun-up status of TS015 at the end of year 30 is used for model initialization, and the experiment is carried out for 7 years, up to year 37.

We have manually chosen two typical days that are representative of Arctic sea ice drift patterns: Dec. 20th and Feb. 6th (Fig. 6.a and b). A winter-time Arctic Oscillation (AO) index is constructed based on sea-level pressure (SLP) of 50-yr's NCEP reanalysis data, and applied to the NYF dataset. Specifically, AO is defined as the leading EOF mode for the weekly mean SLP in the northern hemisphere (20 $^\circ N$ and north) for the extended winter months (November to April) of years 1950 to 2000. The 50-year SLP sequence is detrended and the seasonal cycle is removed for the EOF computations. The leading mode explains 13.9 % of the total variance, with the normalized spatial pattern (unitless) and the principle component (time series) shown in Figure S1. The wintertime AO index of the NYF dataset is shown in Figure 6.c. The winter of the NYF forcing dataset corresponds to an overall neutral AO status, and the variability of wintertime weekly AO index (25 hPa as in Fig. 6.c) is also on par with the average intra-seasonal variability of the 50-year NCEP reanalysis data (22 hPa as in Fig. S1.b). As a reference, the summertime AO of the NYF dataset is mildly negative (Fig. S1.c).

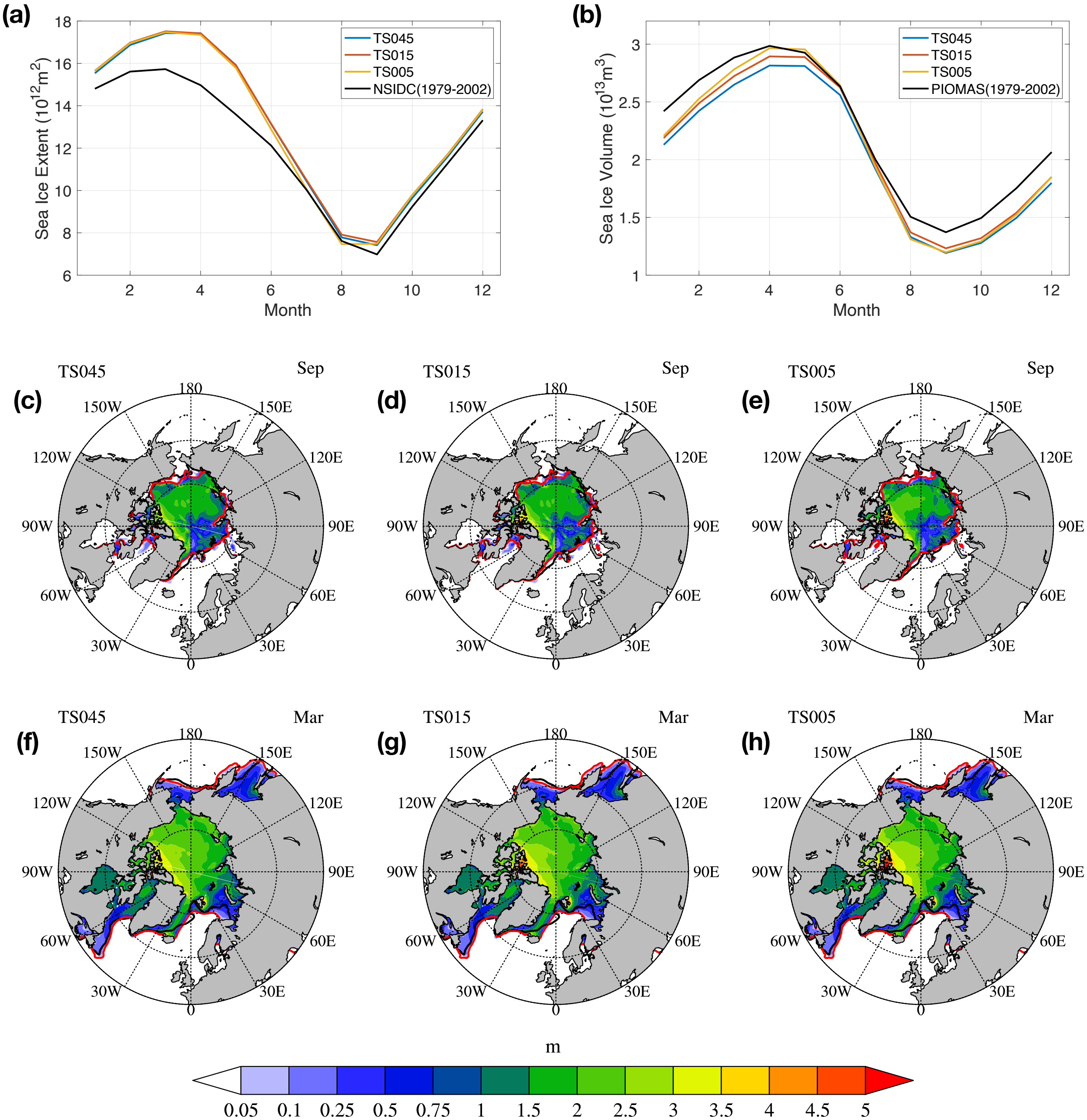


**Figure 5.** Climatological seasonal cycle of Arctic SIE (panel a) and SIV (panel b), computed as 5-year mean of year 33 to 37. September (or March) sea ice thickness fields for TS045, TS015 and TS005 are shown in panel c (or f), d (or g) and e (or h), respectively. Within each panel (c through h), the satellite-observed and modeled sea ice edge (sea ice concentration at 15%) are marked by black and red lines, respectively. The climatology SIE, as well as as March and September sea ice edge, are computed from the NSIDC Arctic sea ice dataset from passive microwave sensors (SSMI/SMMR), for the years between 1979 and 2002. The climatological annual cycle for SIV (in panel b) is computed from PIOMAS dataset for the same period (1979 to 2002).

The two representative days are: (1) Dec. 20th, on which date the high-pressure center resides in Beaufort Sea, and a negative AO index is witnessed, and (2) Feb. 6th, on which date the high-pressure center shifts towards the eastern hemisphere, the low-pressure system in the Atlantic sector extends further into the Arctic, and a slightly positive AO index is present. Furthermore, because asymptotic convergence of sea ice kinematic to increase in the EVP subcycle count is witnessed in existing studies (Lemieux et al., 2012; Koldunov et al., 2019), we limit the analysis of kinematics and scaling to the experiments with the largest EVP subcycles (NDTE=960) for each grid.

Figure 7 shows the deformation fields for Dec. 20th. On the Pacific side, there is divergence in the Beaufort Sea and Chuckchi Sea, and accompanying convergence in East Siberian Sea. Shearing rate of up to 10 $\%/d$ is also present in these regions, with a shearing arc extending from Beaufort Sea across the basin to Severnaya Zemlya and another one along the Siberian Shelf. In the Atlantic sector of the Arctic Ocean, there is extensive divergence to the north of Svalbard, and minor convergence to the north of Greenland. In the regions of thinner ice and marginal ice zones, large deformation rates are present.

The overall deformation pattern on Dec. 20th is consistent across TS045, TS015 and TS005. Comparing TS045 and TS015, we witness much finer structure of the deformation fields in all aforementioned regions. Specifically, both narrower shearing and divergence regions and higher rate of deformation rates are present in TS015. The differences of the kinematics between TS015 to TS005 are mainly present in fine structure of the deformation and shearing events. With TS005, the model simulates more and finer sea ice kinematic features, such as the network of shearing in Beaufort Sea and along the Siberian Shelf.

Figure 8 shows the deformation fields for Feb. 6th. On the Pacific side, the divergence (convergence) region is in Beaufort Sea (Chuckchi Sea). The divergence in Laptev Sea is paired with the convergence to the north of Queen Elizabeth islands (see Fig. 6.b for the sea ice drift). A shearing belt is present across the basin from the Canadian Arctic Archipelago to the north of Franz Josef Land. In the Atlantic sector, the convergence to the north of Barents Sea corresponds to the divergence in the north, including the north of Greenland and the north of Franz Josef Land. The simulation results are consistent across the three grid resolutions, including the major regions of divergence (or convergence) and those of shearing, except for very large shearing belts across the basin.

Similar to Dec. 20th, TS045, TS015 and TS005 simulates consistent deformation fields, including the location and strength of deformation events in the Arctic basin. There is a clear separation of the level of detail for the deformation systems across the resolution. The kinematic features which can be detected by visual inspections, are better defined in TS005. Especially the networks of deformations, such as those in the Davis Strait and to the north of Fram Strait and Greenland, contain over 20 major linear features in TS005. For comparison, the run with TS015 produces much fewer features, while that with TS045 only produces the major 1 or 2 deformation features. However, on both days, there is also evidence that, even at TS005, the model is limited for resolving fine-scale kinematic structures. Some large kinematic features, especially in the central Arctic, have ends that are not well defined, which is clearly not bounded by the grid sizes. This applies to both shearing and divergence. On the grid's native resolution, the simulated kinematic features contain both physical deformation and the deformation caused by numerics. As a consequence, the effective resolution of the model is usually coarser than the grid's native resolution, which we further evaluate using the statistics of sea ice deformation.

We examine the the probability density function of total deformation rates, which were previously investigated for RGPS data (Marsan et al., 2004). Specifically, the region outlined in Figure 7 is used for study, and we show the daily and 3-day cumulative probability distribution function (PDF) for total deformation rates in Figure 9. The 3-day deformation data is computed from the 3-day mean velocity fields for the period of Dec. 19th to Dec. 21th, and Feb. 5th to Feb. 7th, respectively. With higher resolution, the model consistently simulates more extreme deformation events, corresponding to a flatter cumulative PDF for the deformation rates.

Since the three grids have nearly exact grid stepping ratio of 1:3:9, we carry out: (1) the spatial coarsening of the model output of TS005 onto TS015 and TS045, and (2) that of TS015 onto TS045. The cumulative PDFs for each resolution, including modeled with the native resolution as well as scaled from higher resolutions, are shown in each panel in Figure 9 with the same symbol. At larger spatial scales (7.3 km and 22 km), the slopes of the PDFs become steeper for both TS005 and TS015 on Dec. 20th, but witness much smaller changes on Feb. 6th. The slopes of cumulative PDFs from scaled rates of TS005 are shallower than non-scaled rates of TS015, indicating that the effective resolution of the TS015 run is lower than its native resolution of 7.3 km. Similarly, at the spatial scale of TS045's native resolution (22 km), the slopes from TS005 and TS015 are shallower than that from TS045. This indicates that at the scale of 22 km, more extreme deformation events are present in the run with TS005 and TS015 than in TS045. Therefore, in terms of modeling realistic shape of the PDF of sea ice deformation rates, the model's effective resolution is coarser than the grid's native resolution.

By treating the PDF of the scaled results of TS005 as the "truth", we evaluate the effective resolution of grids of coarser resolutions. Specifically, for TS015, we define the effective resolution scale as the scale at which the PDF's tail slope of the scaled results from TS015 reaches that from TS005. We further scale down the model results of both TS005 and TS015 to attain the slopes at spatial scales coarser than 22 km (or 0.45°). We attain same slope of PDF tail for TS015 as TS005 at the scale of 42 km for Dec. 20th. For Feb. 6th, the scale with same PDF tail slope for TS015 and TS005 is 50 km. This result gives certain hint of the effective resolution of TS015 (with grid resolution of about 7.3 km). Regarding the CDF of sea ice kinematics, the effective resolution is variable among days with different kinematic features, and about 6 to 7 times the native resolution of TS015. Also, since we witness flatter cumulative PDF slopes in scaled datasets, we expect the "real" tails of cumulative PDFs at 2.4 km flatter than the modeling result from TS005, which have the slope of -1.0 for Dec. 20th, and -0.5 for Feb. 6th.

For cumulative PDF of 3-day mean sea ice deformation (lower panels of Fig. 9), we witness slight steepening of the PDF tails for both days than those of daily deformations. This is due to the temporal averaging on Eulerian grid points attenuates the large deformations, causing fewer large deformation events in the PDF. On Dec. 20th, the PDF tail slope is -2.7 at the scale of 22 km (from the scaled results of TS005). For reference, the analysis with RGPS data in Marsan et al. (2004) in which the PDF tail slope of -2.5 is found for 13-20 km scale (Fig. 3 of the reference). However, it is worth noting that a Lagrangian-tracking based method of our model output is needed for formally compare the results (Hutter et al., 2018), which we plan to carry out with historical simulations and the new grids.

We further carry out spatial scaling analysis for these two representative days (Fig. 10). Specifically, the moments ($q$) that are adopted to evaluate the structure function of scaling and the multi-fractality are: 0.5, 1, 2 and 3. The polynomial for the least-square fitting of the structure function is: $\beta(q) = a \cdot q^2 + b \cdot q$. At $q = 1$, the three resolutions show slight differences for $\beta$:

for both days, and higher resolution starts with a slightly higher mean deformation rate (0.12 and 0.09 for TS005 on Dec. 20th and Feb. 6th, respectively). At $q = 3$, $\beta(q)$ is in the range of 0.7 (TS045) and 1.1 (TS005) on Dec. 20th, and between 1.1 and 1.6 on Feb. 6th for all three grids. At higher orders (e.g., $q = 2$ or $q = 3$), high-resolution produces faster decay of deformation rates with spatial scales (larger $\beta$) on Dec. 20th, but on Feb. 6th, the differences of decay rates are less pronounced between the grids. For 3-day mean deformation fields, the mean deformation rate is generally lower than at 1-day scale, and the difference on higher orders is also evident between Dec. 20th and Feb. 6th. Furthermore, no negative value of $\beta$ is detected at $q = 0.5$, which is consistent with Marsan et al. (2004) (Fig. 4 of the reference).

The structure function of $\beta(q)$ shows a strong curvature, and this applies to all the grids on both days, indicating multi-fractal spatial scaling of the sea ice kinematics. On Dec. 20th, the curvature level ($a$) is higher in TS005 (0.12) than TS015 (0.09) and TS045 (0.05). On Feb. 6th, the curvature levels are more consistent across the 3 resolutions (0.16 for TS045, 0.17 for TS015, and 0.23 for TS005). The differences in the statistics of scaling is the result of both the localization of the specific deformation field, as well as the resolution of the grid. Besides, there is slight drop in $\beta$ when evaluating 3-day deformation fields with 1-day counterparts. This is consistent with existing works in which formal temporal scaling is carried out, which indicate decrease in $\beta$ with longer time scales. However, our analysis here is based on model outputs on Eulerian grids, and a formal temporal scaling based on Lagrangian diagnostics of our model data is planned in future study.

Based on the numerical experiments with NYF dataset, we show that the sea ice kinematics, including the deformation and its spatial scaling, are distinctive on different days. On the two representative days, the deformation fields show multi-fractality, which is consistent with existing studies with observational datasets and modeling results (Marsan et al., 2004; Rampal et al., 2019). On Feb. 6th, there are more larger deformation events than Dec. 20th: higher 95-th percentile is present for all 3 resolutions, including scaled results (Fig. 9). Large-scale sea ice drift patterns were found to be greatly accurately determined by geostrophic winds and the associated SLP field and AO indices (Rigor et al., 2002). The associated sea ice deformations at smaller spatial and temporal scales, due to the multi-fractality and large scale-small scale linkage, is highly dependent on the atmospheric forcings which contain inherent variability at different scales. Furthermore, the sea ice deformation is also greatly dependent on sea ice status, such as ice thickness and strength. Since the experiments in this study target at climatologlical sea ice states, the ice thickness and multi-year ice coverage is higher than the ice condition when existing satellite observations such as RGPS were carried out. Historical simulations which are driven by high-resolution, inter-annually changing atmospheric forcings, as well as coupling to dynamical atmospheric and oceanic models, are needed to compare with coinciding observations such as RGPS.

### 3.3 Wintertime kinematics

We extend the analysis of spatial scaling to the winter months (Dec. to Feb.). Daily deformation fields are used to construct the time sequence of the spatial scaling exponent $\beta$ for $q = 1$ during this period (Fig. 11). The value of $\beta$ shows very large day-to-day variability throughout the winter, but mostly within -0.1. During winter, the analyzed region (Fig. 7) mainly consists of packed ice, with the ice concentration close to 100% and the mean ice thickness over 2 m (Fig. 5.h). Similarly, as reported by Hutter et al. (2018) which is a model-based study, both packedness and thickness contribute to an exponent close to 0,

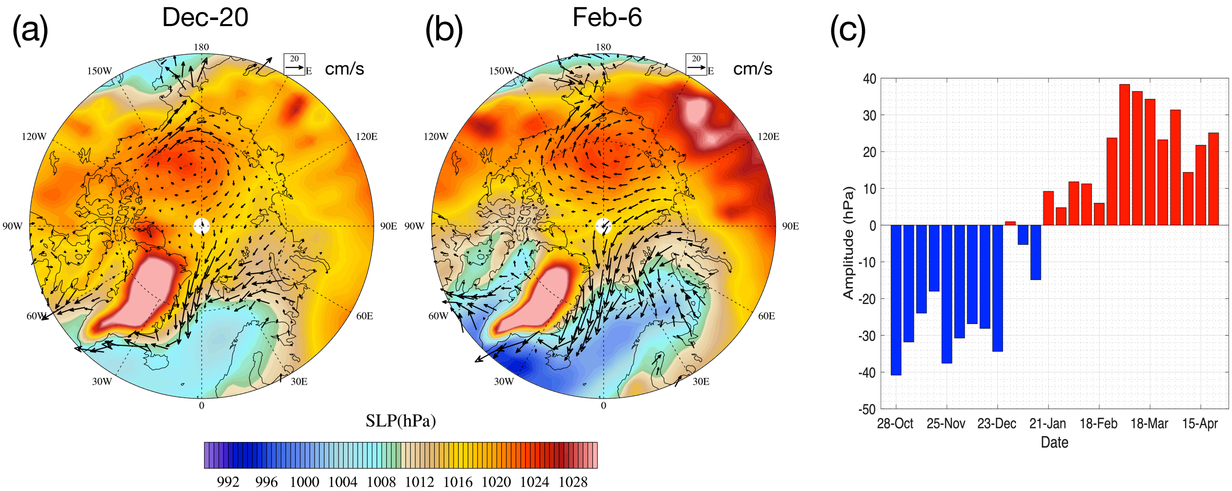


**Figure 6.** Daily sea-level pressure from NYF dataset (filled contour) and modeled sea ice motion by TS045 (vectors) on Dec. 20th (a) and Feb. 6th (b). Wintertime Arctic Oscillation (AO) index of the NYF dataset is in panel c. See the text for detailed methods for the computing of AO.

and the central Arctic shows very low scaling factor ($0 < \beta < 0.09$) in January. This is consistent with our result which also show $\beta$ within 0.1. We do notice that in Hutter et al. (2018), hourly sea ice deformation fields are used to compute the scaling coefficients, compared to daily fields in our current study. However, the spatial-temporal scaling in Hutter et al. (2018) show very close values for $\beta$ between hourly and daily results (Fig. 7 of the reference). We consider the low scaling coefficient as produced by our model runs reasonable for characterizing sea ice kinematics in packed ice.

Furthermore, as revealed in Figure 11, distinctive phases are present during the 3 months. During January, the exponent is between 0.02 and 0.03, and lower (closer to 0) than the previous month of December (mainly between 0.04 and 0.06). The value of $\beta$ also grows (more negative) towards February (around 0.04). There are several potential contributing factors to the differences in $\beta$. First, in order to ensure continuity at the beginning/end of the year, for December, NYF dataset is based on the interpolation of year 1994 and 1995 of NCEP reanalysis. Potentially, the atmospheric processes during this month may contain attenuated spatial and temporal variability. Second, in NYF dataset, the dominant atmospheric variability (AO) shifts from negative in December to positive in January and February. This corresponds to the systematic shift of $\beta$ during this period. However, a simple regression of AO on various scales (daily to weekly) yields no significant statistical correlation with $\beta$. Since the atmospheric forcing dominates large-scale sea ice drift, we conjecture that regarding atmospheric forcing, the fine-scale atmospheric processes (such as spatial and temporal wind variability) serve as the missing link between large-scale drift and small-scale kinematics and statistics. Lastly, sea ice status, including sea ice strength and rheology, dominates the shearing and convergence/divergence failures at local scale. The thickening of the sea ice throughout the winter months may also contribute to the increase of ice strength and the overall decrease in $\beta$.

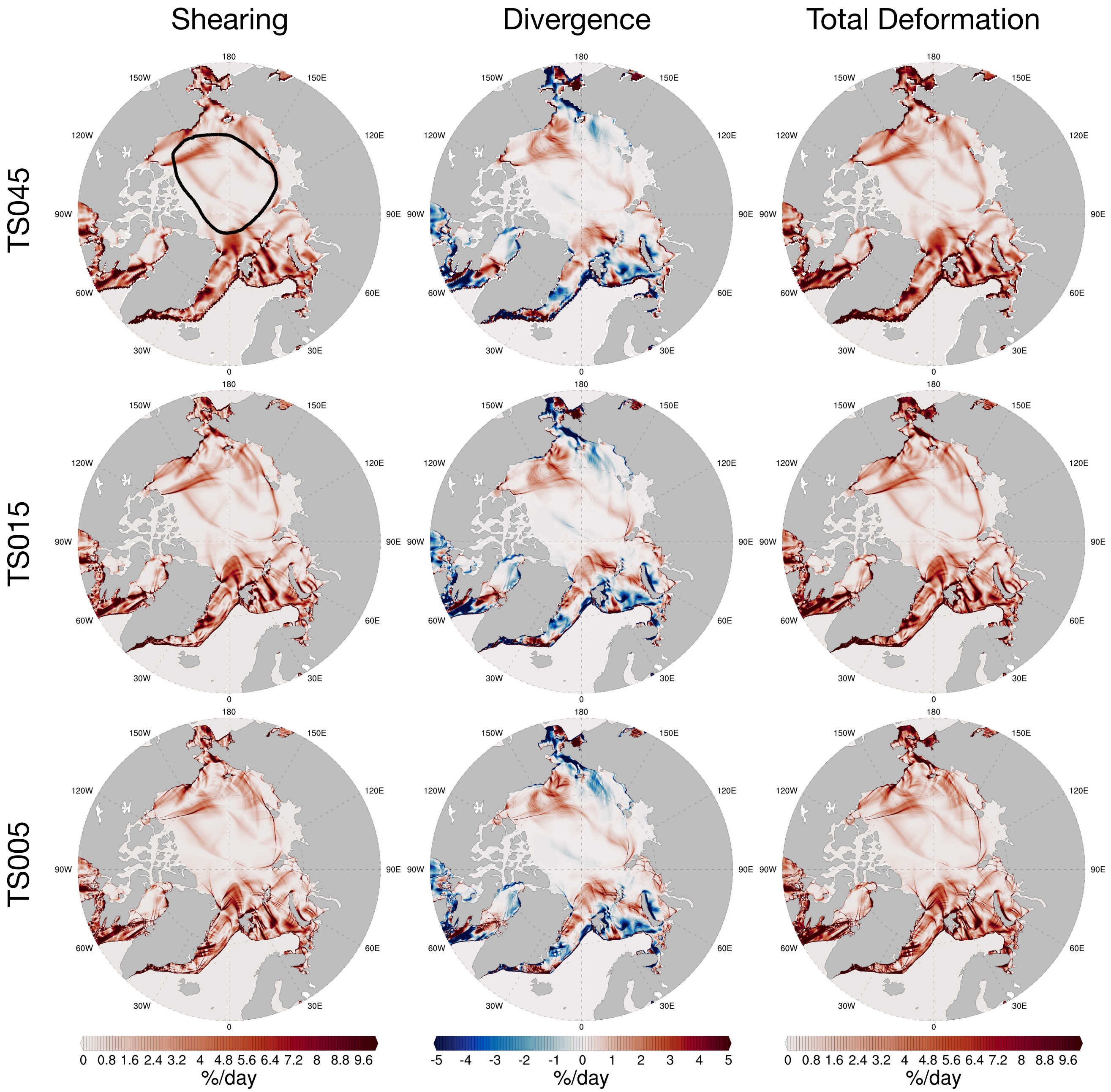


**Figure 7.** Daily deformation fields on Dec. 20th. The first, second and third row show the deformation fields for TS045, TS015 and TS005, respectively. Deformation rates include shearing rate (left), divergence rate (middle) and total deformation rate (right). The region for further statistical analysis including spatial scaling is outlined in black in the first panel.

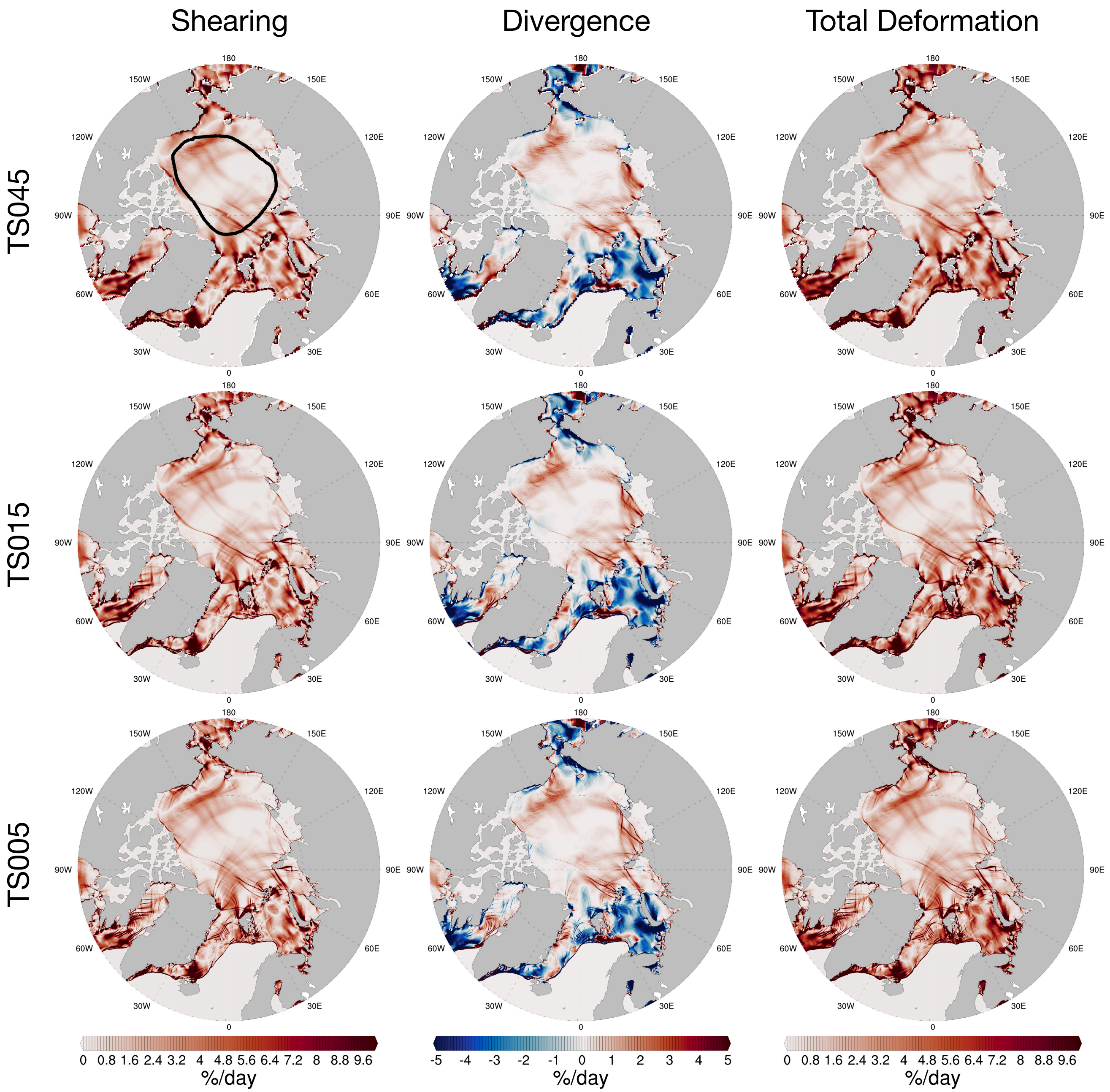


**Figure 8.** Same as in Fig. 7, but for Feb. 6th.

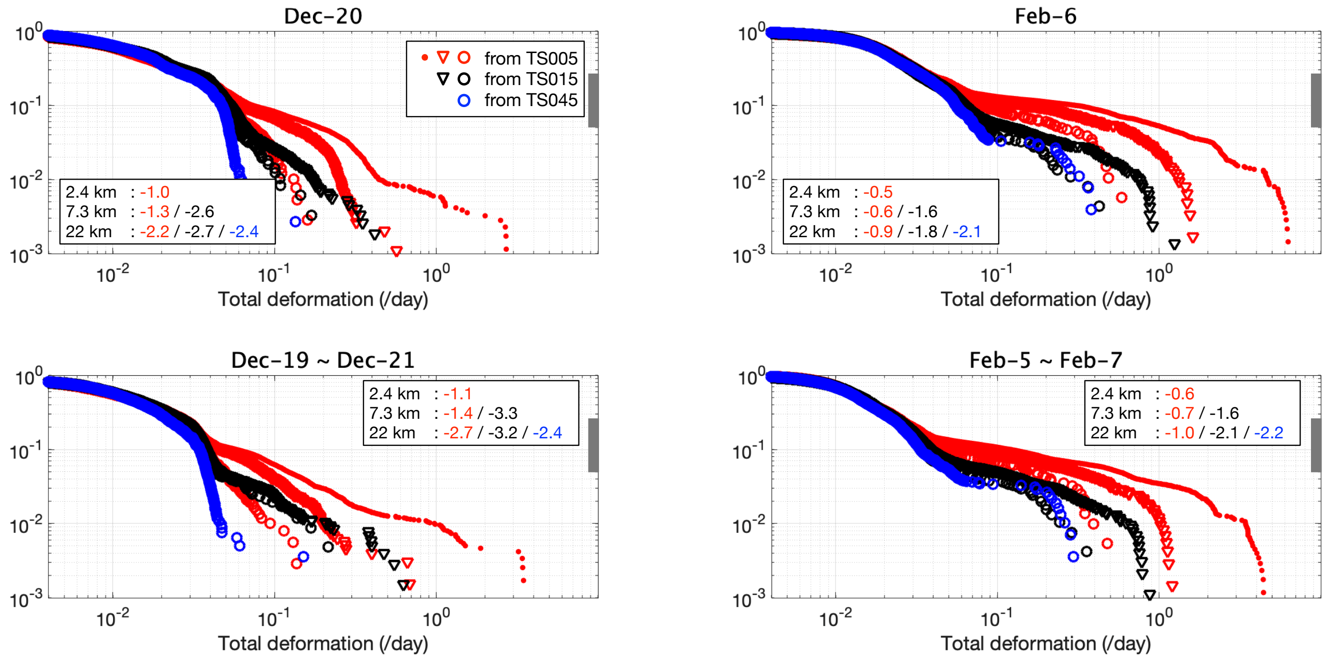


**Figure 9.** Cumulative distributions for the total deformation rates on Dec. 20th and Feb. 6th. Region of study is outlined in Fig. 7 and Fig. 8. Daily rates are shown in the first row and 3-day rates on the second row. Colors indicate the cumulative PDF from the model results from different grids (red: TS005; black: TS015; blue: TS045). With spatial coarsening of TS005, we compute the cumulative PDF at the spatial scales corresponding to native resolution of TS015 and TS045. In turn, the spatial coarsening with TS015 is also applied to compute the cumulative PDF at the equivalent resolution of TS045. The 3 spatial scales are marked by different shapes: 22 km (or TS045's native resolution) in circles; 7.3 km (or TS015's native resolution) in triangles; 2.4 km (or TS005's native resolution) in dots. Slopes are computed for the range of the cumulated probability between 0.05 and 0.25 for all cumulative PDFs (marked out in grey in each panel), which correspond to 95th and 75th percentile of the deformation fields, respectively.

### 3.4 Numerical convergence of EVP

In this section we evaluate the sensitivity of the modeled sea ice kinematics to the EVP subcycling and asymptotic convergence. The elastic wave term introduced the EVP is more effectively damped with more subcycles, leading to consistent deformation fields. This asymptotic convergence of the deformation fields to EVP subcycling is examined in this study. In Figure 12 we show the probability density function (or PDF) of daily deformation rates during wintertime (Dec. to Feb.) for the three grids. All the simulations attain a good shape for the tail of of the PDF, approaching the slope of -3. For the total deformation rate, there exists a well defined mode at $0.1\%/d$ to $0.2\%/d$ for runs with NDTE=960, and at NDTE=120, a slight shift of mode to higher values (between $0.5\%/d$ to $1\%/d$ for TS015 and TS005). At different resolutions, the EVP subcycling count plays a different role in the shape of PDF. For TS045, the PDF is consistent between different subcycle counts. But for TS015 and TS005, there are much more evident differences: (1) with larger NDTE, there are more regions with smaller shearing and

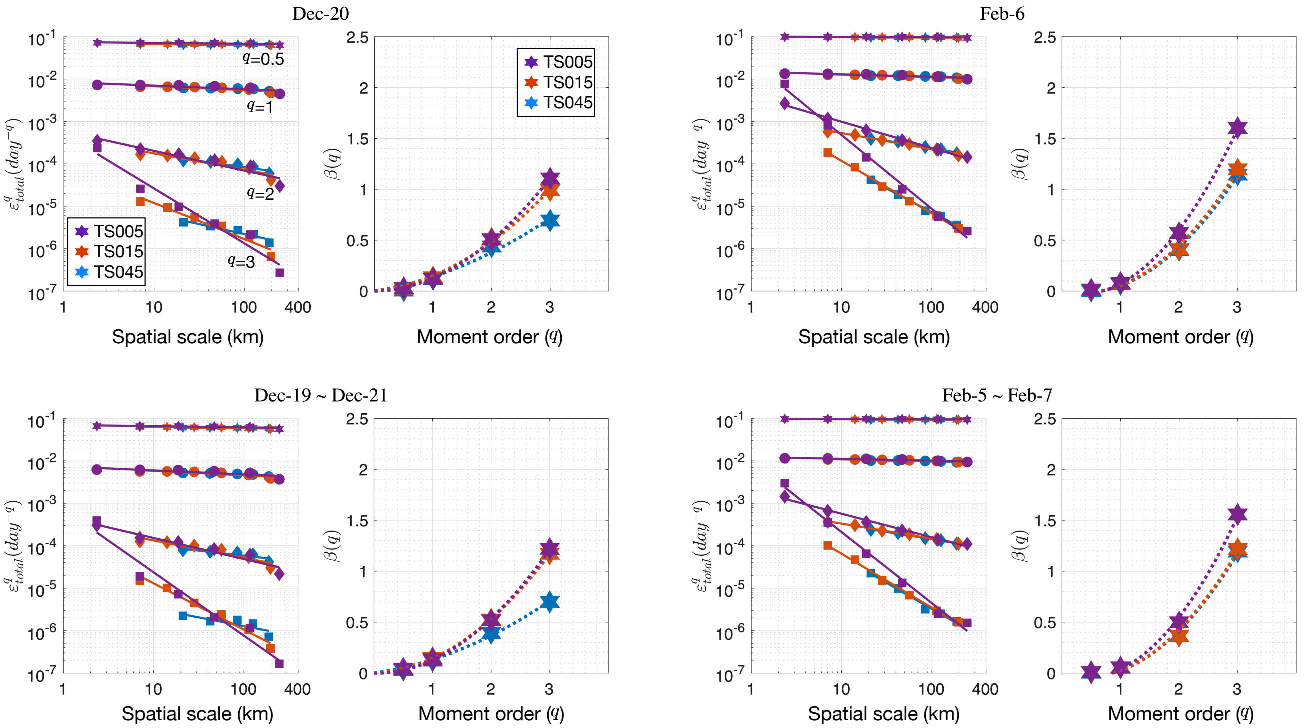


**Figure 10.** Spatial scaling of total deformation rate for daily deformation fields (top row) and 3-day mean deformation fields (lower row). The daily mean velocity fields on Dec. 20th and Feb. 6th, as well as the 3-day mean velocity fields centering on Dec. 20th and Feb. 6th are used to derive the scaling curves. Each panel contains the scaling curves and the structure function relating the scaling coefficients ($\beta$'s) to the moment of order ($q$). Detailed methodology used to compute the deformation rates with the model outputs is outlined in Appendix B.

divergence (less than 0.1 $\%/d$); (2) there is general convergent behavior of the shape of the PDF when NDTE is large (e.g., NDTE>480 for TS015). This behavior also applies for specific days (see Fig. S2 and Fig. S3 for the PDF on Dec. 20th and Feb. 6th, respectively). Besides, the PDFs of high-resolution runs (TS015 and TS005) show better tail structure, and furthermore, the slopes are also better characterized (i.e., closer linear fittings at -3) with larger values of NDTE. For TS045, the tail of the PDF suffers from the lack of samples for large deformation events. This indicates that insufficient EVP subcycle count leads to overall non-convergent deformation rate distributions.

A visual inspection of the deformation fields reveals the loss of the kinematic features when the convergence is not attained. Figure 13 shows the daily total deformation fields on Dec. 20th as simulated with different NDTE values for each grid. The more remarkable difference is between the runs with NDTE=120 and NDTE=960 with the highest resolution (i.e., TS005). Although the linear kinematic features are well defined with NDTE=960, the deformation field is much noisier for the run with NDTE=120, with only the larger features detectable. The noise level is at about 1 $\%/d$, which corresponds to the mode of PDF in Figure 12. With larger values of NDTE, the noise level decreases and the deformation rate around the linear kinematic features becomes smaller. As a result, a convergent PDF and linear feature maps are attained. One exemplary region is the

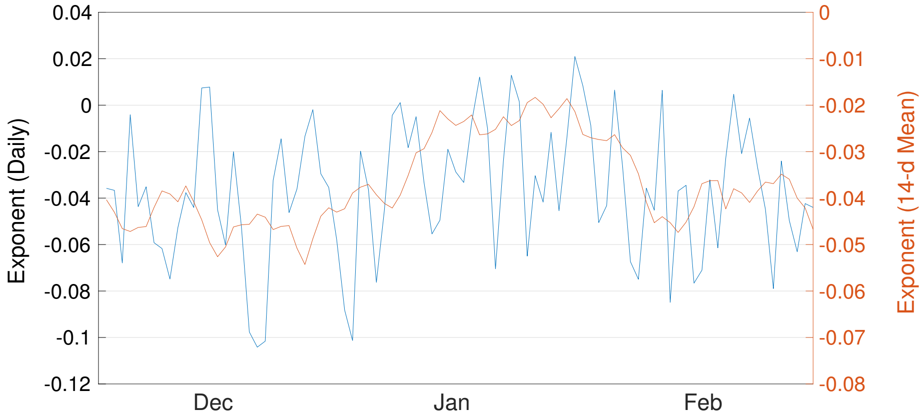


**Figure 11.** Spatial scaling exponents of the total deformation for $q$=1 for daily fields during winter. The region analyzed is outlined in the first panel of Fig. 7. Model output with TS005 grid is used for the analysis. Exponent sequence from daily fields (blue line, left y-axis) is accompanied by its 14-day running mean (orange line, right y-axis).

Canadian Arctic Archipelago (CAA), where the landfast sea ice dominates during winter in the model run with NDTE=960. For example, Figure S4 shows that the 2-week mean sea ice velocity within the CAA is lower than $5\times10^{-4}m/s$ (Lemieux et al., 2015). The detailed total deformation rate field within the CAA for TS005 (third row of Figure 13) is further shown in Figure S5. The experiment with NDTE=120 show much higher and noisier sea ice deformation fields than that with NDTE=960. Overall, the results show that with the traditional EVP implementation, with higher resolution, even more subcycles are needed to reach convergence for the simulated kinematics. This causes further increase in simulation cost, given that the dynamics time step is already decreased in high-resolution runs, due to CFL conditions in processes such as advection (Tab. 2).

For TS045, although the PDF of the deformation rates are similar among runs with different NDTE values, the deformation field is also slightly more noisy in runs with NDTE=120 and NDTE=240 than that with NDTE=960. The region with the biggest difference is within the Canadian Arctic Archipelago. We further evaluate the effect of subcycling by carrying out the experiments with NDTE=240 and NDTE=960 for TS045 further to year 45 (Fig. 4). We show the difference of March (September) sea ice thickness between NDTE=960 run and NDTE=240 run on year 45 in Figure 14.a (14.b). Although there is only less than 1% difference in the basin-scale ice volume between the two experiments, the sea ice is remarkably thinner in the CAA in the run with NDTE=960.

The difference in ice thickness is all-year around (i.e., in both September and March). Specifically, in the run of NDTE=960, an ice arch forms by the eastern end of the Lancaster Sound and near Amund Ringnes Island, resulting in thicker ice in these regions. In other parts of the CAA, the ice is thinner by about 15 to 20 cm on average, and up to 1 meters thinner in certain areas. As shown in Figure 14.c, the run with NDTE=240, which started from year 1, has already attained equilibrium in sea ice thickness and volume in the CAA well before year 35. However, in the run with NDTE=960 which starts from year 35, the model status gradually shifts to another equilibrium status for ice thickness towards year 45. The overall volume difference is uniformly 100 $km^3$ in March and September, which consists of about 6.5% of the total volume in September. We further attribute the difference of winter ice thickness to the thermodynamic (Fig. 14.d), advection (Fig. 14.e), and dynamical ridging/rafting (Fig. 14.f) contributions during the freeze-up seasons, computed as multi-year mean fields for December, January and February (DJF) of year 41 to 45. Specifically, in CICE model, the 3-month mean ice volume tendencies due to thermodynamic growth, ice advection, and ridging are computed from the model diagnostics for ice volume budget at Eulerian grid points. As compared with the run with NDTE=960, there exist small deformation events in the CAA in the run with NDTE=240, which are arguably due to non-convergent EVP solutions (see also Fig. 13 for comparisons of deformation fields). Therefore, there is more ice thickness increase in the run with NDTE=240 due to these events (Fig. 14.f). Also, since September ice is thinner in the run with NDTE=960, it is intuitive that the winter thermodynamic ice growth should be higher for NDTE=960. On the contrary, the thermodynamic ice thickness growth is in general lower in the run with NDTE=960, except for regions with the biggest thickness decrease in September as compared with the run with NDTE=240 (Fig. 14.d and Fig. 14.b). This is mainly due to the fact that the thermodynamic ice growth is also closely tied to the kinematics processes. With more noisy sea ice movement fields in the run with NDTE=240, the sea ice formation and growth is also promoted with very small deformation events, resulting in more thermodynamic growth in the run with NDTE=240. As compared with ridging and rafting, the sea ice advection is mainly responsible for redistributing the ice mass and thus plays a minor role for the overall ice volume in the CAA in our experiments (Fig. 14.e).

The dependence of the modeled sea ice thickness in the CAA on EVP convergence in our study is purely numerical, but calls for further attention from both modelers and modeling data users. It highlights the importance of numerical convergence of EVP (or any other candidate solvers to VP) on the modeled sea ice climatology in fast ice regions. Since the experiments are idealized in this study, the effects in realistic simulations may be also subjected to grid resolution and staggering, as well as coupling and feedback processes.

## 4 Summary and discussion

In this paper we carried out sea ice simulations with a multi-resolution framework with Community Earth System Model. A grid hierarchy is constructed with the resolution range spanning climate simulations (0.45°) to sub-mesoscale modeling (0.05°). At 0.05°, the grid resolution in the Arctic region is approximately 2.45 km. The grid hierarchy is incorporated into CESM, and by using atmospherically forced experiments, we simulate and evaluate sea ice kinematics and scaling properties with a multi-resolution approach. We have found good consistency of the Arctic sea ice climatology and kinematics across the resolution range. As shown in the spatial scaling analysis on the representative days, multi-fractal sea ice deformation is accurately modeled by all three resolutions. In our study, high-resolution (0.05°) runs yield the most trustworthy kinematic features, and the multi-resolution simulations provide a unique approach for evaluating sea ice kinematics in lower resolutions. Furthermore, the convergence of Elastic-Viscous-Plastic rheology model is evaluated, which show significant impact of EVP convergence on kinematic statistics, as well as landfast ice in Canadian Arctic Archipelago. The framework of utilizing the grid hierarchy, including TS045, TS015 and TS005, provides an infrastructure for multi-resolution simulations for both ocean

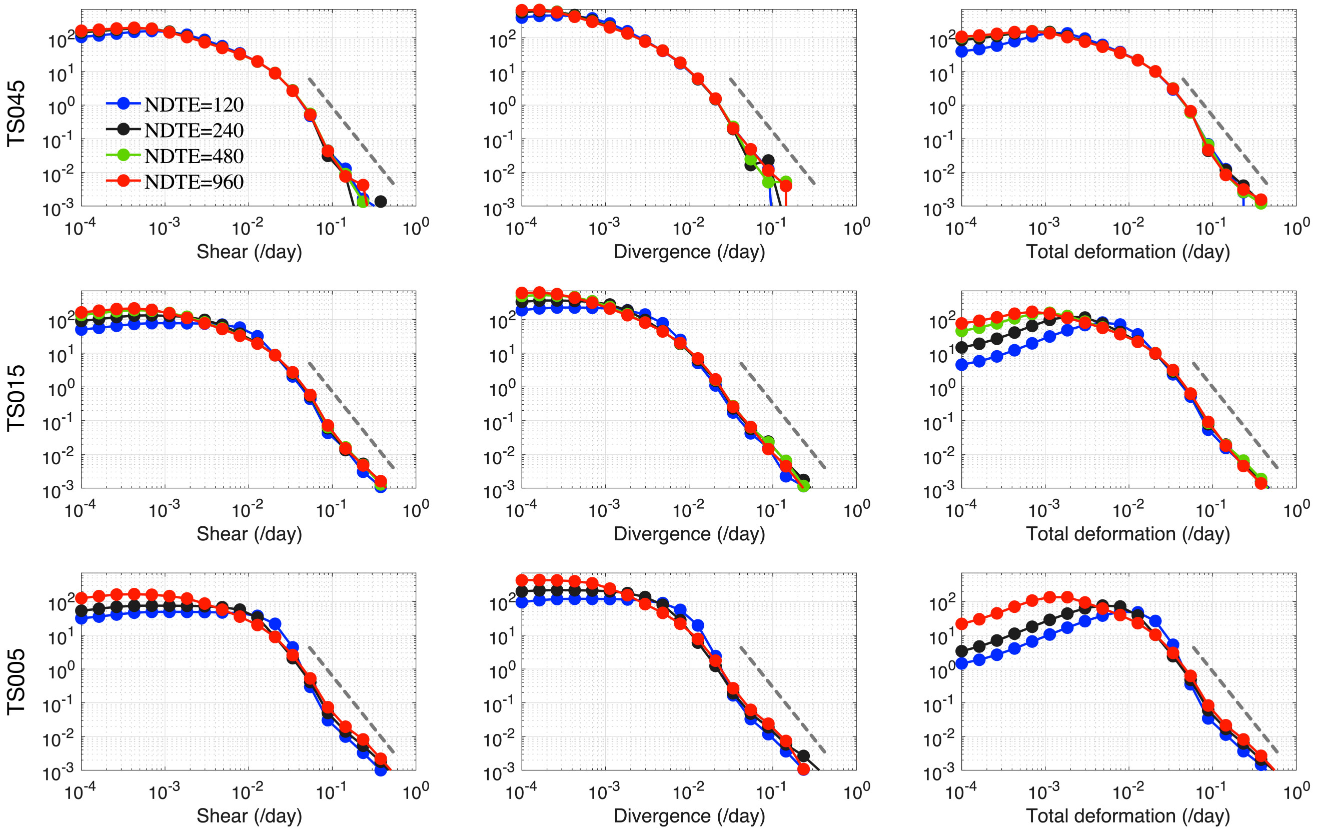


**Figure 12.** Probability density of modeled daily deformation rates during winter months (Dec. to Feb.) with TS045 (first row), TS015 (second row) and TS005 (third row). The region of study is outlined in Fig. 7. Shearing rate (left column), divergence rate (central column) and total deformation rate (right column) are shown. Runs with different EVP configurations (NDTE from 120 to 960) are marked by the same color as in Fig. 4.a. The theoretical slope for the PDF tail of -3 is shown in each panel for reference (grey dashed line).

and sea ice in the future. The three grids and the model integration are openly provided for public use for the version 1.2.1 of CESM.

Sea ice kinematics has been the focus of the high-resolution sea ice modeling community in recent years. Based on SAR remote sensing such as ASAR and RADARSAT, kilometer-level or finer observations of sea ice drift and deformation are made possible, and serve as the backbone for the validation of high-resolution sea ice simulations. Modeling studies with structured grids such as MITgcm (Spreen et al., 2017; Hutter et al., 2018) are similar to our study, although model specifics are different. The sea ice deformation and scaling can be easily derived with model output for spatial scaling, but Lagrangian based diagnostics is required for the full analysis of temporal scaling. In our study, we mainly utilized model output for the study of spatial scaling properties in Section 3.2, with initial study of 3-day mean drift fields. Specifically, the process dependent scaling properties were found for representative days for sea ice drift and AO index. As future work, a full exploration of AO and ice condition dependent scaling analysis is planned with the grid hierarchy and CESM. Besides, the scaling analysis remains an

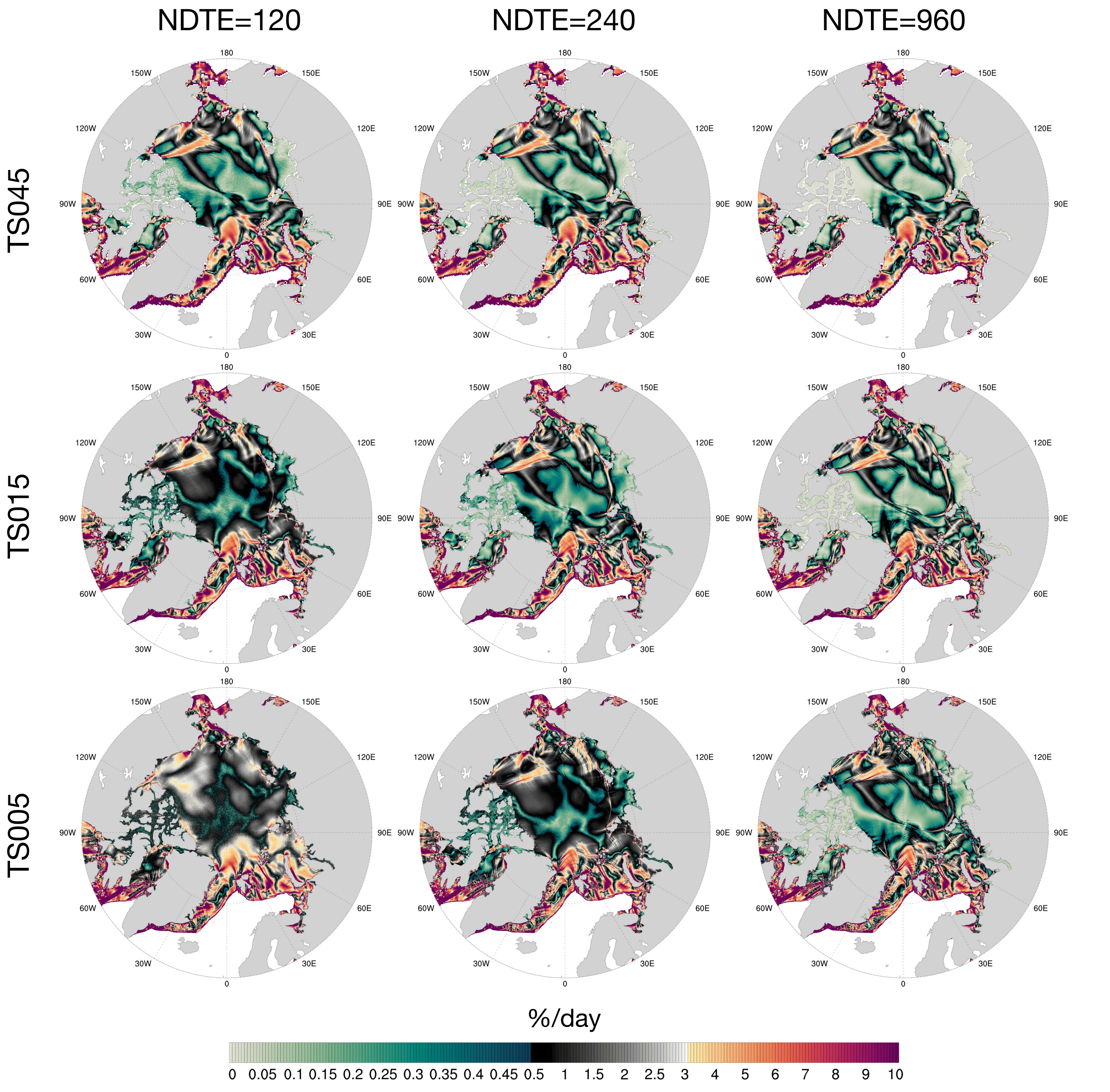


**Figure 13.** Total deformation rate on Dec. 20th with NDTE=120 (left), 240 (central) and 960 (right). Each row represents a specific grid, including: TS045 (top), TS015 (middle) and TS005 (bottom). Results with NDTE=960 are reproduced from Fig. 7. Colormap is adjusted from Fig. 7 for increased resolution of under 1 $\%/d$.

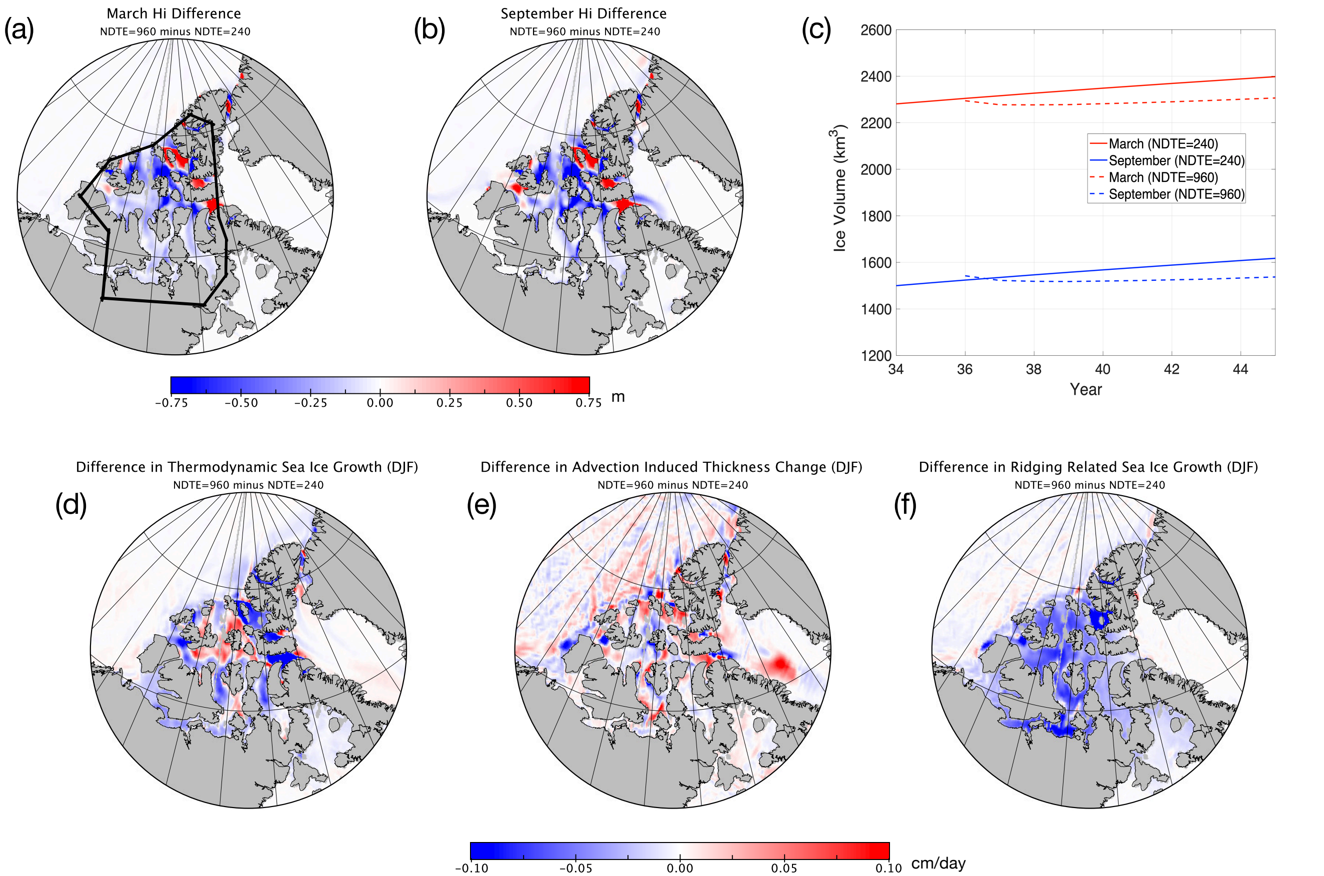


**Figure 14.** March (a) and September (b) sea ice thickness difference between the run with NDTE=240 and that with NDTE=960 of year 50 for TS045 (NDTE=960 minus NDTE=240). Sea ice volume in March and September within the CAA (outlined in panel a) since year 41 are shown in panel c. Differences in mean sea ice growth rate due to thermodynamics (d), advection (e), and dynamic ridging (f) during winter months (DJF) are computed for multiple winters (DJF of years 41 to 50). Blue (red) color indicates lower (higher) ice growth during freeze-up in the run with NDTE=960 than NDTE=240 during winter.

important tool for evaluating sea ice kinematics, but it maybe insufficient for fully evaluating the sea ice deformation properties. Novel statistics based on linear kinematics features (LKF) are proposed in recent studies, such as Hutter and Losch (2020) and Ringeisen et al. (2019). The utilization of a full suite of diagnostics in our modeling framework, including temporal-spatial scaling and LKF based approaches, serve as an important direction for future work.

In this study, the NYF dataset of CORE 2 is utilized. This potentially compromises the comparability of the model results with satellite observations such as SAR-based sea ice kinematics (Kwok et al., 2008; Marsan et al., 2004). The inter-annual forcing dataset (IAF) of CORE 2 and the JRA-55 used by Ocean Model Intercomparison Project, phase 2 (OMIP2) can be utilized for historical simulations with the proposed grids. Furthermore, comparison can be made with specific satellite observations such as RGPS (Kwok et al., 2008). This work is planned as future work with higher versions of the coupled model (i.e., version 2 of CESM). Besides, the attribution of the scaling statistics is planned regarding the resolution of the atmospheric forcing. Specifically, new reanalyses datasets (such as JRA-55) can be utilized and compared with NCEP CORE 2, in order to study the effect of resolution of the forcing dataset. Also, we plan to explore the potential of coupling to the interactive atmospheric model (with different resolutions) in CESM. A similar multi-resolution approach can be attained for both the atmosphere and the ice component in CESM for the study of sea ice kinematics.

Sea ice rheology models are key to the simulation of sea ice dynamics and reproducing linear kinematic features. Together with other parameter schemes including the sea ice strength (H79 in this study) and ridging, parameters of these schemes are utilized for tuning the models towards certain observations (Bouchat and Tremblay, 2017). In specific, sea ice strength parameter ($P^*$) and eccentricity of the elliptic yield curve of EVP are found to be tunable parameters to improve the modeling of sea ice dynamics. During the tuning of the sea ice models, the aforementioned novel statistics can also be integrated for improving rheology models such as the yield curve shape (Ringeisen et al., 2019). With high-resolution grids in the Arctic region (e.g., 2.4 km for TS005), we plan to to carry out simulations and comparative studies with anisotropic rheology models such as EAP (Tsamados et al., 2013). Specifically, with the updated version of the sea ice component model (version 5 of CICE) as well as the coupled model of CESM, we carry out the model integration of the grid hierarchy and associate numerical experiments.

While EVP provides a numerically stable and easy-to-implement solver for the traditional VP model, the convergence of EVP solutions to VP model is the focus of many recent efforts (Lemieux et al., 2012; Kimmritz et al., 2015; Koldunov et al., 2019). Based on a traditional implementation of EVP in our model, we have witnessed asymptotic converging behavior of sea ice kinematics fields with increased EVP subcycle count. Based on a traditional implementation of EVP in our model, we have witnessed asymptotic and converging behavior of modeled kinematics by the increasing EVP subcycle count. But this comes at a large computational overhead: at 960 subcycles per step for TS005, the simulation speed has halved compared with 240 subcycles per step, and over 50% of the computational time is consumed in EVP, with less than 0.5 SYPD with 1920 processor cores. Ideally, an efficient and scalable implicit solver promises a more elegant and numerically sound solution to the solving problem of VP model (Lemieux et al., 2010). Also, adaptive methods that complements the convergence and efficiency problems of traditional EVP solver, such as Kimmritz et al. (2015) and Koldunov et al. (2019), are considered in our future work for the integration of the upgraded version of the coupled or sea ice model.

In Sec. 3.4, we have shown that the mean states for ice thickness and volume can be systematically shifted due to the numerical behavior of EVP solver. Since this issue is purely numerical, the uncertainty caused by it is different from other factors, such as the choice of ice strength parameterization scheme. In our study, the region which is most sensitive is landfast ice in the CAA, where significant decrease of ice volume is witnessed when solver convergence is attained with enough subcycle counts. Furthermore, more subcycling is required for higher resolution to reach convergence. Given the wide adoption of VP and EVP in climate models, using the model outputs for climate research and applications (such as the projection of shipping routes) could face potential compromises if the convergence issue is overlooked. Especially, careful choices should be made for configuring EVP at different resolutions (Kiss et al., 2020). Besides, since asymptotic behavior of the sea ice kinematics to EVP subcycling is investigated in this study, the convergence of VP solver needs further formal definition for the strict intercomparison of multiple solvers in the future (Lemieux et al., 2012). In Koldunov et al. (2019) the authors also discovered sensitivity of modeled ice thickness to EVP subcycling, but an increase in ice thickness with more EVP subcycles (Fig. 2 of the reference). Also the region with most significant thickness change is different in Koldunov et al. (2019), covering both regions in the CAA and north of CAA and Greenland. Compared to our study, the different behavior to EVP subcycling in Koldunov et al. (2019) may be due to the differences in the numerical experiments, as well as model physics, including grid resolutions, ice thickness distribution settings, etc. Although both show relationship of ice thickness to rheology model, more analysis is needed for the attribution and explanation of aforementioned differences. Besides, tidal processes and interactions with sea ice are potentially important for the simulation of landfast ice (Lemieux et al., 2018). Since these processes are absent in our current model, we plan to include parameterization schemes that account for the their influence on sea ice kinematic in the future.

With the wide availability of high-performance computing utilities and the progress in model developments, high-resolution and even multi-resolution simulations are becoming more common for climate modeling community. While 1° models are still dominant in Coupled Model Intercomparison Projects (CMIP), high-resolution models are informative of potential model biases and parameterization improvements. For example, three resolutions (1°, 0.25° and 0.1°) are built into ACCESS-OM model for ocean-sea ice coupled simulations (Kiss et al., 2020). In GFDL's most recent ocean-sea ice model [OM4.0, (Adcroft et al., 2019)], two resolutions are adopted, including OM4p5 (0.5°) and OM4p25 (0.25°). Parameterization schemes in the ocean and the sea ice models are chosen and tuned to each specific resolution. For example, mesoscale eddy induced mixing parameterization is usually adopted for low-resolution ocean models (0.5° or coarser), but inactive for higher resolutions. In our study, we use three resolutions for the study of Arctic sea ice kinematics, including: 0.45°, 0.15° and 0.05°. As is shown in the scaling analysis, this multi-resolution framework enables comparative analysis across the resolution. Given that the modeled sea ice climatology is reasonable and consistent among the three resolutions, we consider the results adequate for the analysis of kinematics and scaling based on the coupling to the Slab Ocean Model. Beyond the lower computational overhead of this approach, we can also attain an equilibrium status for the sea ice with fewer model years. Especially for 0.05° grid (TS005), the computational cost and the duration is prohibitively high to fully spin-up the ocean-sea ice coupled model. Furthermore, it reduces the uncertainty of ocean's modeling on the sea ice, including: (1) ocean model's parameterization schemes that are not aligned and potentially not well-tuned between the different resolutions; and (2) the avoidance of ocean and ocean-sea ice coupled internal variability that may potentially compromise the comparability across the resolutions. In the future, we plan to carry out spin-up and long-term simulation of the ocean-sea ice coupled system using the proposed multi-resolution framework, which will introduce variability to the modeled sea ice states from the oceanic dynamic processes and coupled processes. Specifically, the migration of the status from cheap, low-resolution runs (TS045) to TS015 and TS005 is planned, in order to facilitate faster spin-up for high-resolution runs. This is accompanied by historical, inter-annual forcing datasets, for the production of realistic simulations and comparison with coinciding satellite observations of the sea ice kinematics.

*Acknowledgements.* The authors would like to thank the editors and referees for their invaluable efforts in improving the manuscript. This work is partially supported by: National Key R & D Program of China (no.: 2017YFA0603902), the General Program of National Science Foundation of China (no.: 42030602), and Tsinghua University Initiative Scientific Research Program (no.: 2019Z07L01001). This work is also partially supported by Center for High-Performance Computing and System Simulation, Pilot National Laboratory for Marine Science and Technology (Qingdao). The authors would also like to thank the National Supercomputing Center at Wuxi for the computational and technical supports during the numerical experiments.

The authors gratefully acknowledge the CESM development team at NCAR and the user community of CESM for providing the open-source usage of CESM and its component models, and their great help. We also would like to express sincere thanks for using ESMF utilities during the integration of TS grids in CESM.

*Code and data availability.* The three grids in this article (TS045, TS015 and TS005) are openly provided in the binary grid format of POP and CICE. Modifications to CESM (version 1.2.1) are made to incorporate the new grids, with model configurations of CICE and coupling with atmospheric forcing dataset (T62). Auxiliary datasets are also provided, including: (1) coupling interpolators of TS grids to T62, and (2) CICE monthly history files during March. The grids and model integration is also available for Community Integrated Earth System Model [CIESM, (Lin et al., 2020)]. All the code and data are hosted at: https://doi.org/10.5281/zenodo.3842282.

CESM code and ESMF regridding utility are available for download at: http://cesm.ucar.edu (last accessed: 2020-Feb-20) and https://www.earthsystemcog.org/projects/esmf/regridding (last accessed: 2020-Mar-12).

## Appendix A: Orthogonal grid for northern patch

The construction of the orthogonal grid in the northern patch (NP, as in Sec. 2) involves a numerical process of two steps. First, a series of embedding ellipses is constructed on the stereographic projection of NP from the North Pole (Fig. A1.a). The outermost ellipse is a circle defined by the boundary between NP and SP. The innermost ellipse is a direct line that crosses the North Pole and links the two grid poles, which are prescribed locations on land. A smooth transition from the circle to the innermost ellipse is achieved, by controlling the semi-major axes ($a$'s) and semi-minor axes ($b$'s) of the ellipses. Without the loss of generality, we rescale the projected NP, so that the outermost ellipse is the unit circle and the innermost ellipse resides on the $x$-axis, and the layout is shown in Figure A1.a. Therefore, we have: (1) for the outermost ellipse, $a = b = 1$; and (2) for the innermost ellipse, $a = \alpha$ and $b = 0$, where $\alpha$ is half of the distance between the two grid poles. To ensure a continued change of meridional grid scales on NP-SP boundary, the change in $b$ should be equal to that in $a$ on the outermost ellipse. In Figure A1.b we show a possible relationship between $a$ and $b$: $a = \alpha \cdot b^2 + \beta \cdot b + \alpha$, where $\beta = 1 - 2\alpha$. It can be computed that the slope of the curve equals 1 when $a$ (or $b$) approaches 1, ensuring same change speed in $a$ and $b$ and a smooth meridional scale transition on the NP-SP boundary. The ellipses, including $a$'s, $b$'s and center locations, can then be determined according to these configurations and the required resolution. In this paper, we have chosen the following parameters for TS grids: the NP-SP boundary ($\phi$) at about $10°N$, and the two poles at $(63°N, 104°W)$ and $(59.5°N, 76°E)$, which are $180°$ apart but on different latitudes (red squares in Fig. A1.a).

Second, with the embedded ellipses, the orthogonal grid can be constructed from the outermost circle. Since NP is directly linked to SP at latitude of $\phi$, we specify the grid points on this boundary (i.e., the outermost circle), and extend into NP to form the meridional grid lines. The construction process is iterative, starting from these points on the outermost ellipse, and for each step constructing lines between two adjacent ellipses. In each step, the ending locations of the lines are located on the inner ellipse, under orthogonality constraints. Fig. A1.a shows a specific example between two adjacent ellipses (marked by blue and dash-blue). This whole approach is similar to the grid generation methods that are based on numerical integration processes, as in Madec and Imbard (1996) and Xu et al. (2015).

Figure A2 show the meridional and zonal grid scales ($dx$ and $dy$) along typical meridional grid lines for TS005. As is shown, there is smooth transition of the meridional grid scale on the boundary of SP and NP (at about J=2520 for TS005). Also the overall grid scale anisotropy is kept lower than 1.5 in the oceanic areas.

## Appendix B: Sea ice model (CICE) configuration and parameters

CICE (version 4.0) is the sea ice component of the CESM (version 1.2.1). CICE is a full thermodynamic-dynamic model for sea ice, and with the coupling framework in CESM, CICE is forced with NCEP CORE atmospheric forcings and coupled to the Slab Ocean Model. Sea ice thickness distribution with 5 categories is adopted in our experiments, which is also the default configuration for CICE in CESM. In the vertical direction, we use 4 ice layers and 1 snow layer. The sea ice dynamics mainly include four components: (1) Elastic-Viscous-Plastic rheology model with an elliptic yield curve and the aspect ratio of 2 (Hunke and Dukowicz, 1997); (2) the ice strength model in Hibler (1979), refereed as H79, in which the ice strength is related to the mean ice thickness; and (3) the ice ridging scheme as in (Lipscomb et al., 2007); (4) the advection scheme of transport-remapping (Dukowicz and Baumgardner, 2000). For thermodynamics, the Delta-Eddington (D-E) radiation scheme is adopted, with explicit meltpond formulation (Briegleb and Light, 2007). Key parameters of CICE in our experiments are shown in Tab. B1

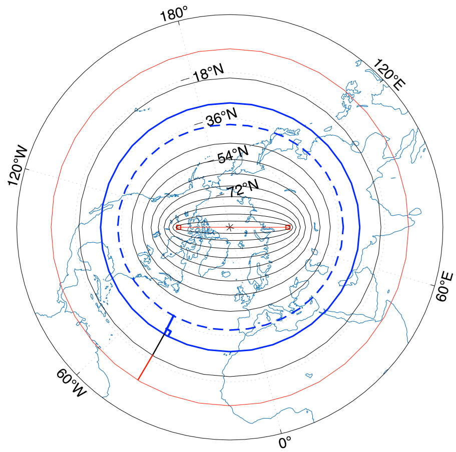


(a) Embedding ellipses

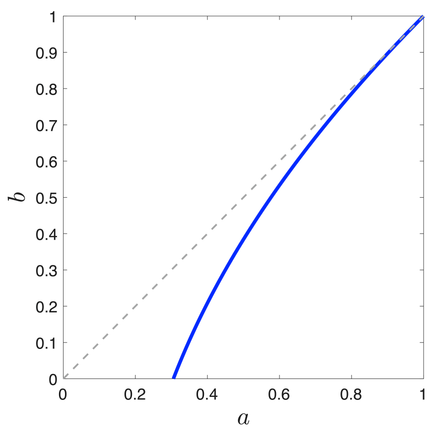


(b) Relationship between ellipses' axes

**Figure A1.** Construction of the embedding ellipses and the orthogonal grid. In panel a, we show in red the outermost ellipse (a circle) and the innermost ellipse (the direct link between the two grid poles marked by red square). The numerical process of constructing an orthogonal grid is carried out between two adjacent ellipses, starting with points the outermost ellipse, and recursively down to the innermost one. The construction of a single step on the current ellipse (blue) to the next ellipse (dashed blue) is shown in panel a. In panel b, we show the relationship between the major axis and minor axis of the ellipses under a quadratic form (see Sec. A for details).

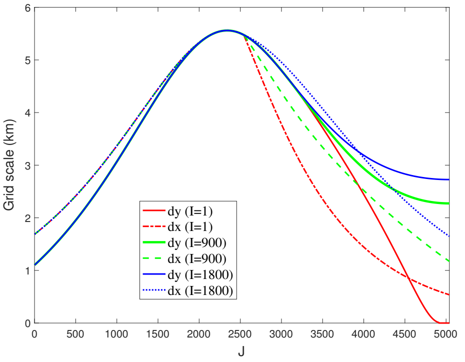


**Figure A2.** Grid sizes along the "meridional" grid lines for TS005 (I & J dimensions are 7200 and 5040). Three typical lines are chosen: I=1, I=900 (1/8 in the I-direction), and I=1800 (1/4 in the I-direction). Grid sizes in both I and J directions retain continued changes. The corresponding grid lines are also shown in Figure 2 with the same color coding. Note that when I=1, $dy$ (meridional grid size) approaches zero when J is close to the northern end (J=5400), which does not affect the model's time stepping since it is near the grid pole which resides on the land.

**Table B1.** Key model parameters of CICE in numerical experiments

| Parameter | Value | Notes |
|---|---|---|
| $P^*$ | 2.75 $\times 10^4 N/m$ | Ice strength parameter for H79 |
| $C$ | 20 | Empirical constant parameter for H79 |
| $a^*$ | 0.5 | $e$-folding scale for participation function during ridging |
| $\mu_{rdg}$ | 4 $m^{0.5}$ | $e$-folding scale for ice ridging |
| $\rho_s$ | 330 $kg/m^3$ | Snow density (used in D-E) |
| $R_{fresh}$ | 100 $um$ | Freshly-fallen snow grain radius (used in D-E) |
| $R_{nonmelt}$ | 500 $um$ | Seasoned snow grain radius (used in D-E) |
| $R_{melt}$ | 1000 $um$ | Melting snow grain radius (used in D-E) |

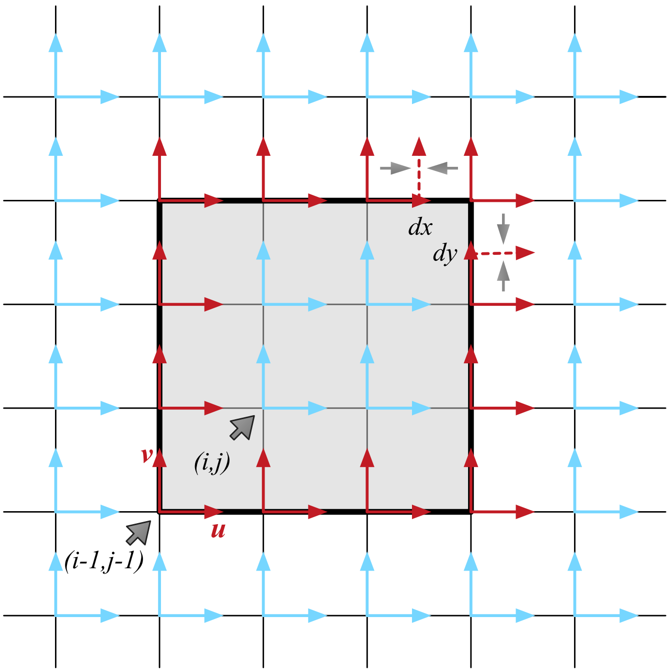


**Figure C1.** Example for spatial scaling analysis with a local area of 9 (i.e., 3×3) model cells. The horizontal (or vertical) direction is in the model's eastern (or northern) direction, indexed by discrete indices of $i$ (or $j$). The sea ice drift velocities that are used to compute the line integral for $\frac{\partial u}{\partial x}$ and $\frac{\partial v}{\partial y}$ are marked by red. For contrast, other velocities are marked by blue. Since velocities are defined on the top-right corner of each cell, they are interpolated on the cell edges to compute the integral. The interpolated velocites are marked by dashed vectors, corresponding to the averaging operation in Eqs. C2.

## Appendix C: Scaling analysis for kinematics

With Arakawa-B grid staggering in CICE, we carry out the spatial scaling analysis of sea ice drift fields according to Marsan et al. (2004). A exemplary case with 9 local grid cells is shown in Figure C1. For the computing of a specific spatial derivate (i.e., $\frac{\partial u}{\partial x}$), the line integral is computed to calculate the flux through the boundary of the specified area (Eqs. C2). The deformation rates can be computed according to Eqs. 1 through Eqs. 3. For the area from $i_1$ to $i_2$ and $j_1$ to $j_2$, the line integral consists of the flux computation over the eastern ($i = i_2$), western ($i = i_1 - 1$), northern ($j = j_2$), and southern ($j = j_1 - 1$) boundaries. The spatial scale is defined as the square root of the integrated cell areas.

$$\frac{\partial u}{\partial x}|_{Length} = \frac{1}{Area}\oint u \cdot dy \tag{C1}$$

$$\frac{\partial u}{\partial x}|_{i_1,i_2,j_1,j_2} = \frac{1}{\sum_{i=i_1}^{i_2}\sum_{j=j_1}^{j_2} dx_{i,j} \cdot dy_{i,j}} \left(\sum_{j=j_1}^{j_2} \frac{u_{i_2,j-1} + u_{i_2,j}}{2} \cdot dy_{i_2,j} - \sum_{j=j_1}^{j_2} \frac{u_{i_1-1,j-1} + u_{i_2-1,j}}{2} \cdot dy_{i_1-1,j}\right) \tag{C2}$$

*Author contributions.* SX designed the grid generation algorithm and carried out grid generation. SX and JM carried out model integration of TS grids in CESM, as well as numerical experiments. SX, LZ, JM and YZ analyzed the model outputs. All the authors contributed to the writing fo the manuscript.

*Competing interests.* The authors declare no conflict of interest.

## References


ETOPO1 Global Relief Model, https://www.ngdc.noaa.gov/mgg/global/, doi:10.7289/V5C8276M, date accessed: 2019-Aug-10.

Adcroft, A., Anderson, W., Balaji, V., Blanton, C., Bushuk, M., Dufour, C. O., Dunne, J. P., Griffies, S. M., Hallberg, R., Harrison, M. J., Held, I. M., Jansen, M. F., John, J. G., Krasting, J. P., Langenhorst, A. R., Legg, S., Liang, Z., McHugh, C., Radhakrishnan, A., Reichl, B. G., Rosati, T., Samuels, B. L., Shao, A., Stouffer, R., Winton, M., Wittenberg, A. T., Xiang, B., Zadeh, N., and Zhang, R.: The GFDL Global Ocean and Sea Ice Model OM4.0: Model Description and Simulation Features, Journal of Advances in Modeling Earth Systems, 11, 3167–3211, doi:10.1029/2019MS001726, 2019.

Bouchat, A. and Tremblay, B.: Using sea-ice deformation fields to constrain the mechanical strength parameters of geophysical sea ice, Journal of Geophysical Research: Oceans, 122, 5802–5825, doi:10.1002/2017JC013020, 2017.

Briegleb, B. P. and Light, B.: A Delta-Eddington Multiple Scattering Parameterization for Solar Radiation in the Sea Ice Component of the Community Climate System Model (No. NCAR/TN-472+STR), Tech. rep., University Corporation for Atmospheric Research, doi:doi:10.5065/D6B27S71, 2007.

Chelton, D. B., deSzoeke, R. A., Schlax, M. G., El Naggar, K., and Siwertz, N.: Geographical Variability of the First Baroclinic Rossby Radius of Deformation, Journal of Physical Oceanography, 28, 433–460, doi:10.1175/1520-0485(1998)028<0433:GVOTFB>2.0.CO;2, 1998.

Dansereau, V., Weiss, J., Saramito, P., and Lattes, P.: A Maxwell elasto-brittle rheology for sea ice modelling, The Cryosphere, 10, 1339–1359, doi:10.5194/tc-10-1339-2016, 2016.

Dukowicz, J. K. and Baumgardner, J. R.: Incremental Remapping as a Transport/Advection Algorithm, Journal of Computational Physics, 160, 318 – 335, doi:10.1006/jcph.2000.6465, 2000.

Dupont, F., Higginson, S., Bourdallé-Badie, R., Lu, Y., Roy, F., Smith, G. C., Lemieux, J.-F., Garric, G., and Davidson, F.: A high-resolution ocean and sea-ice modelling system for the Arctic and North Atlantic oceans, Geoscientific Model Development, 8, 1577–1594, doi:10.5194/gmd-8-1577-2015, https://www.geosci-model-dev.net/8/1577/2015/, 2015.

Girard, L., Bouillon, S., Weiss, J., Amitrano, D., Fichefet, T., and Legat, V.: A new modeling framework for sea-ice mechanics based on elasto-brittle rheology, Annals of Glaciology, 52, 123–132, doi:10.3189/172756411795931499, 2011.

Griffies, S. M., Danabasoglu, G., Durack, P. J., Adcroft, A. J., Balaji, V., Böning, C. W., Chassignet, E. P., Curchitser, E., Deshayes, J., Drange, H., Fox-Kemper, B., Gleckler, P. J., Gregory, J. M., Haak, H., Hallberg, R. W., Heimbach, P., Hewitt, H. T., Holland, D. M., Ilyina, T., Jungclaus, J. H., Komuro, Y., Krasting, J. P., Large, W. G., Marsland, S. J., Masina, S., McDougall, T. J., Nurser, A. J. G., Orr, J. C., Pirani, A., Qiao, F., Stouffer, R. J., Taylor, K. E., Treguier, A. M., Tsujino, H., Uotila, P., Valdivieso, M., Wang, Q., Winton, M., and Yeager, S. G.: OMIP contribution to CMIP6: experimental and diagnostic protocol for the physical component of the Ocean Model Intercomparison Project, Geoscientific Model Development, 9, 3231–3296, doi:10.5194/gmd-9-3231-2016, https://www.geosci-model-dev.net/9/3231/2016/, 2016.

Hallberg, R.: Using a resolution function to regulate parameterizations of oceanic mesoscale eddy effects, Ocean Modelling, 72, 92 – 103, doi:https://doi.org/10.1016/j.ocemod.2013.08.007, http://www.sciencedirect.com/science/article/pii/S1463500313001601, 2013.

Hibler, W. D.: A Dynamic Thermodynamic Sea Ice Model, Journal of Physical Oceanography, 9, 815–846, doi:10.1175/1520-0485(1979)009<0815:ADTSIM>2.0.CO;2, 1979.

Hunke, E. C. and Dukowicz, J. K.: An Elastic-Viscous-Plastic Model for Sea Ice Dynamics, Journal of Physical Oceanography, 27, 1849–1867, doi:10.1175/1520-0485(1997)027<1849:AEVPMF>2.0.CO;2, 1997.

Hunke, E. C. and Lipscomb, W. H.: CICE: the Los Alamos Sea Ice Model Documentation and Software User's Manual Version 4.0 LA-CC-06-012, Tech. rep., Los Alamos National Laboratory, 2008.

Hutter, N. and Losch, M.: Feature-based comparison of sea ice deformation in lead-permitting sea ice simulations, The Cryosphere, 14, 93–113, doi:10.5194/tc-14-93-2020, https://www.the-cryosphere.net/14/93/2020/, 2020.

Hutter, N., Losch, M., and Menemenlis, D.: Scaling properties of Arctic sea ice deformation in a high-resolution viscous-plastic sea ice model and in satellite observations, Journal of Geophysical Research: Oceans, 123, 672–687, doi:10.1002/2017JC013119, 2018.

Jahn, A., Sterling, K., Holland, M. M., Kay, J. E., Maslanik, J. A., Bitz, C. M., Bailey, D. A., Stroeve, J., Hunke, E. C., Lipscomb, W. H., and Pollak, D. A.: Late-Twentieth-Century Simulation of Arctic Sea Ice and Ocean Properties in the CCSM4, Journal of Climate, 25, 1431–1452, doi:10.1175/JCLI-D-11-00201.1, 2012.

Kimmritz, M., Danilov, S., and Losch, M.: On the convergence of the modified elastic-viscous-plastic method for solving the sea ice momentum equation, Journal of Computational Physics, 296, 90 – 100, doi:10.1016/j.jcp.2015.04.051, http://www.sciencedirect.com/science/article/pii/S0021999115003083, 2015.

Kiss, A. E., Hogg, A. M., Hannah, N., Boeira Dias, F., Brassington, G. B., Chamberlain, M. A., Chapman, C., Dobrohotoff, P., Domingues, C. M., Duran, E. R., England, M. H., Fiedler, R., Griffies, S. M., Heerdegen, A., Heil, P., Holmes, R. M., Klocker, A., Marsland, S. J., Morrison, A. K., Munroe, J., Nikurashin, M., Oke, P. R., Pilo, G. S., Richet, O., Savita, A., Spence, P., Stewart, K. D., Ward, M. L., Wu, F., and Zhang, X.: ACCESS-OM2 v1.0: a global ocean–sea ice model at three resolutions, Geoscientific Model Development, 13, 401–442, doi:10.5194/gmd-13-401-2020, https://www.geosci-model-dev.net/13/401/2020/, 2020.

Koldunov, N. V., Danilov, S., Sidorenko, D., Hutter, N., Losch, M., Goessling, H., Rakowsky, N., Scholz, P., Sein, D., Wang, Q., and Jung, T.: Fast EVP Solutions in a High-Resolution Sea Ice Model, Journal of Advances in Modeling Earth Systems, 11, 1269–1284, doi:10.1029/2018MS001485, https://agupubs.onlinelibrary.wiley.com/doi/abs/10.1029/2018MS001485, 2019.

Kwok, R., Hunke, E. C., Maslowski, W., Menemenlis, D., and Zhang, J.: Variability of sea ice simulations assessed with RGPS kinematics, Journal of Geophysical Research, 113, doi:10.1029/2008JC004783, 2008.

Lemieux, J.-F., Tremblay, B., Sedláček, J., Tupper, P., Thomas, S., Huard, D., and Auclair, J.-P.: Improving the numerical convergence of viscous-plastic sea ice models with the Jacobian-free Newton-Krylov method, Journal of Computational Physics, 229, 2840 – 2852, doi:10.1016/j.jcp.2009.12.011, http://www.sciencedirect.com/science/article/pii/S0021999109006822, 2010.

Lemieux, J.-F., Knoll, D. A., Tremblay, B., Holland, D. M., and Losch, M.: A comparison of the Jacobian-free Newton-Krylov method and the EVP model for solving the sea ice momentum equation with a viscous-plastic formulation: A serial algorithm study, Journal of Computational Physics, 231, 5926 – 5944, doi:10.1016/j.jcp.2012.05.024, 2012.

Lemieux, J.-F., Tremblay, L. B., Dupont, F., Plante, M., Smith, G. C., and Dumont, D.: A basal stress parameterization for modeling landfast ice, Journal of Geophysical Research: Oceans, 120, 3157–3173, doi:10.1002/2014JC010678, 2015.

Lemieux, J.-F., Lei, J., Dupont, F., Roy, F., Losch, M., Lique, C., and Laliberté, F.: The Impact of Tides on Simulated Landfast Ice in a Pan-Arctic Ice-Ocean Model, Journal of Geophysical Research: Oceans, 123, 7747–7762, doi:10.1029/2018JC014080, 2018.

Lin, Y., Huang, X., Liang, Y., Qin, Y., Xu, S., Huang, W., Xu, F., Liu, L., Wang, Y., Peng, Y., Wang, L., Xue, W., Fu, H., Zhang, G. J., Wang, B., Li, R., Zhang, C., Lu, H., Yang, K., Luo, Y., Bai, Y., Song, Z., Wang, M., Zhao, W., Zhang, F., Xu, J., Zhao, X., Lu, C., Chen, Y., Luo, Y., Hu, Y., Tang, Q., Chen, D., Yang, G., and Gong, P.: Community Integrated Earth System Model (CIESM): description and evaluation, Journal of Advances in Modeling Earth Systems, 12, e2019MS002 036, doi:10.1029/2019MS002036, 2020.

Lindsay, R. W. and Stern, H. L.: The RADARSAT Geophysical Processor System: Quality of Sea Ice Trajectory and Deformation Estimates, Journal of Atmospheric and Oceanic Technology, 20, 1333–1347, doi:10.1175/1520-0426(2003)020<1333:TRGPSQ>2.0.CO;2, 2003.

Lipscomb, W. H., Hunke, E. C., Maslowski, W., and Jakacki, J.: Improving ridging schemes for high-resolution sea ice models, Journal of Geophysical Research - Oceans, 112, doi:10.1029/2005JC003355, 2007.

Locarnini, R. A., Mishonov, A. V., Antonov, J. I., Boyer, T. P., Garcia, H. E., Baranova, O. K., Zweng, M. M., Paver, C. R., Reagan, J. R., Johnson, D. R., Hamilton, M., and Seidov, D.: NOAA Atlas NESDIS 73 World Ocean Atlas 2013, Volume 1: Temperature, 2013.

Madec, G. and Imbard, M.: A global ocean mesh to overcome the North Pole singularity, Climate Dynamics, 12, 381–388, doi:10.1007/BF00211684, 1996.

Marsan, D., Stern, H., Lindsay, R., and Weiss, J.: Scale Dependence and Localization of the Deformation of Arctic Sea Ice, Phys. Rev. Lett., 93, 178 501, doi:10.1103/PhysRevLett.93.178501, https://link.aps.org/doi/10.1103/PhysRevLett.93.178501, 2004.

Rampal, P., Weiss, J., Marsan, D., Lindsay, R., and Stern, H.: Scaling properties of sea ice deformation from buoy dispersion analysis, J. Geophys. Res., 113, doi:10.1029/2007JC004143, 2008.

Rampal, P., Dansereau, V., Olason, E., Bouillon, S., Williams, T., Korosov, A., and Samaké, A.: On the multi-fractal scaling properties of sea ice deformation, The Cryosphere, 13, 2457–2474, doi:10.5194/tc-13-2457-2019, https://www.the-cryosphere.net/13/2457/2019/, 2019.

Rigor, I. G., Wallace, J. M., and Colony, R. L.: Response of Sea Ice to the Arctic Oscillation, Journal of Climate, 15, 2648–2663, doi:10.1175/1520-0442(2002)015<2648:ROSITT>2.0.CO;2, 2002.

Ringeisen, D., Losch, M., Tremblay, L. B., and Hutter, N.: Simulating intersection angles between conjugate faults in sea ice with different viscous-plastic rheologies, The Cryosphere, 13, 1167–1186, doi:10.5194/tc-13-1167-2019, 2019.

Scholz, P., Sidorenko, D., Gurses, O., Danilov, S., Koldunov, N., Wang, Q., Sein, D., Smolentseva, M., Rakowsky, N., and Jung, T.: Assessment of the Finite-volumE Sea ice-Ocean Model (FESOM2.0) – Part 1: Description of selected key model elements and comparison to its predecessor version, Geoscientific Model Development, 12, 4875–4899, doi:10.5194/gmd-12-4875-2019, https://www.geosci-model-dev.net/12/4875/2019/, 2019.

Schweiger, A., Lindsay, R., Zhang, J., Steele, M., Stern, H., and Kwok, R.: Uncertainty in modeled Arctic sea ice volume, Journal of Geophysical Research: Oceans, 116, doi:10.1029/2011JC007084, 2011.

Spreen, G., Kwok, R., Menemenlis, D., and Nguyen, A. T.: Sea-ice deformation in a coupled ocean-sea-ice model and in satellite remote sensing data, The Cryosphere, 11, 1553–1573, doi:10.5194/tc-11-1553-2017, 2017.

Tsamados, M., Feltham, D. L., and Wilchinsky, A. V.: Impact of a new anisotropic rheology on simulations of Arctic sea ice, Journal of Geophysical Research: Oceans, 118, 91–107, doi:10.1029/2012JC007990, 2013.

Wang, Q., Wekerle, C., Danilov, S., Wang, X., and Jung, T.: A 4.5 km resolution Arctic Ocean simulation with the global multi-resolution model FESOM 1.4, Geoscientific Model Development, 11, 1229–1255, doi:10.5194/gmd-11-1229-2018, https://www.geosci-model-dev.net/11/1229/2018/, 2018.

Weiss, J. and Dansereau, V.: Linking scales in sea ice mechanics, Phil.Trans. R. Soc. A, 375, doi:10.1098/rsta.2015.0352, 2017.

Xu, S., Song, M., Liu, J., Wang, B., Li, L., Huang, W., Liu, L., Xia, K., Xue, W., Pu, Y., Dong, L., Shen, S., Hu, N., Liu, M., and Sun, W.: Simulation of sea ice in FGOALS-g2: Climatology and late 20th century changes, Advances in Atmospheric Sciences, 30, 658–673, doi:10.1007/s00376-013-2158-4, 2013.

Xu, S., Wang, B., and Liu, J.: On the use of Schwarz-Christoffel conformal mappings to the grid generation for global ocean models, Geoscientific Model Development, 8, 3471 – 3485, doi:10.5194/gmd-8-3471-2015, http://www.geosci-model-dev.net/8/3471/2015, 2015.

Zweng, M., Reagan, J., Antonov, J., Locarnini, R., Mishonov, A., Boyer, T., Garcia, H., Baranova, O., Johnson, D., Seidov, D., and Biddle, M.: NOAA Atlas NESDIS 74 WORLD OCEAN ATLAS 2013, Volume 2: Salinity, 2013.